SIMULATION OF A HIGH DISC LOADING
FREE PROPELLER IN A CROSS FLOW
BY THE VORTEX-LATTICE METHOD

R. L. Parker, Jr. and F. L. Heltsley

ARO, Inc.

November 1972

Approved for public release; distribution unlimited.

ARNOLD ENGINEERING DEVELOPMENT CENTER
AIR FORCE SYSTEMS COMMAND
ARNOLD AIR FORCE STATION, TENNESSEE

NOTICES

SIMULATION OF A HIGH DISC LOADING FREE PROPELLER IN A CROSS FLOW BY THE VORTEX-LATTICE METHOD

R. L. Parker, Jr. and F. L. Heltsley
ARO, Inc.

FOREWORD

The research reported herein was performed by the Arnold Engineering Development Center (AEDC), under sponsorship of the Air Force Flight Dynamics Laboratory (AFFDL), Air Force Systems Command (AFSC), under Program Element 64207F, Project 69BT. Project monitor was Capt Carlos Tirres, Research and Development Division, Directorate of Technology, AEDC.

The results presented were obtained by ARO, Inc. (a subsidiary of Sverdrup & Parcel and Associates, Inc.), contract operator of the Arnold Engineering Development Center (AEDC), AFSC, Arnold Air Force Station, Tennessee, under Contract F40600-73-C-0004. Much of the effort was conducted under the direction of Dr. R. A. Kroeger. The study was conducted from November 10, 1969, to June 1971, under ARO Project Numbers BD5026 and BC5132. The manuscript was submitted for publication on June 26, 1972.

This technical report has been reviewed and is approved.

CARLOS TIRRES
Captain, USAF
Research and Development
    Division
Directorate of Technology

ROBERT O. DIETZ
Acting Director
Directorate of Technology

ABSTRACT

A study was conducted to develop an analytical model for the investigation of flow fields about intermediate disc loading lift devices for VTOL applications. Classical vortex-lattice theory was used in conjunction with experimental data for representing a free propeller in a crossflow. The jet phenomena to be simulated by the model are discussed. A number of previous attempts at vortex-lattice modeling are presented. Analytical streamlines and field vectors are compared with available experimental data. The results are evaluated and recommendations are made for further model development.

CONTENTS

APPENDIXES

I. ILLUSTRATIONS

Figure

NOMENCLATURE

C_{pt}	Total pressure coefficient
D	Circular diameter of propeller area
G	Normal velocity component
$\{G\}$	N-component column vector
$[H]$	N x N matrix
$[H]^{-1}$	N x N matrix (inverse of $[H]$)
$\{I\}$	N-component column vector
K	Flow coefficient
$\overline{n}$	Unit vector normal to a surface
U_{max}	Jet centerline velocity
V	Velocity
$\overline{V}$	Velocity vector
V_e	Effective velocity ratio, V_∞/V_j
x, y, z	Coordinates related to airframe axes
$\{\Gamma\}$	N-component column vector
δ	Thrust vector angle
ρ	Density

Subscripts

inlet	Fan inlet station
j	Jet
∞	Free stream

SECTION I
INTRODUCTION

Recent interest in medium to high disc loading jet supported vertical takeoff and landing aircraft has introduced a requirement for accurately representing this type vehicle analytically. Such a model would permit the designer to make accurate predictions of the interactions between lift and control jets and the various aircraft surfaces. Numerous experimental and analytical studies have been conducted in the general area although most are concerned with either very low disc loading lift devices such as helicopter rotors or very high disc loading ones such as turbojet exhausts. The analytical techniques currently available are either too simplified to provide useful information or too cumbersome for use by the average designer.

This effort is an attempt to provide a workable analytical model capable of generating flow fields for the intermediate disc loading devices. Classical vortex-lattice theory is used in conjunction with experimental data to develop the quasi-empirical representation of the propeller disc and jet. The modular nature of the program permits the designer to construct the desired vehicle configurations by assembling various combinations of propeller jets and solid surfaces. In addition to its value as an aircraft design tool, the resulting model can be useful in computing wind tunnel wall interference for a wide variety of vehicle configurations and lift producing devices. The technique is relatively easy to use and is not extremely time consuming on a digital computer.

SECTION II
PROPERTIES OF THE PROPELLER JET

Prior to the development of an analytical model such as this one it is necessary to observe the physics of the phenomena involved. A detailed simulation of jet phenomena can become quite complex. In order to meet the objectives, namely to provide a usable design tool, the phenomena will be dealt with as simply as possible. At the same time, the intent is to retain sufficient accuracy to adequately reproduce the flow field about the model. To accomplish this task, concentration will be placed on the gross effects of the chosen configuration on the external stream, and little time will be spent discussing the flow within the jet boundary.

When the development of this propeller representation began, quantitative information about the flow field surrounding a propeller was found to be far from adequate. Although jet trajectories and skew angle data were available from a number of sources for a wide variety of test conditions, no satisfactory far field velocity vector measurements could be located. Jet cross-sectional shape information was limited and most of that available pertained to either high speed jets or low disc loading rotor wing downwash. Likewise, no inlet velocity distributions could be found for the particular configurations and empirical entrainment values were limited to axisymmetrical jets. It was decided to conduct a brief experimental investigation to supplement the information contained in the literature and provide further insight into the physical phenomenon.

The study was conducted in the 9-ft-diam low-speed wind tunnel at the Georgia Institute of Technology. A 9-in.-diam, three-bladed propeller driven by a high-speed, 2-hp electric motor was used to provide a flow field similar to that associated with moderately high disc loading propulsion devices. Figure 1a (Appendix I) is a close-up of the model and the cruciform rake used in the experiment. The rake was rotated to various positions about the propeller axis to provide the total pressure distribution in the plane immediately beneath the propeller disc.

Velocity vectors were recorded at selected locations in the flow field for various ratios of mean propeller efflux velocity to tunnel velocity. Figures 1b and 1c show the probe used to measure the vector velocities and directions. The 3 degree-of-freedom traverse system upon which the probe was mounted is shown in Fig. 1d as it was installed in the tunnel. The portion of the experimental vector data used in the analytical study is tabulated in Fig. 2, and the flow directions are plotted in two views.

In addition to the quantitative data obtained during this study, a hand-held tuft probe was used to provide a great deal of qualitative information. The skew angle and jet trajectory were roughly traced using reference points on the tunnel window. Except for the presence of a skew angle, the vena contracta, and an uneven velocity distribution through the propeller disc, the propeller efflux was seen to behave in much the same manner as a pure jet exhausting into a crossflow. This was probably due to the high rotational rate and the high solidity ratio of the propeller. It was interesting to note that in the locations where the propeller was stalled the reverse flow velocity was small relative to the velocities through the lifting portion of the face.

Several references were used in this study to provide additional information relating to the jet internal structure and the associated external flow fields. The following discussion is intended to give the reader a more complete understanding of the phenomena with which this report deals.

One of the first attempts to describe a jet exhausting into a cross-flow was made by Shandarov and is included in Ref. 1. Figure 3 contains the original data along with a qualitative interpretation of the information. Here, the contours representing the jet boundary and constant total pressure potential core are placed along the jet trajectory at positions corresponding to the stations where the measurements were made. In this figure, the jet expansion and deformation into the classical horseshoe can be seen.

Although Shandarov's data were obtained for a jet exhausting from a flat plate, the flow field generated is very similar to that associated with the propeller at the same effective velocity ratio.

As the fluid proceeds away from the propeller, it is decellerated, having transferred part of its energy to the free stream. As this occurs, the particles on the sides tend to be swept in the downstream direction at a higher rate than those in the jet center. This results in a rollup of the jet into the classical contra-rotating vortex pair and a net bending of the mean jet path. Simultaneously, the jet cross section increases because of the entraining of free-stream fluid. As the process continues, the direction of the jet path asymptotically approaches the free-stream direction, and the axial velocity excess within the jet becomes minutely small, leaving only the contra-rotating vortex pair. Finally, at a great distance downstream, this too succumbs to the viscocity of the stream. Figure 4 is an attempt by the authors to illustrate the effects of the propeller and its exhaust jet on the surrounding fluid. Arrows have been placed in various positions in the flow field to represent imaginary stream surfaces. A letter has been placed on the upstream end of each arrow to indicate the manner in which that portion of the flow behaves. Those marked with the letter (I) represent the fluid captured by the propeller inlet. This fluid receives energy directly from the propeller and becomes the initial jet flow. As the jet proceeds along its path, other fluid is captured or entrained from the surrounding stream. This is brought about by two mechanisms which will be discussed later. Let us call them turbulent and nonturbulent entrainments, denoted by the letters (T) and (NT), respectively. The letter (D) which appears next to the remaining arrows signifies that this fluid is merely deflected by the presence of the jet. Those arrows are shown here to be converging toward the downstream side of the jet, replacing the fluid captured by

either the inlet or by jet entrainment. This illustrates the near field
sink effect which characterizes all high disc loading V/STOL aircraft
in the jet supported flight mode.

To fully understand the formation of the propeller jet, a close look
at the two previously mentioned entrainment mechanisms is in order.
A discussion of the processes as they pertain to a jet exhausting from a
flat plate is contained in Ref. 2. Platten and Keffer describe the entrain-
ment depicted by the letter (T) in Fig. 4 as "normal turbulent shear flow."
This is the same mechanism which is responsible for entrainment into
jets exhausting into quiescent air and is due to mean velocity differences
within the flow. When such jets are deflected by a crossflow, an addi-
tional phenomenon occurs. This mechanism results from the presence
of the contra-rotating vortex pair and is responsible for the entrainment
of nonturbulent fluid. Reference 2 also states that the entrainment rate
due to this additional phenomenon may be an order of magnitude greater
than that associated with jets exhausting into quiescent air.

The effect can be clearly seen for a laminar jet since the turbulent
mixing does not occur until the free-stream fluid is well within the jet
boundary. The flow takes on the appearance of a double jelly roll.
Figure 5, which is a photograph from Ref. 3, is a good example. The
cut is taken normal to the trajectory of a jet exhausting from a flat plate.
Fluid issuing from the jet exit is seeded with smoke and is illuminated
by a thin slit light beam. The wind tunnel flow is clean and appears
black. A dark spiral is visible within the white, jet flow. This fluid is
seen to have entered the back side of the jet cross section, becoming
part of the jet before turbulent mixing took place.

Figure 6 clearly shows the fluid entering the jet back side. However,
the jelly roll appearance is lost because of turbulent mixing. In this pho-
tograph, taken in the ONERA water tunnel, the jet flow is seeded with
milk while the free-stream fluid contains larger particles.

Fricke, et al (Ref. 4) Volume I, observed that a jet deflected by a
crossflow experiences more rapid decay than a free jet. Their data are
presented in Fig. 7. Since the rate of decay is directly proportional to
entrainment of fluid from the free stream, these data indicate that the
entrainment rate is significantly higher for the deflected jet case.

In summary, then, the free propeller exhausting normal to the cross-
flow has many of the same characteristics as a pure jet exhausting from
a plate. The primary differences are the skew angle, the vena contracta
and the unsymmetrical exhaust velocity distribution. The surrounding
flow fields are also similar except in the region downstream of the

exhaust. The propeller associated flow exhibits a high degree of down-
wash into the wake region while the flow behind the jet does not. This
is seen to be due to the restraint added by the presence of the plate.
Flow into the wake region must come around the jet in the form of a
side wash.

SECTION III
VORTEX LATTICE METHOD

The analytical description of a turbulent jet deflected by a crossflow
has been attempted by quite a large number of individuals employing at
least as many approaches. Much of the work has involved selecting appro-
priate mathematical expressions and combining them to provide a com-
plete formulation of the jet. Empirical data are then called upon to deter-
mine values for the coefficients used. Some of these techniques have been
shown to predict jet trajectories rather well, whereas others yield insight
into the entrainment mechanisms.

Potential theory has formed the basis for a great deal of the analyt-
ical work which has been performed. A majority of the resulting models
can be used to compute plate surface data, as well as pressures induced
elsewhere in the flow field. Most of the models depend on an empirical
trajectory equation to provide geometric locations for the chosen poten-
tial singularities. Some require entrainment data to determine singu-
larity strength distributions. As with the mathematically formulated
models, many of the techniques are capable of moderately accurate pre-
dictions, whereas others leave much to be desired.

Vortex lattice theory is used in this development to provide the re-
quired analytical simulation. The discussion which follows is intended
to provide a basic understanding of the method. An in-depth description
is given by Fitch (Ref. 5) and Rubbert (Ref. 6).

An aerodynamic surface in potential flow can be represented by a
suitable sheet of vorticity. Green's Theorem shows that any solution
for the disturbance potential can then be expressed in terms of this dis-
tribution of vorticity in the boundary.

A good approximation of the surface distribution can be obtained by
replacing the continuous sheet of vorticity with concentrated vortex

filaments. Two-dimensional flow situations can be represented by a set of straight, parallel, infinitely long filaments of vorticity. The spacing between the filaments is normally even. However, in some situations, it is expedient to space them unevenly. When this occurs, it is necessary to account for the uneven spacing in the placement of the associated boundary conditions. The simulation of three-dimensional flows is somewhat more difficult. One concept resolves the three-dimensional distribution into components in two different directions. The two distributions are then represented by concentrated vortex filaments. Since, Hemholtz's theorem states that a vortex may not end in the fluid, the strength of the two vortex sheets must be related. By representing the surface with a network of horseshoe or ring vortices this requirement is automatically satisfied.

Although the spacing of the vortices in one sheet is independent of the other, there is usually an optimum relationship. In general, the vortices should be spaced more closely in the direction of higher vorticity gradient, especially if the associated vortex strengths are higher than those in the other direction. For example, in modeling the solid surfaces in Fig. 8, the vorticity gradients are larger in the streamwise direction. The vortices involved (i. e. those running generally perpendicular to the flow) are of higher strength. As can be seen in the figure, the spacing can be adjusted to suit the particular need. In situations where the model will be run at various attitudes and the number of vortices used is of little concern, the filaments can be placed close together in both directions. The size of the available digital computer sometimes yields the latter technique impractical.

In generating a vortex lattice model of a lifting system, it is necessary that at least one vortex pair be extended to infinity. A more realistic representation can, of course, be obtained by simulating the shed vortex sheet by using a number of vortex filaments. The points from which the vorticity is shed should correspond to those of the case being simulated. Best results are provided if the vortex filaments travel along streamlines after leaving the model. Satisfactory data can be obtained in most cases, however, when the filaments are run straight to infinity in the downstream direction.

Nonlifting systems can be represented by a lattice of ring vortices or by forcing both sides of all horseshoe vortices to extend to infinity along the same path, thus canceling each other.

Development of any model first requires the geometric definition of all surfaces by appropritate vortex lattice networks. A description of

6

the model input procedure is contained in Appendix II. This being completed, the vorticity distribution is determined by requiring that the flow be everywhere parallel to the surface. This is accomplished by placement of control points within the lattice. Figure 9 shows a typical lattice of horseshoe vortices along with the corresponding control points. The boundary condition at each control point can be written in the form:

$$\overline{V}_i \cdot \overline{n}_i = G_i \tag{1}$$

where:
$\overline{V}$ = velocity vector induced by all vortices and the free stream

$\overline{n}$ = unit vector normal to the surface

G = magnitude of velocity component normal to the surface

i = control point number

This produces a set of N linear algebraic equations which must be solved for the individual vortex strengths. These equations can be written in matrix notation in the form

$$[H] \{\Gamma\} - \{I\} = \{G\} \tag{2}$$

Unlike the previous equation the free-stream velocity and the velocity induced by the vortex lattice have been separated. The elements of the matrix [H] are the scalar products of the unit normal and the influence coefficients computed from the geometry of the vortex network. The column matrix $\{\Gamma\}$ contains the unknown vortex strengths. The scalar products of the unit normals and the free-stream velocity vector appear in the column matrix $\{I\}$. The elements of the column matrix $\{G\}$ are the individual normal velocity components specified at the control points. Vortex strengths are determined by inverting the matrix [H]. The equation can then be written as

$$\{\Gamma\} = [H]^{-1}\Big[\{I\} + \{G\}\Big] \tag{3}$$

Once the vortices are known, forces, moments, and pressures on the model can be computed along with velocities and pressures at any point in the surrounding field.

SECTION IV
REVIEW OF VORTEX LATTICE JET MODELS

A number of individuals have utilized vortex lattice theory in the investigation of viscous jet aerodynamics. Monical presented a jet model in Ref. 7 based on the above technique. His model (shown in Fig. 10) was constructed of a vortex network deformed into a tube having a square cross section. The tube was bent in the downstream direction to simulate the deflection of a real jet in a crossflow. The shape of the curve was determined by an empirical jet trajectory equation. The primary difficulty encountered in the use of this model results from the method by which the inlet velocity was obtained.

Flow was induced through the tube by flaring the last set of tube surfaces, thus causing a pressure differential between the tube ends. The flare angle was indirectly determined by iterating on the proper mass flow. Simulation of the hover flight mode was found to be impossible, since the method was dependent on pressures induced by the freestream.

Monical's model was constructed of solid surfaces, i. e., no flow in the direction normal to the lattice. This permitted use of a simplified version of Eq. (1) in the form

$$\overline{V}_i \cdot n_i = o, \quad i = 1, \, n \tag{4}$$

Relatively good correlation with test data was obtained using this analytical model in conjunction with a wing planform to represent a fan-in-wing V/TOL configuration. However, the method provides poor simulation of a deflected free propeller jet. The flow in the downstream region is especially bad. This phenomenon is discussed in more detail in Section V.

The technique of Monical was improved by Fitch (Ref. 5) by eliminating the iteration requirement. In order to induce mass flow through the tube, a control point was added at the jet face center. A nonzero boundary condition was satisfied at this control point to provide the necessary flow into the tube entrance. Fitch found that, in order to operate at a particular effective inlet velocity, the nonzero boundary condition specified had to be 1. 5 times larger than the selected velocity. Expressed in equation form this becomes

$$V_{inlet} = K_{inlet}G_{inlet} = 1.5G_{inlet} \tag{5}$$

The multiplier (K_{inlet}) is referred to in this report as the inlet lattice flow coefficient.

Addition of this generalized boundary condition required solution of the nonhomogeneous form of Eq. (1), i.e., at least one G_i was nonzero. The flared end of the efflux tube was replaced by a ring vortex. The efflux mass flow rate was then independent of the free-stream velocity magnitude and direction and could be directly specified. The remainder of the tube, as with Monical's model, was made up of solid surfaces. Figure 11 shows the model used by Fitch to represent a fan-in-wing configuration. Although not illustrated, a sheet of vortex filaments was attached to the wing trailing edge to simulate the shed vorticity. This configuration was capable of producing moderately good flow field data. However, as in the case of Monical's model, questionable results were generated when the jet was used without the wing.

A typical set of streamlines generated by the tube alone in the plane of symmetry is shown in Fig. 12. Note that the fluid which was not captured by the inlet relaxes immediately to the free-stream direction. This indicates that the downwash velocities present in the real case aft of the inlet are not being properly induced by the model. The streamlines on the jet interior are shown although no attempt has been made to accurately reproduce that portion of the flow field. The flow is merely being ducted away to provide proper inlet simulation. Connecting the efflux model to a wing planform produces flow fields of the type illustrated in Fig. 13. Here, bundles of streamlines are released at selected points upstream of the model to produce stream tubes. A visual indication of the velocities along the path of each bundle is provided by the relative areas of various tube cross sections. Note the contraction of the tubes which enter the inlet, indicating fluid acceleration. In some situations, deformation of the tube makes it difficult to estimate the cross-sectional area. Such is the case with the third tube from the top. Extreme stretching in the vertical direction gives the appearance of flow expansion when, in reality, the fluid is being accelerated through the wing trailing votex sheet.

The effect of a coarse vortex grid is illustrated by the waviness of the streamlines near the tube surface. For the situation shown, tighter filament spacing in the jet axial direction would tend to reduce the scale of these disturbances.

Figure 14 shows a highly sophisticated jet representation from Rubbert, et al (Ref. 6). In this model the jet velocity is specified in a manner similar to that used by Fitch. The single jet face boundary condition is seen to have been replaced by a vortex grid with numerous

control points permitting the specification of an inlet velocity distribution. In addition, the tube cross section is a 15-sided polygon instead of a square. This made it possible to provide more precise data in the field surrounding the wing-jet juncture.

Data generated by the model was found to correlate well with experimental results. As with the models of Monical and Fitch, however, the tube was constructed using solid surface panels. Here again, the jet has been represented by a solid cylinder submerged in a potential cross-flow.

The previously mentioned generalized boundary condition from Ref. 5 was used by Schulz (Ref. 8) to simulate viscous jet entrainment. The configuration investigated by Schulz was identical to that shown in Fig. 11 except that the solid surface panels used to construct the jet tube were replaced by porous ones. This was accomplished by specifying a nonzero normal inflow velocity component at each of the associated control points. Schulz also used a form of the lattice flow coefficient to provide the effective normal velocity through the tube surface. The value required however was somewhat different from that used by Fitch. According to Schulz, the coefficient may range in value from 0.25 through 0.5. Solution of Eq. (1) was required with the boundary conditions on the surface of the plate set equal to zero and those located on the tube surface given values to represent various entrainment rates. In addition, a single boundary condition was placed in the entrance of the tube to specify the jet exhaust velocity. Schulz also presents a model of a jet exhausting into a static region. It is illustrated in Fig. 15.

Figure 16 shows two vortex models used by West (Ref. 9) to provide simulation of both the plate pressure distribution and flow field velocities for a jet exhausting from a flat plate. Although this work did not include deflected jets, it is included here to further illustrate the method of viscous entrainment simulation. The modeling technique was similar to that used by Schulz with one exception; the jet control points were placed on a surface approximating the expanding jet boundary while the vortex tube maintains its uniform cross section. This was done in order to provide more precise flow simulation in the region near the jet boundary. Computations are included in the reference for determining values for the individual jet boundary conditions based on the distance from the jet exit and the vortex lattice spacing. Empirical velocity fields were obtained by West using strobe photography to track soap bubbles as they were entrained into the jet. Correlation of these data with analytical results showed the two to be in excellent agreement. Figure 17 is typi-

cal of the information presented. West states that the models in Fig. 16 provide nearly identical flow fields at distances greater than one jet diameter from the lattice surface. This is to be expected based on the vorticity gradient effect previously discussed. Because of the symmetry involved in the lattice construction, the net vorticity in the axial direction is found to vanish leaving only a column of ring vortices of various strengths. Addition of axial filaments merely changes the shape of the rings. Unless the spacing of the rings along the axis is also modified, no significant effect should be expected.

It should be noted that the distance of singularity disturbance propagation using this particular model is a function of jet diameter because of the inherent equality of jet diameter and vortex spacing in the axial direction.

Use of West's model to represent a fan exhaust deflected by a crossflow is suggested by Fitch (Ref. 5) although no data are presented. A schematic drawing of the model is shown in Fig. 18. The authors found that this mathematical representation is capable of providing smoother near field flow. However, very little effect can be seen in the far field.

SECTION V
DEVELOPMENT OF THE PRESENT MODEL

The first attempt to represent a propeller exhausting into a cross wind is shown in Fig. 19 and will be referred to a Model 1. It combines a jet similar to that developed by Fitch with a means of specifying an inlet velocity distribution similar to that used by Rubbert. The octagonal cross section provides better near field data than a square tube without requiring excessive digital computer time.

The configuration is made up of five "wing parts" (see Appendix II) as shown in the exploded view in Fig. 20. In each case, the rectangular array of vortex quadrilaterals has been deformed into the shape of a particular model surface. The ring at the tube exit (wing part 5) is constructed from a single quadrilateral by using "extra points."

Note that the vortices trailing from wing parts 1, 2, and 5 are forced to cancel, thus forming a nonlifting wing part. The vorticity from the remainder of the model trails to infinity in the downstream direction from the lower end of the jet tube.

A digital computer program was written to generate the geometric coordinates of the propeller disc and tube surface. As shown in Fig. 20, the propeller was replaced by an octagonal grid to permit the imposition of an uneven velocity distribution. This can be done by specifying velocity values at the 25 boundary points located within the grid; 24 in wing-parts 1 and 2 and one, associated with wingpart 5, located in the center of the grid.

Based on the uncertainty introduced by Fitch and Schulz with regard to the lattice flow coefficient, computations were made using Model 1 for a range of coefficient values. It was found that the most realistic inlet flow was produced when the flow coefficient was set at 1.125.

The jet tube is generated by constructing octagons at various distances along a trajectory and connecting them to form quadrilateral grid. The size of the octagons is decreased just below the propeller disc in an attempt to include the effect of the classical vena contracta associated with a device of this type. It should be noted that the resulting tube is not an attempt to reproduce a particular surface which exists in the real jet but is merely a portion of the overall simulation.

The trajectory of the jet tube is computed using an equation per Margason (Ref. 10). The equation can be written:

$$\frac{X}{D} = -\frac{V_e^2}{4\sin^2\delta_j}\left(\frac{Z}{D}\right)^3 - \frac{Z}{D}\ \delta_j\sqrt{\frac{\rho_\infty V_\infty^2}{\rho_j V_j^2}} \tag{6}$$

where D = jet exit diameter

V_e = effective velocity ratio

X, Z = dimensions parallel and normal to the free-stream velocity in the plane of the trajectory

δ_j = angle between jet exit centerline and the free stream

The coordinate system used throughout this study is shown in Fig. 21.

For the propeller in a crossflow problem, the jet exit diameter (D) is assumed to correspond to the diameter of the propeller. An average velocity was obtained for flow through the propeller disc from the data measured in the Georgia Institute of Technology wind tunnel. By using

this value for V_j and assuming that the fluid density does not change, the effective velocity ratio is determined by

$$V_e = \frac{V_\infty}{V_j} \tag{7}$$

The angle (δ_j) is assumed to correspond to the skew angle of the mean flow through the propeller disc. For a propeller with its axis of rotation oriented normal to the wind, this angle can be approximated by

$$\delta_j = \tan^{-1}\!\left(\frac{V_\infty}{V_j}\right) \tag{8}$$

Analytical streamlines generated by Model 1 at a velocity ratio of 2.15 are shown in Fig. 22 representing the flow near the geometrical plane of symmetry, i.e., $Y = 0$. The vectors illustrated are those measured in the Georgia Institute of Technology wind tunnel for the same velocity ratio. Note the absence of downwash in the downstream flow field. Figure 23 is a comparison of the empirical data with vectors computed using Model 1.

As was expected, this configuration provided flow fields similar to those generated by the models of other authors. Although computed for a much lower velocity ratio, the flow field shown in Fig. 22 exhibits the same characteristics as the field illustrated in Fig. 12. As fluid disappears into the inlet, the surrounding flow fills in as it would aft of a point sink. In both cases, the streamlines relax immediately to the free-stream direction. Fluid passes around the jet tube in a nearly two-dimensional manner as can be seen by the additional streamlines in Fig. 19. The imposition of entrainment into the tube was found to have little effect on the downwash. In fact, the two-dimensional character of the flow was hardly disturbed.

As stated previously, models of this type provide more realistic flow fields when used in conjunction with a wing. It was decided to investigate further, hoping that a key could be found for the improvement of the modeling technique.

It has been proposed by a number of authors that the jet affects the surrounding flow as if it were replaced by a lifting body shape or warped delta wing at high angle of attack (see Fig. 24). In both cases vorticity is shed along the lateral edges. The sheets thus formed roll up into a single contra-rotating vortex pair. A more digital approach might be a series of low aspect ratio, high lift wings placed along the jet trajectory.

Here, the continuous sheet of vorticity shed from the lateral edges is replaced by discreet vortices from the wing tips.

If a jet can be described in this manner, it is not surprising that Model 1 is inadequate, since it provides no means of shedding vorticity except from the extreme lower end of the tube. Attaching the jet model to a wing provides that means, since vortices are shed from the wing model's trailing edge. Calculations were made using a configuration similar to that shown in Fig. 11. Although the jet tended to reduce the net lift of the wing, it was sound that the vortex pair trailing from the wing-jet juncture was drastically strengthened. The trailing vorticity distribution along the span was similar to the type produced by the superposition of the wing alone and a much shorter, very high lift wing. No experimental data were available for showing to what extent this occurs in real life.

A new vortex lattice model was needed which could adequately simulate these phenomena. The first attempt referred to as Model 2 appears in Fig. 25. The inlet and the downstream side of the octagonal tube were represented in the same manner as in Model 1. To provide trailing vorticity on the sides of the model, the wing parts forming the upstream side of the tube were rotated 90 deg. This placed the wing part leading edges in the geometric symmetry plane and the trailing edges on either side of the tube. As can be seen in Fig. 25, no attempt was made to position the filaments of trailing vorticity. They were simply run straight to infinity in the downstream direction. In order to conserve the Model 1 trailing geometry at the tube exit, the last panel of the upstream half of the tube was not rotated. This is illustrated schematically in Fig. 26. Note also that the remainder of the upstream portion of the tube was divided into two pairs of wing parts. This was required because of a six panel width limitation of the computer program.

Figures 27 and 28 are comparisons of the empirical vector data with analytically generated streamlines and vectors, respectively. The changes in the model are seen to have resulted in a marked increase in downwash in the aft flow field. Note the increase in upwash upstream of the inlet also pointing to the increase in circulation. The streamlines in Fig. 25 show that the flow is far from two dimensional. The downwash near the geometric symmetry plane is accompanied by a high degree of upward flow outside the sheet of trailing vorticity.

A question arose at this time concerning the possibility of trailing the filaments from the downstream half of the jet tube instead of from the front half. The model shown in Fig. 29 was generated to investigate the effect of such a change. This representation, referred to as Model

2a, is identical in appearance to Model 2. The primary difference is illustrated schematically in Fig. 30. Computations using the modified configuration showed a reversal in the sense of trailing vorticity. Since this resulted in upwash near the geometric symmetry plane and downward flow outside the vortex sheets, Model 2a was abandoned.

Model 3 was generated next in an effort to reduce the large circulatory effect produced by Model 2. The new configuration (shown in Fig. 31) was formed by the addition of one extra point to the path of each vortex filament making up the trailing sheets of Model 2. The points were chosen in such a way as to lower the vortices and move them outward from the geometric symmetry plane. The vortex sheets thus formed provided data much nearer the experimental vectors. Analytical streamlines are shown in Fig. 32.

Since the downwash was still found to be excessive, the decision was made to add an intermediate set of extra points to the trailing vortex paths. In this manner, the sheet could be lowered farther than in Model 3, at the same time providing a smoother transition to the downstream direction. The resulting configuration, called Model 4, appears in Fig. 33. As can be seen in the figure, an error occurred in the input of one of the extra point coordinates. Since no serious effects were observed, corrective action was not taken. The expected decrease in downwash was achieved and is shown in Figs. 34 and 35. Although the flow field immediately behind the propeller is seen to have been over-relaxed, the angularity in the far aft field remained higher than the experimental values. The sink effect of the inlet is indicated by the flow directions above and on either side of the propeller disc. The lateral inflow angles generated by the model correlate well with empirical data; however, the upwash at both locations is excessive.

At this point, it was noted that the shape of Model 4 was tending toward the empirical jet contours of Shandarov (Fig. 3). It was decided that a configuration which duplicated these data more closely might be the answer. This resulted in the construction of Model 5 illustrated in Fig. 36. As shown in the figure, numerous changes were made in the trailing sheet geometry. Eight extra points were added to the path of each vortex filament in an attempt to match the Shandarov data. The position of each individual point at each station was determined by the technique illustrated in Fig. 37. The new contour was lower and wider than Model 4 and provided a much smoother transition to the downstream direction.

The streamlines and vectors resulting from Model 5 are shown in Figs. 38 and 39, respectively. As was expected, the inlet conditions were nearly identical to those exhibited by Model 4. The new configu-

ration, however, caused an increase in downwash in the aft field. The data seem to indicate that the model scale has been increased, i. e., the circulatory effects are propagated farther into the surrounding fluid. At the same time, the flow property changes occur more gradually suggesting that the net strength of model vorticity remained relatively constant.

Comparison of the Model 5 data with the experimental results reveals an important characteristic. At each of the geometric locations used in the correlation, the flow angularity generated analytically is greater than the experimental values. Closer examination shows that the induced inlet flow is excessive indicating that the chosen value of the lattice flow coefficient was too high.

An investigation was initiated to define the optimum coefficient value for this model. The vector data presented in Fig. 40 was generated by Model 5 with the inlet lattice flow coefficient reduced to unity. Comparison with Fig. 39 shows a decrease in flow angularity throughout the flow field of nearly 10 percent. However, the angles were still higher than those measured in the wind tunnel, indicating that further reduction of the coefficient was in order.

As a matter of convenience, an attempt to determine the sensitivity of Model 5 to selected geometrical changes was integrated into the investigation at this point. Two additional configurations were constructed, the geometry of each varying slightly from Model 5. In one version, called Model 6, the wing parts which formed the vortex panels on the lower front of the jet tube were rotated 90 deg, placing their leading edges in the geometric symmetry plane. Hopefully, the flow field would prove insensitive to this change since it simplified the modeling technique somewhat. An additional modification was included in Model 6 in an effort to adjust the downwash imbalance produced by Model 5. The uppermost filament of the trailing sheet on each side of the model was lowered to coincide with the path of the second filament from the top. This change was intended to result in a slight decrease in downwash in the aft flow field without significantly affecting the inlet region.

Vector data generated by Model 6 for two values of inlet lattice flow coefficient are presented in Figs. 41 and 42. Comparison of Fig. 41 with Fig. 39 shows a maximum difference in flow angularity between corresponding points in the field of less than 5 percent. Differences of less than 1 percent are seen to exist in the aft region.

An examination of Fig. 42 suggests that an inlet coefficient of 0.5 was too low since most of the flow angles generated are less than the experimental values.

In addition to Model 6, another configuration was generated in order to separate the effects of the two previous geometric changes. The result was identical to Model 6 except that the uppermost filament of the trailing sheet was returned to its original (Model 5) position. The new jet representation, referred to as Model 7, was used to compute the vectors shown in Figs. 43 and 44. Again, two values of the inlet flow coefficient were used.

A comparison of Models 5, 6, and 7 can be made using Figs. 39, 41, and 43, respectively, since they were all computed for a coefficient value of 1.125.

The effect of the wing part rotation alone can be seen in Figs. 39 and 43. Very small changes occurred in the inlet region; however, downwash values in the aft region were increased by as much as 4 percent.

In summary, the wing part rotation caused an increase in aft region downwash without affecting the inlet region. Lowering the uppermost filament of the trailing sheet resulted in a decrease in downwash in the aft region in addition to changes in the flow near the inlet. Thus, the two modifications combined yielded only minor changes in the flow field.

The results, using an inlet coefficient of 0.675, are shown in Fig. 44. Flow angularity values in the aft region correlate well with experimental data; however, two primary discrepancies are present in the flow field. The upwash on either side of the inlet is approximately 50 percent too high although the inflow angles at the same locations are lower than the experimental values. In addition, the downwash directly above the inlet is too low. The latter conditions indicate that insufficient flow was being induced into the inlet. The high upwash values suggest that the influence of the lift system of the jet was too strong in that region.

Figure 45 is an attempt to graphically display the information obtained from the investigation of Models 4, 5, 6, and 7. Flow angles computed at various geometric points using the different models have been plotted versus inlet lattice flow coefficient. In addition, the empirical values have been included. They appear as horizontal lines on the plot.

The effects of the previously described geometrical modifications to the model can be seen along with the variations due to changes in the inlet flow parameter. It should be pointed out that differences in the arrangement of data along a vertical line exist for Models 4 and 5 while in general they do not for Models 5, 6, and 7. This confirms the aforementioned conclusion that the geometrical changes which produced Models 5, 6, and 7 were relatively insignificant.

The trends present in the plot indicate that it is possible to predict rather precisely the behavior of a particular geometric configuration. The curves illustrated represent the expected variations of flow angularity generated by a configuration similar to Model 5. As can be seen, no single value of flow coefficient can provide a flow field identical to the empirical one. A value of 0.33 yields satisfactory upwash angles in front and on either side of the propeller. The inlet flow and downwash in the aft flow field, however, are much too small. Increasing the coefficient to 0.45 provides sufficient wake angularity although such a change causes too much upwash. Flow into the inlet is still found to be below the required value. The rate of flow into the inlet can be properly adjusted by using a coefficient of 0.75. This results in both excessive upwash on either side and downwash aft of the propeller. Although not included in the plot a close examination of the inflow angles on either side of the propeller indicates that a flow coefficient value of 1.1 is needed to properly simulate the empirical data at those points.

Total simulation requires that the vertical arrangement of the points in Fig. 45 conform to that of the experimental results. Changes in point order are primarily dependent on modifications to model geometry rather than variations in the inlet flow parameter.

Since the effect of lowering the uppermost filament of the trailing sheet in Model 6 produced desirable results, a similar alteration was incorporated into the new representation. This was done in the manner shown in Fig. 46, again utilizing the data from Shandarov. As can be seen in the figure, the outermost extra points were moved inward and corresponding changes were made to the positions of the remaining points. In order to remove the drudgery of placing the extra points by hand, a curve fit was generated using the outermost point from each cross section. A computer program was written capable of computing an outermost point at any selected station along the jet trajectory. The remainder of the points at each station were spaced equally between the outermost point and the side of the jet tube. This resulted in a narrower more dense vortex sheet since the number of vortex filaments remained unchanged. Although the lower wing part rotation carried out in Models 6 and 7 resulted in slight adverse flow angularity changes, the modification was also incorporated into Model 8 since it added simplicity to the geometric input. Intuitively the effect could be easily rendered insignificant by extending the jet tube farther downstream.

Model 8 is illustrated in Fig. 47. Corresponding vectors and stream-lines are presented in Figs. 48 and 49, respectively. Since the data were computed using an inlet flow coefficient of 1.125, the analytical flow angles are higher than the empirical values. By plotting the infor-

mation as shown in Fig. 50 and comparing it with the Model 5 curves, it can be seen that the arrangement of the points has indeed been altered. With the exception of point 8, the order is similar to that of the wind tunnel data.

By assuming that the behavior of Model 8 could be predicted as with previous models, an inlet flow coefficient of 0.906 was seen to provide optimum inlet simulation. The results of the computations made using the reduced coefficient value have been included in Fig. 50. In addition, streamline and vector information is compared with experimental data in Fig. 51 and 52, respectively. Note the improved flow conditions, especially in the region immediately above the propeller disc. The primary problem areas are seen to be the excessive upwash on either side of the disc and the strong downwash at point 8 in the far aft field. It is suggested that the former is due to the singularity effect of the vortex lattice which serves to simulate the propeller while the latter can be attributed to the lack of viscous decay in the potential model.

Figure 53 is included here to demonstrate the capability of the vortex lattice technique to provide three-dimensional flow simulation. The streamlines shown were generated using Model 5; however, close examination of the figure reveals the jet configuration illustrated to be Model 6.

The configuration shown in Fig. 54 was constructed to lend an insight into the mechanics of vortex lattice modeling. Although called Model 9, it was not intended to provide a jet simulation. As can be seen in the figure, it is geometrically simular to Model 1. With respect to the number of wing parts and their respective orientations, Model 9 is essentially Model 8 with the trailing sheet collapsed against the side of the jet tube. The exercise indicates that wing part orientation does not affect the net results as long as the geometric construction is not modified. Such information is encouraging, especially if the user is more scientist than artist.

A number of additional concepts were envisioned during the process of this study. Among them was the configuration illustrated in Fig. 55. By using this representation, called Model 10, an attempt was made to simulate the effect of the low energy wake region.

Although the lattice structure is geometrically identical to Model 2, an additional set of boundary points can be seen in the plane of each trailing vortex sheet. Mechanically, this was done by attaching an additional wing part to either side of Model 1. By specification of the boundary conditions at the new control points, the amount of flow through the

trailing sheets could be controlled without disturbing the tube boundary conditions. In effect, this provided a means by which the direction of flow into the wake region could be specified. The downwash angle could be decreased by increasing the amount of inflow at the sheet control points. Figures 56 and 57 contain the data generated by this model for an inflow velocity of zero. Both figures show excessive flow angles, both in the aft region and on either side of the disc. Close examination of the streamlines plotted in Fig. 53 indicated that an outflow was being induced through the sheets. The location of the control points near the tube appears to have resulted in a strong coupling between the tube and sheet boundary conditions.

In an effort to provide the intended representation, Model 11 was constructed. As illustrated in Fig. 58, the new model was identical to Model 10 except that the sheet boundary points were located farther downstream. Figure 59 indicates fair correlation between the experimental vector data and analytically generated streamlines. The approach was abandoned, however, for two reasons. First, the illustrated streamlines were generated for an inlet flow coefficient of 1.125. If a lower coefficient value had been used to provide more reasonable inlet simulation, it was felt that the resulting reduction in downwash would have produced streamlines quite different from those present in the empirical flow. The second and primary reason was based on the lack of physical justification for placing the singularities in the aft flow field. Very unrealistic flow patterns can be seen in Fig. 58 in the vicinity of the trailing vortices.

On the inside of the sheets, the downwash was extremely high, whereas an upward and outward flow was induced in the exterior region. Although such a model might provide adequate simulation in the remainder of the flow field, any attempt to compute flow characteristics directly downstream of the propeller disc would be futile because of the proximity of the similarities. In addition, little experimental data exist which can be used to specify the amount of inflow through the sheets.

Model 12, shown in Fig. 60 was the last jet representation investigated. Basically, the model is a combination of the concept used in Models 10 and 11, and the geometry of Model 8. The streamline and vector data generated by this representation with the sheet boundary conditions set equal to zero are illustrated in Figs. 61 and 62, respectively. It appears that the imposition of the additional restraint resulted in a decrease in trailing sheet strength. No attempt was made to alter the boundary condition values, again due to the lack of physical justification from empirical data.

SECTION VI
CONCLUSIONS AND RECOMMENDATIONS

A vortex lattice model has been presented for analytically representing a propeller exhausting into a crossflowing stream. In addition to detailed descriptions of each configuration investigated in this study, a discussion of vortex lattice models used by other investigators is included to provide background information.

The reported model is similar to many of the previously used vortex lattice representations with one major exception; sheets of trailing vortex filaments have been attached to either side of the jet tube. Addition of this mechanism for shedding vorticity along the axis of the jet has shown a large improvement in flow field behavior. The modification facilitates the simulation of the roll-up characteristic present in real jets, a phenomenon heretofore unaccounted for in vortex lattice modeling.

It has been shown that the reported model is capable of generating analytical flow fields which correlate well with empirical data. Although the technique is quite flexible, computations have been made for one particular flow condition. The geometric program is currently capable of generating a vortex lattice representation for any reasonable velocity ratio and fan attitude.

Generalization of the model is limited by the absence of adequate experimental data. It is recommended that, at such time data are made available, an attempt be made to define the influence of changes in velocity ratio and thrust vector angle upon such variables as trailing sheet position and inlet lattice coefficient. Such information would provide a more general model.

Small improvements could be made to the existing model for even closer flow field simulation. The data showed that the singularities on the inlet face were producing too strong an influence on the flow near the disc inlet. This suggests that the effective vortex model inlet should be smaller than the actual jet to be represented. Attempts have been made to include jet entrainment in the vortex lattice jet model. The desired results have not been attained. More study and thought into the entrainment mechanism is necessary for its inclusion in the analytical model. More data are needed, in particular, those off the plane of symmetry, before these additions can be made successfully.

The development of a free propeller model is discussed in this report. The model as it exists can easily be attached to a surface for

investigating flows of jet-wing or jet-fuselage configurations. Such investigations have been carried out at the AEDC by the authors. A publication containing the results is being prepared.

REFERENCES

1. Abramovich, G. N. The Theory of Turbulent Jets. MIT Press, Massachusetts Institute of Technology, Cambridge, Massachusetts, 1963.

2. Platten, J. L. and Keffer, J. F. "Entrainment in Deflected Asisymmetric Jets at Various Angles of the Stream." University of Toronto, Canada, UTME-TP 6808, June 1968.

3. Kamotani, Yasuhiro and Greber, Isaac. "Experiments on a Turbulent Jet in a Cross Flow." NASA CR-72893, June 1971.

4. Fricke, L. B., Wooler, P. T., and Ziegler, H. "A Wind Tunnel Investigation of Jets Exhausting into a Crossflow." Volumes I, II, and III, AFFDL-TR-70-154, December 1970.

5. Fitch, Clark R. "Three-Dimensional Aerodynamics Representation of V/STOL Wings by the Vortex-Lattice Method." Master's Thesis, University of Tennessee, August 1967.

6. Rubbert, P. E. "Theoretical Characteristics of Arbitrary Wings by a Non-Planar Vortex-Lattice Method." Boeing Company Document DG-9244, The Boeing Company, Seattle, Washington, August 1962.

7. Monical, Richard E. "A Method of Representating Fan-Wing Combinations for Three-Dimensional Potential Flow Solutions." Institute of Aerospace Sciences Paper Number 65-85. Presented at the IAS Second Aerospace Sciences Meeting, New York, New York, January 25-27, 1965.

8. Schulz, R. J. "Simulation of Jet Entrainment in a Potential Field." AEDC-TR-67-217 (AD822341), November 1967.

9. West, R. H. A. "Investigation of the Entrainment Produced by a Jet Exhausting into a Quiescent Region." Master's Thesis University of Tennessee, August 1967.

10. Margason, Richard J. "The Path of a Jet Directed at Large Angles to a Subsonic Free Stream." NASA TND 4919, 1968.

APPENDIXES
I. ILLUSTRATIONS
II. VORTEX LATTICE PROGRAM
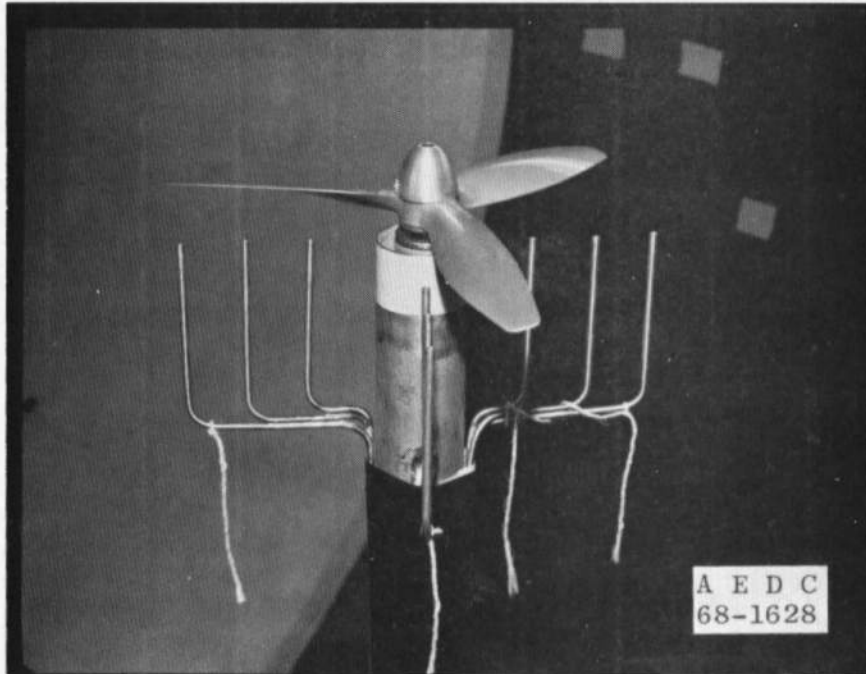
a. Propeller Model and Cruciform Rake as Mounted in 9-Ft Tunnel
at Georgia Institute of Technology (GIT)
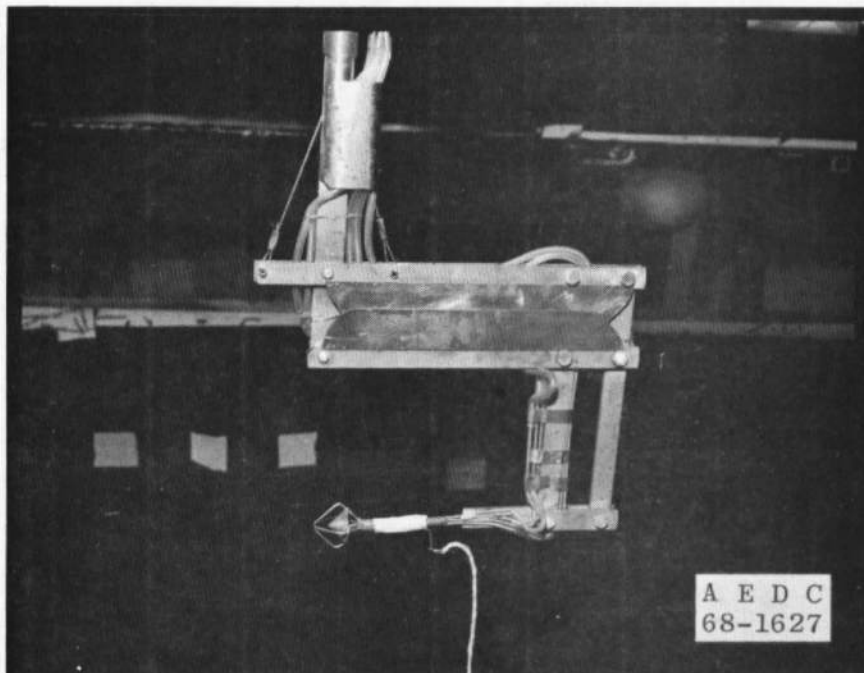
b. Claw Probe for Measuring Velocity Vectors
Fig. 1 Experimental Apparatus
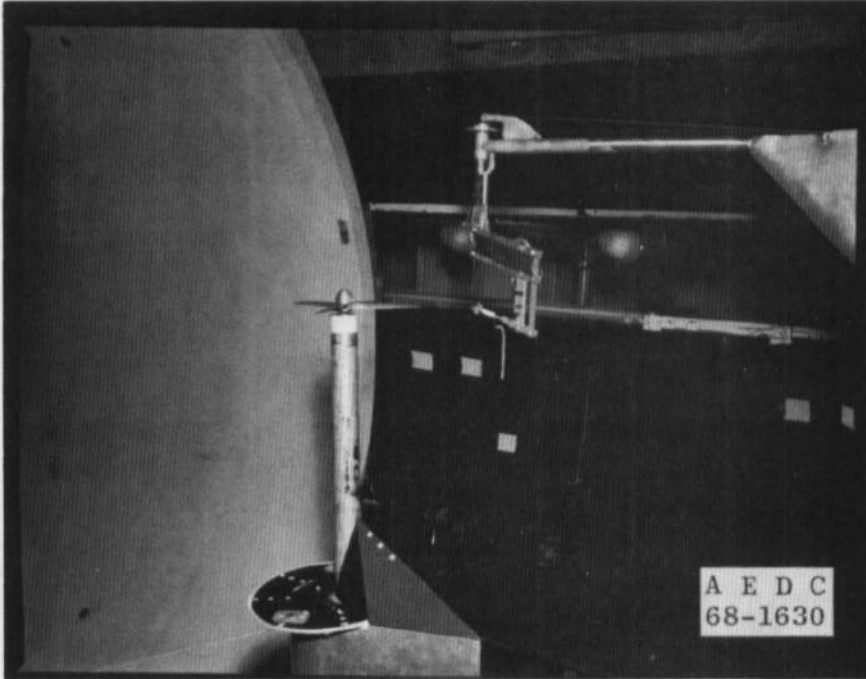
c. Propeller Model and Probe in GIT Tunnel
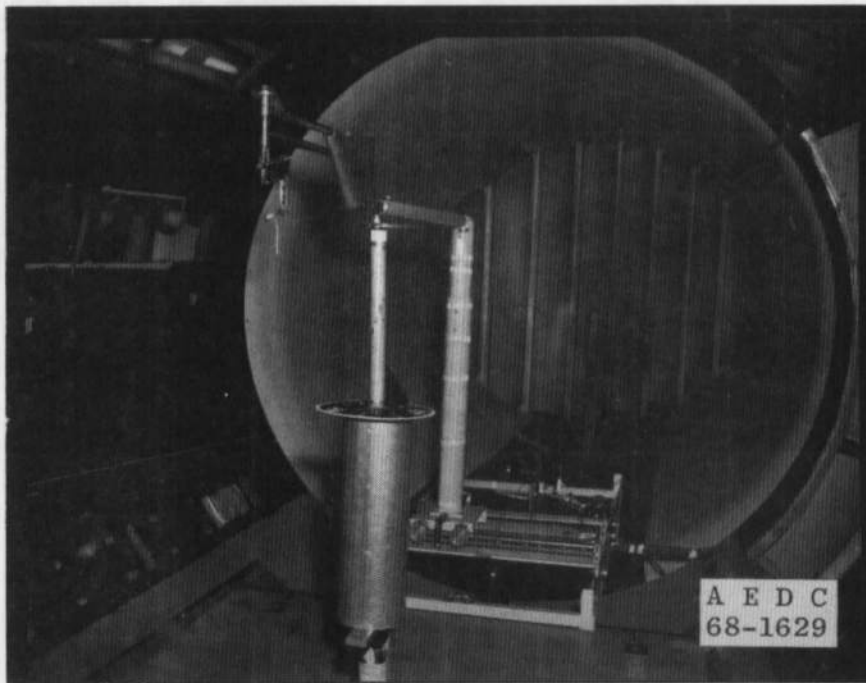
d. Probe-Traverse System
Fig. 1 Concluded

	Point Coordinates			Flow Vector		
Point	X	Y	Z	Vel.	Pitch	Yaw
1	-11.0	0	0		-2.94	1.62
2	0	-7.0	0		-9.49	13.83
3	11.0	0	0		23.20	-6.44
4	0	+7.0	0		-6.54	-8.65
5	11.0	0	-4.0		10.50	0.01
6	0	0	-4.0		24.30	-4.10
7	4.0	0	-4.0		24.70	-0.87
8	21.25	0	4.0		17.40	-3.04

Top View

Side View
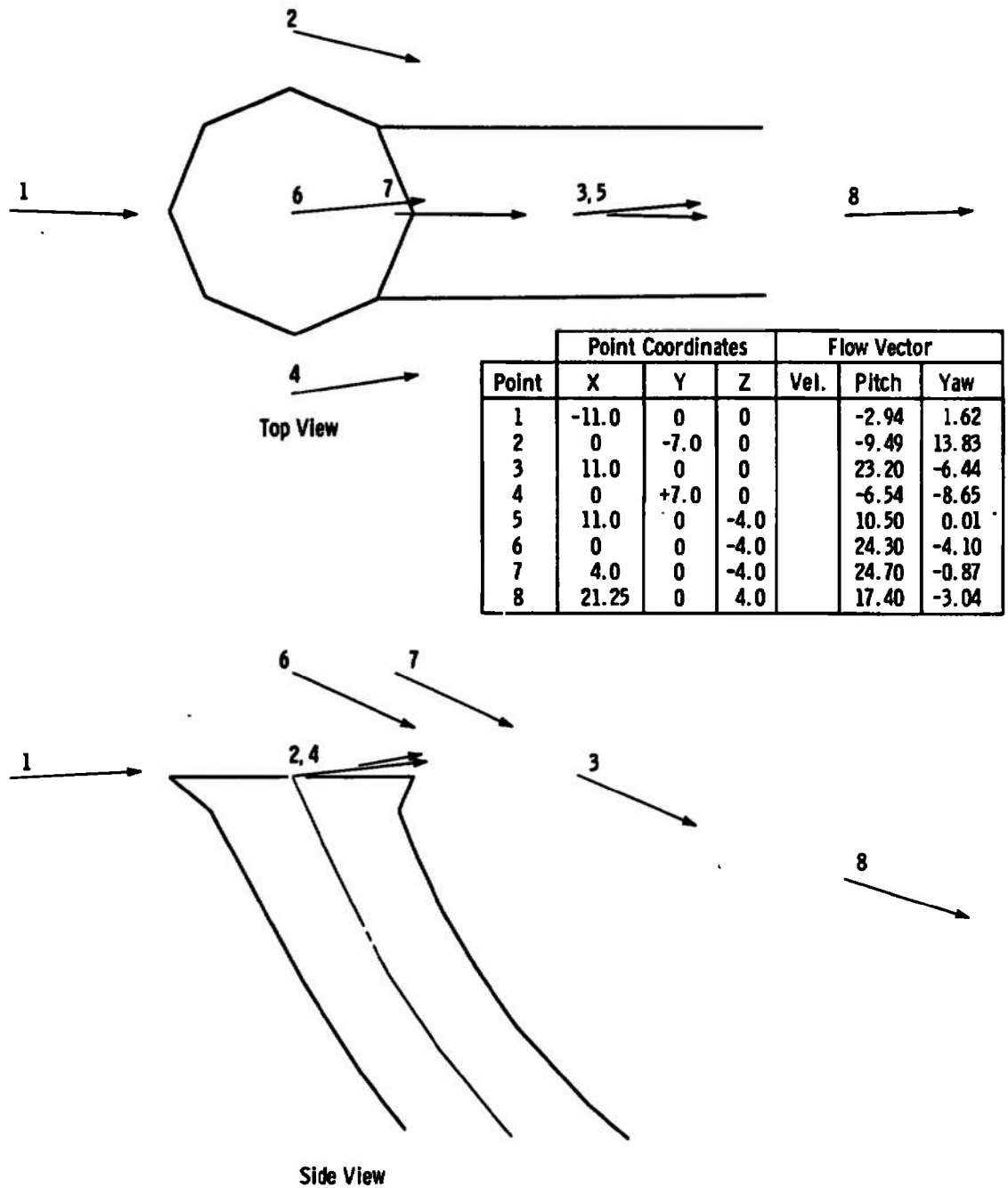
Fig. 2 Data Measured in the Georgia Institute of Technology 9-Ft Wind Tunnel
for Jet-to-Tunnel Velocity Ratio of 2.145
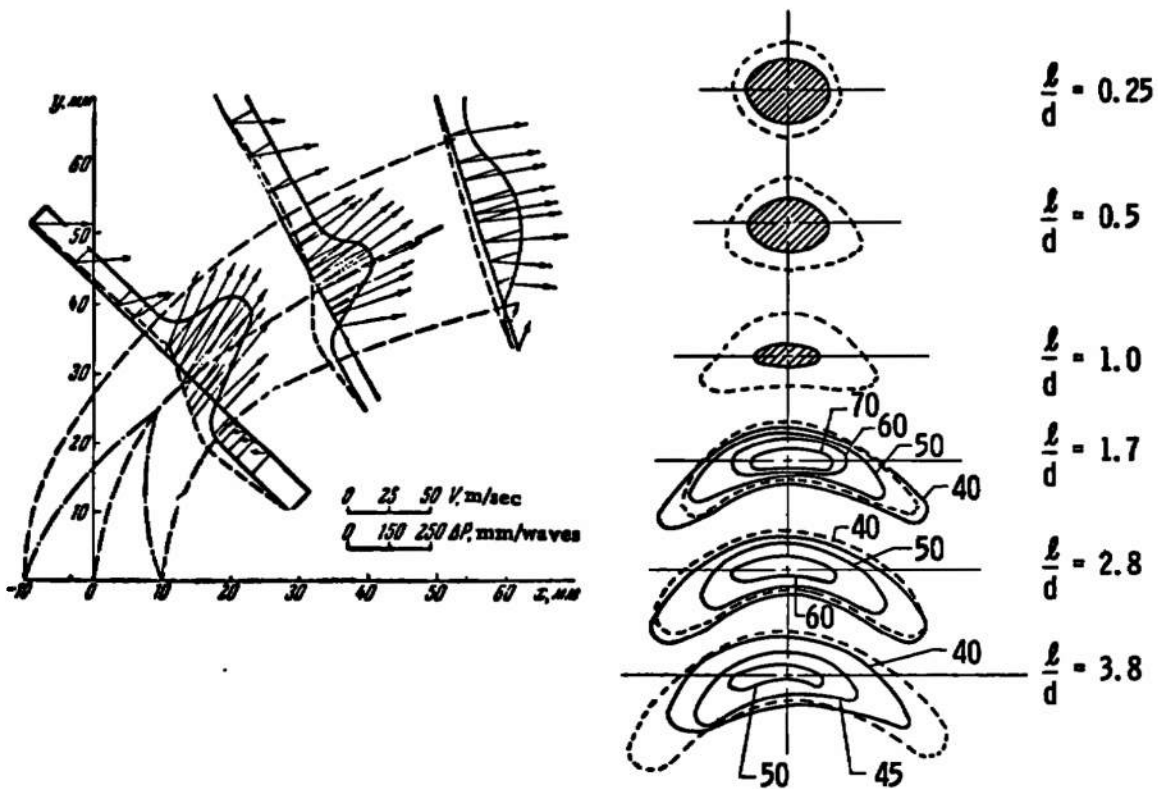
a. Velocity and Pressure Contours
Fig. 3 Velocity and Pressure Contours (Shandarov)
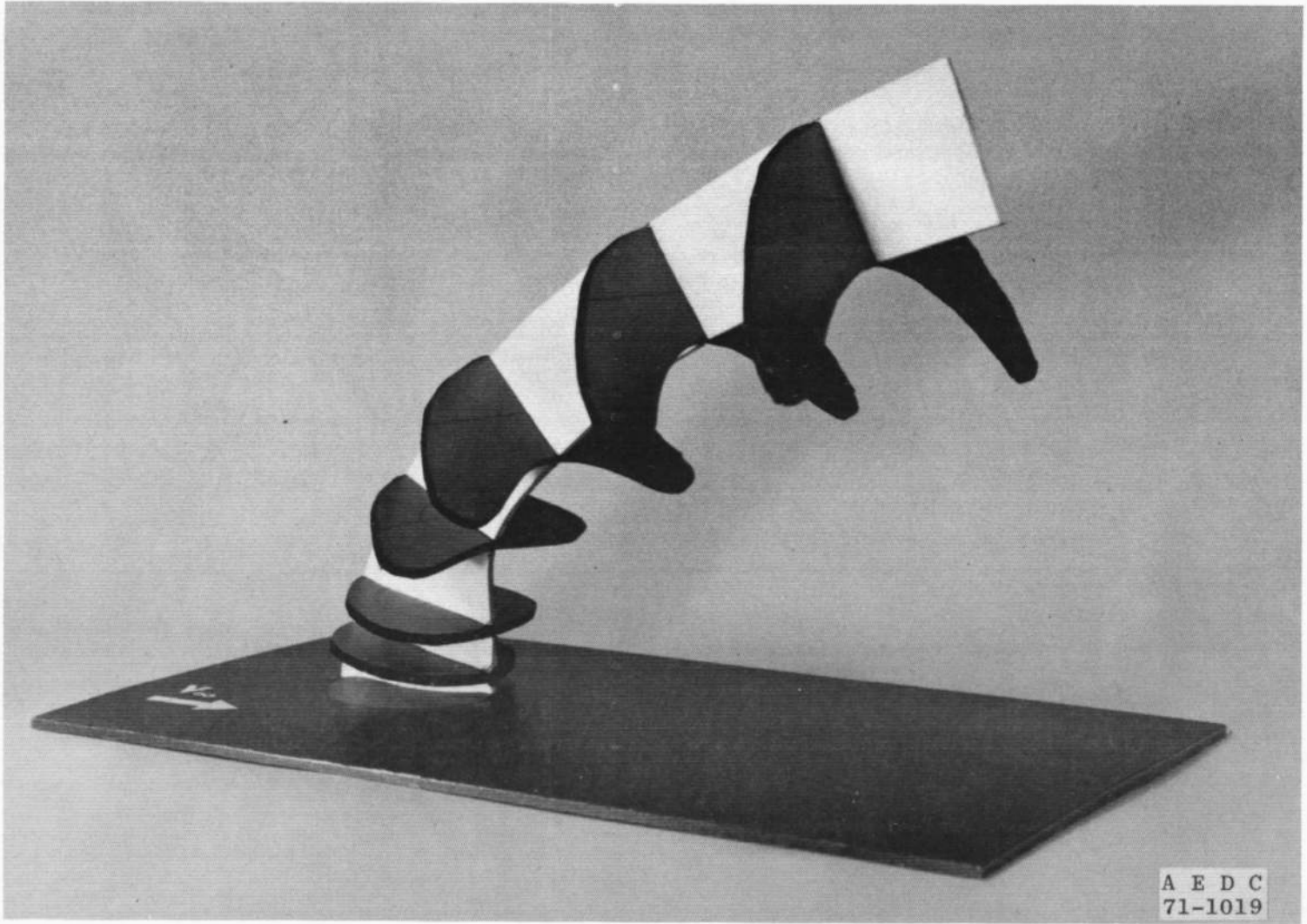
b. Interpretation of Jet Contour
Fig. 3 Concluded
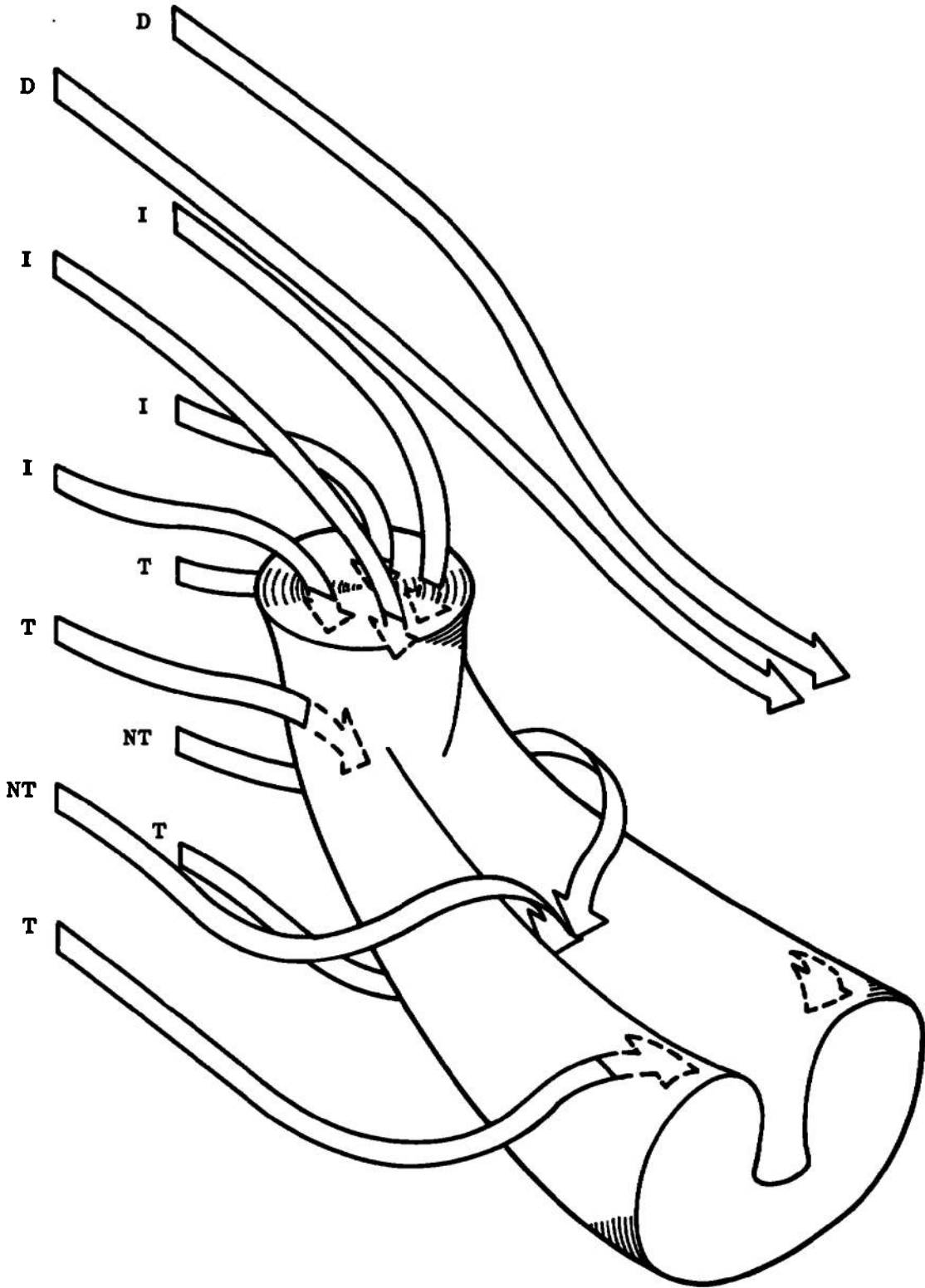
Fig. 4 Interaction of a Jet and the Surrounding Fluid
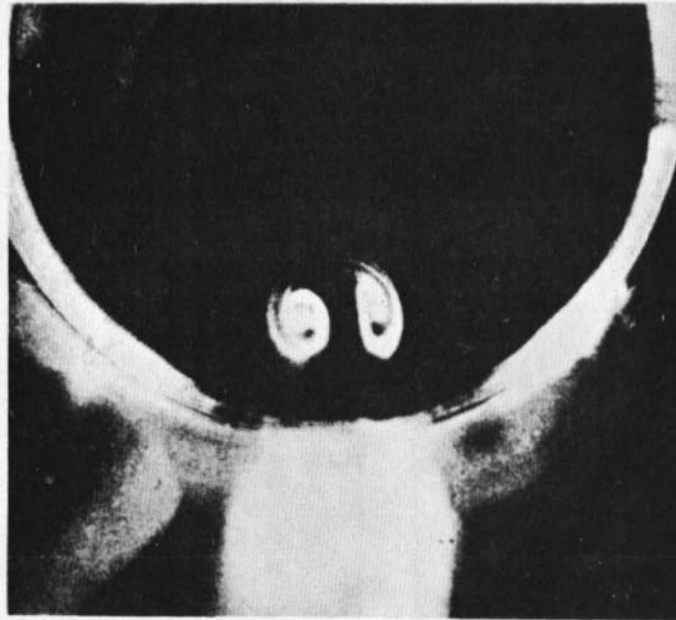
Fig. 5 Laminar Jet Exhausting Normal to the Free Stream
(Free Stream Out of Paper)
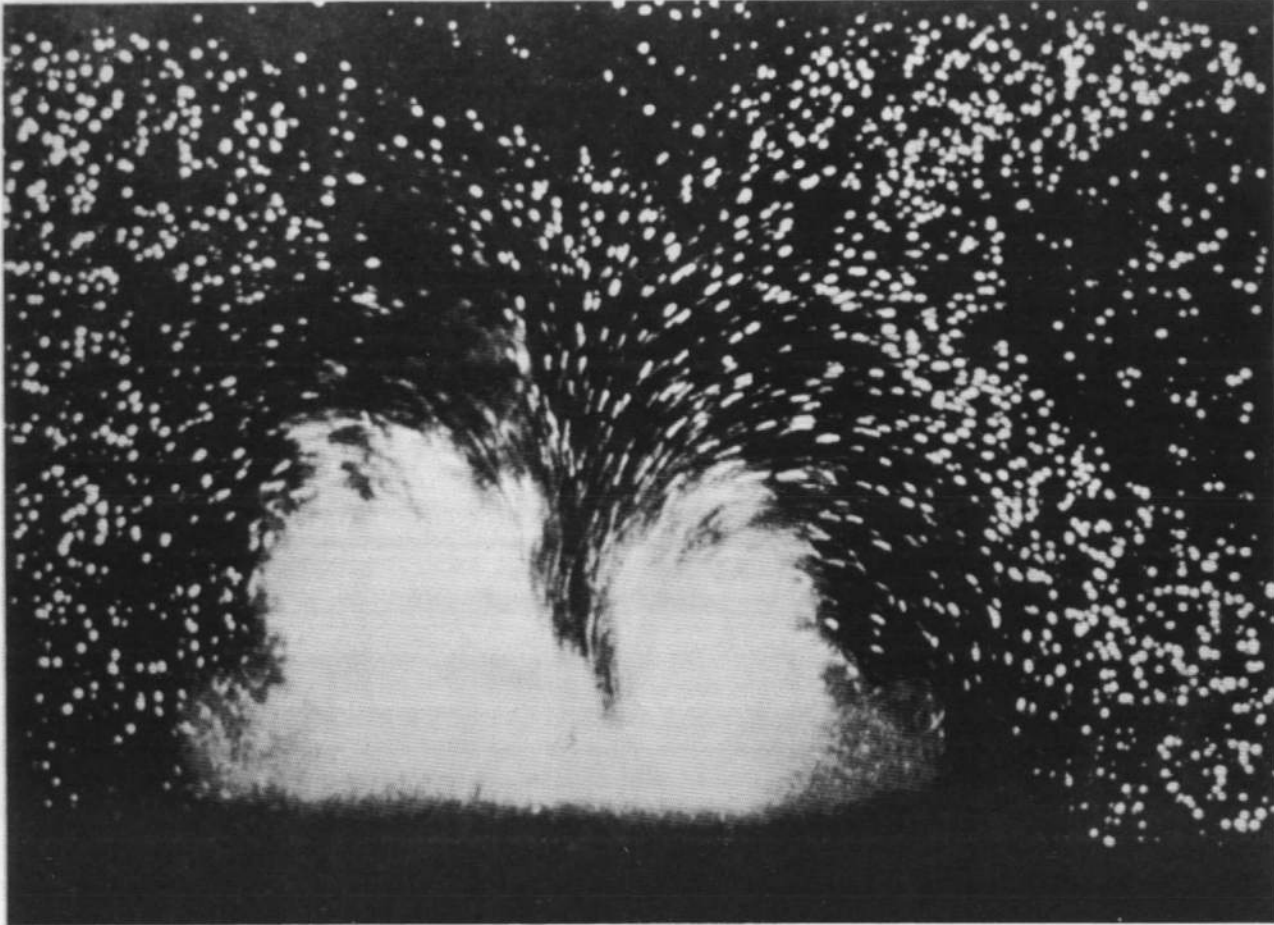
Fig. 6 Cross Section of the Wake of a Jet Exiting Perpendicular to the Free Stream in a Water Tunnel
(Photograph from O.N.E.R.A. Film No. 575 Entitled "Flows with Large Velocity Flunctuations")
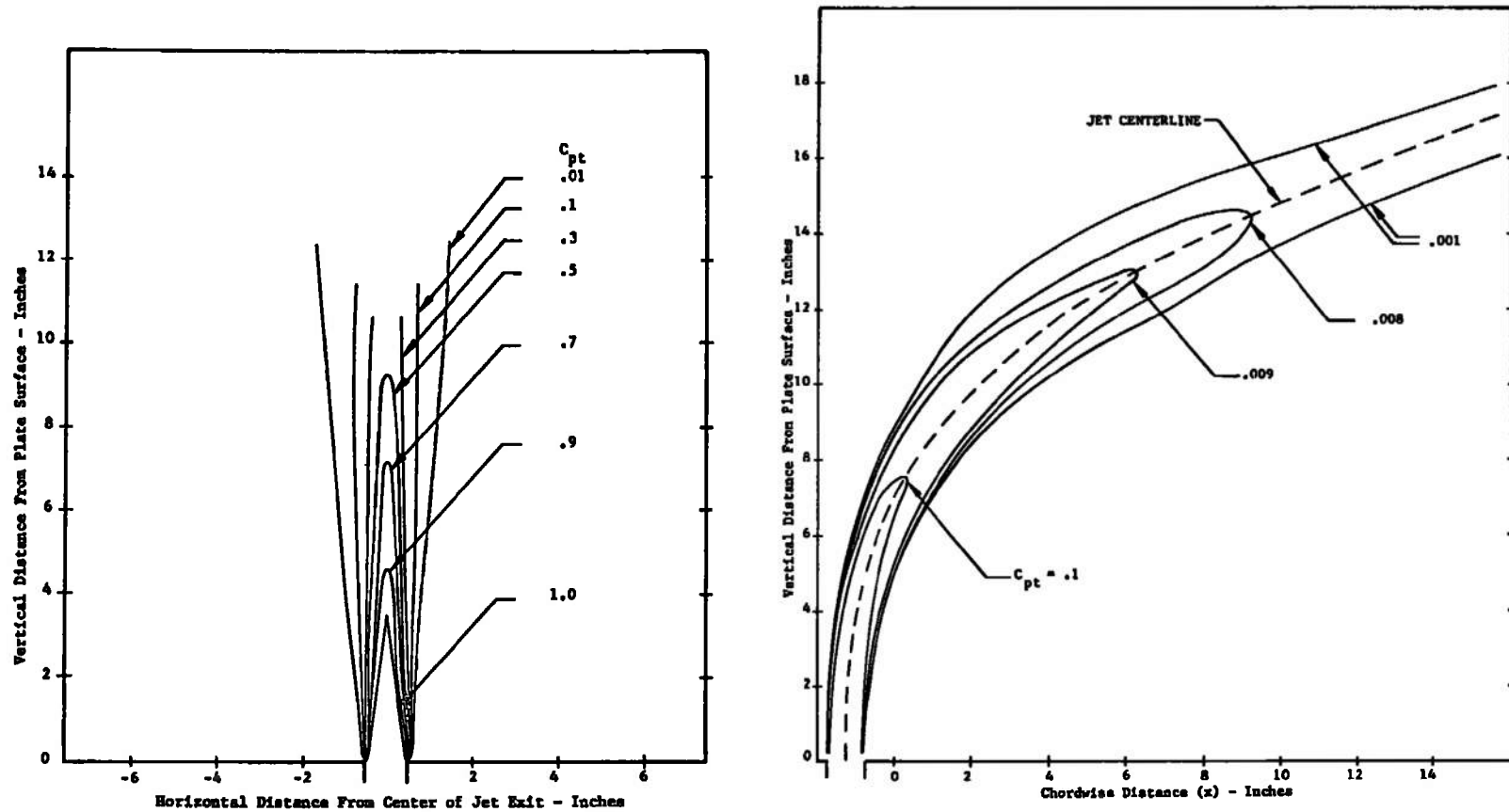
Fig. 7 Jet Decay Rate
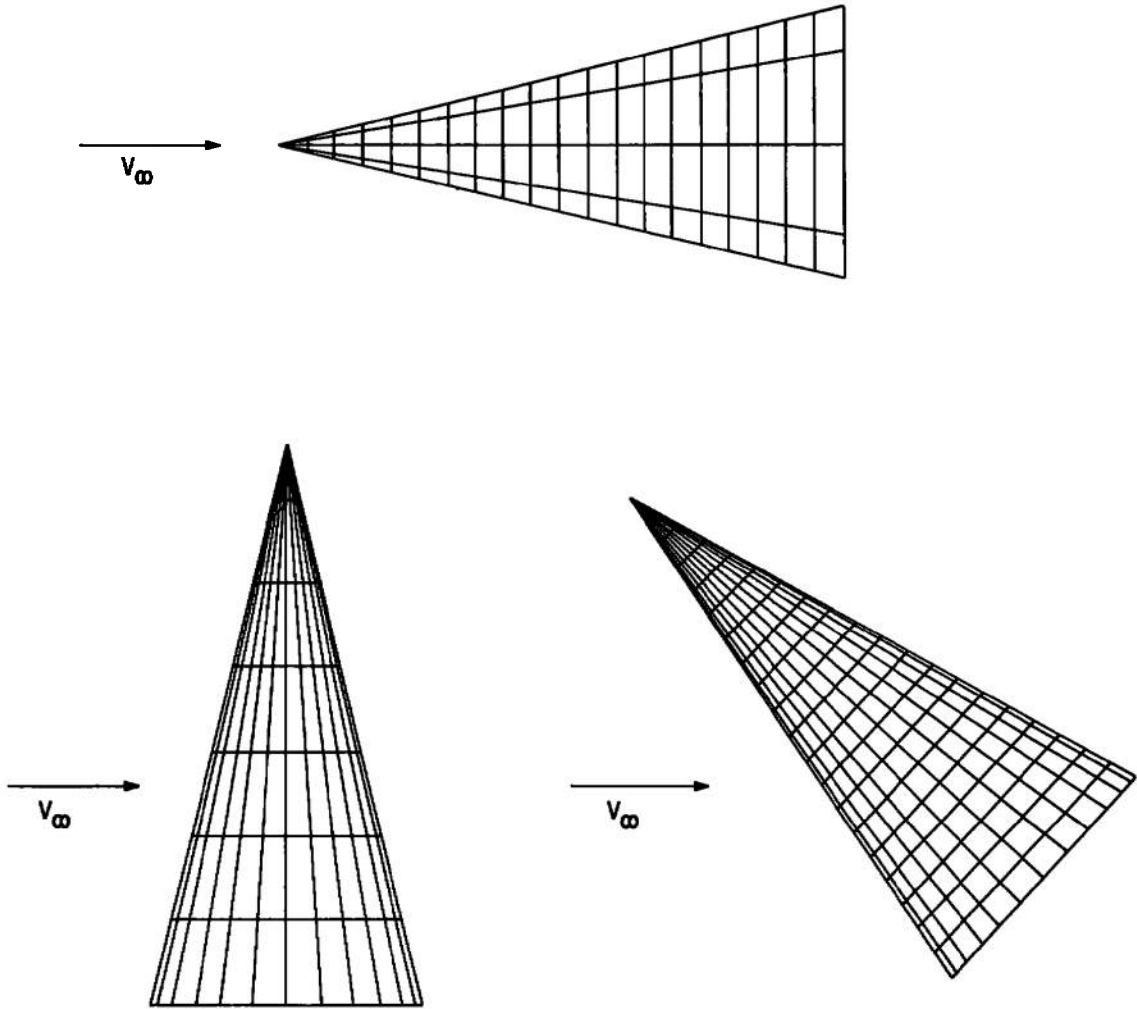
Fig. 8 Effect of Model Attitude on Optimum Vortex Spacing
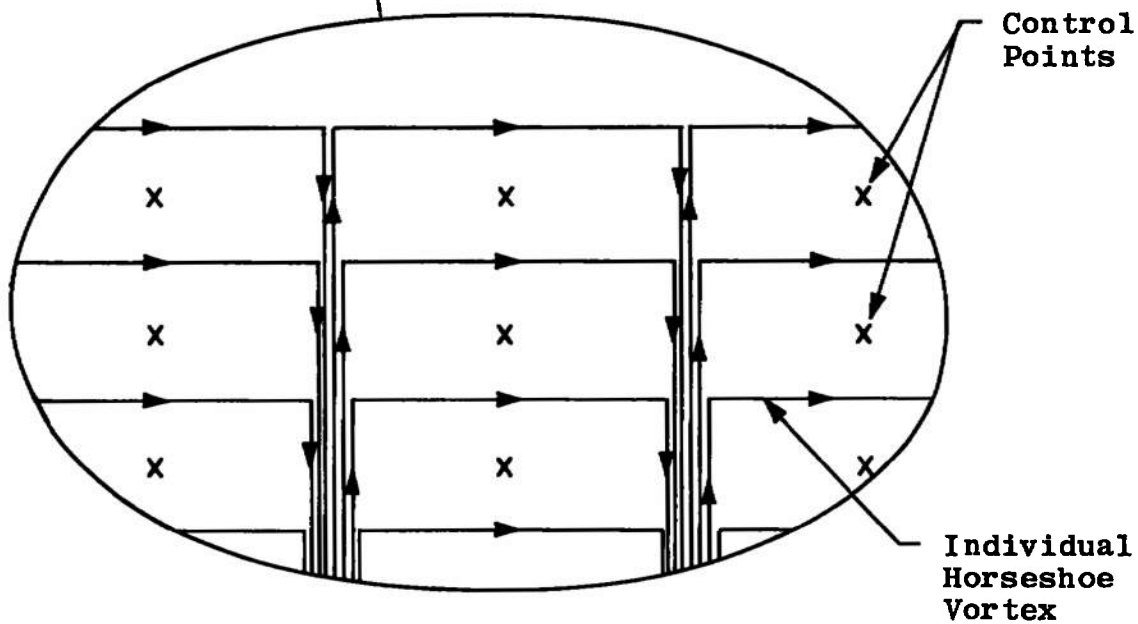
Fig. 9 Distribution of Individual Horseshoe Vortices
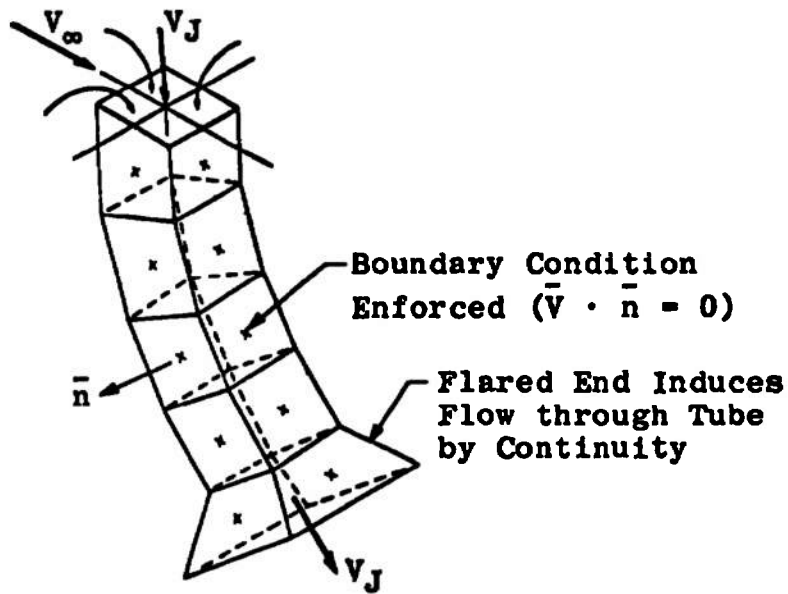
Fig. 10 Original Jet Model (Monical)
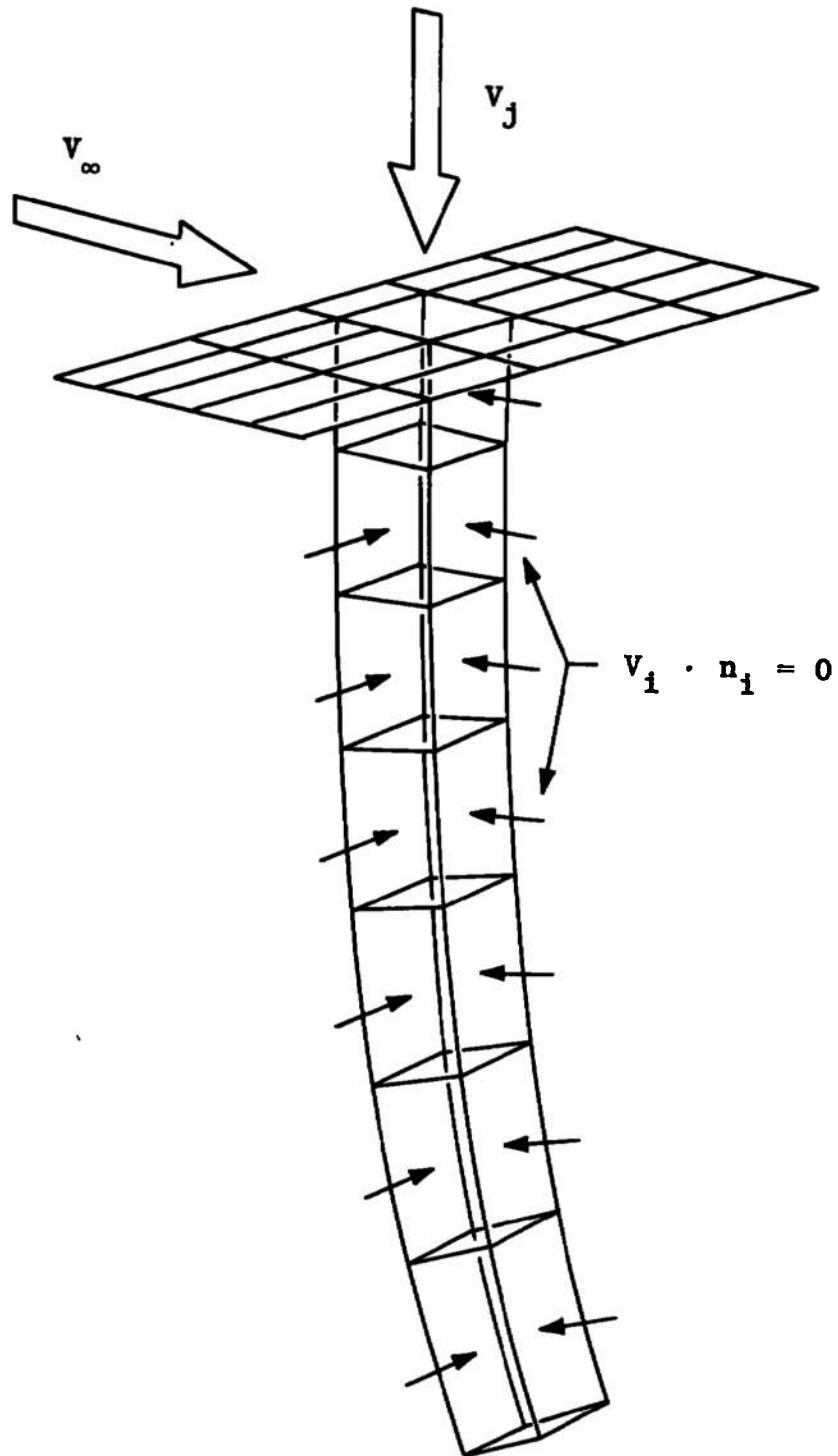
Fig. 11 Fan-in-Wing Model (Fitch)
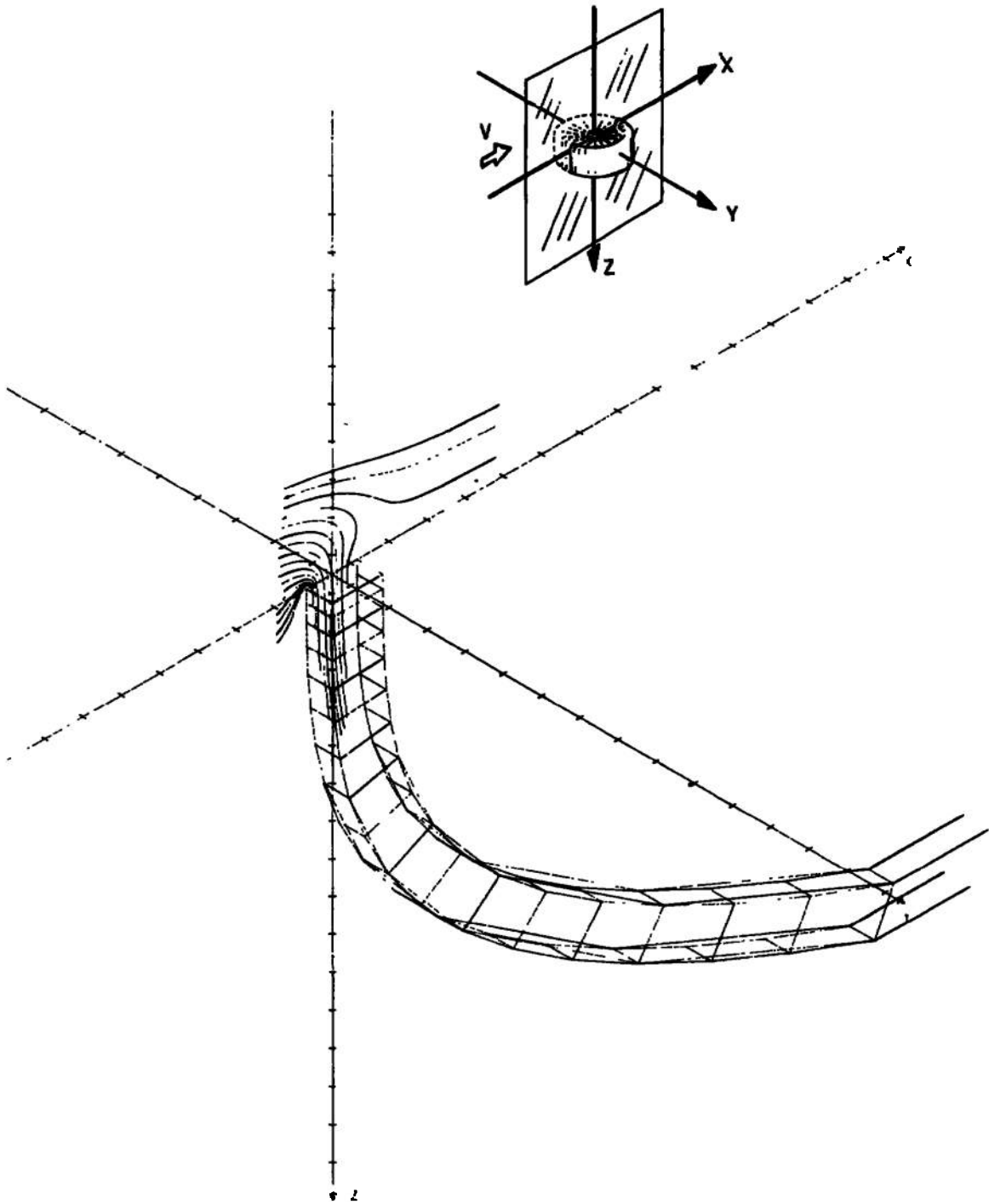
Fig. 12 Propeller Tube Model (Fitch)
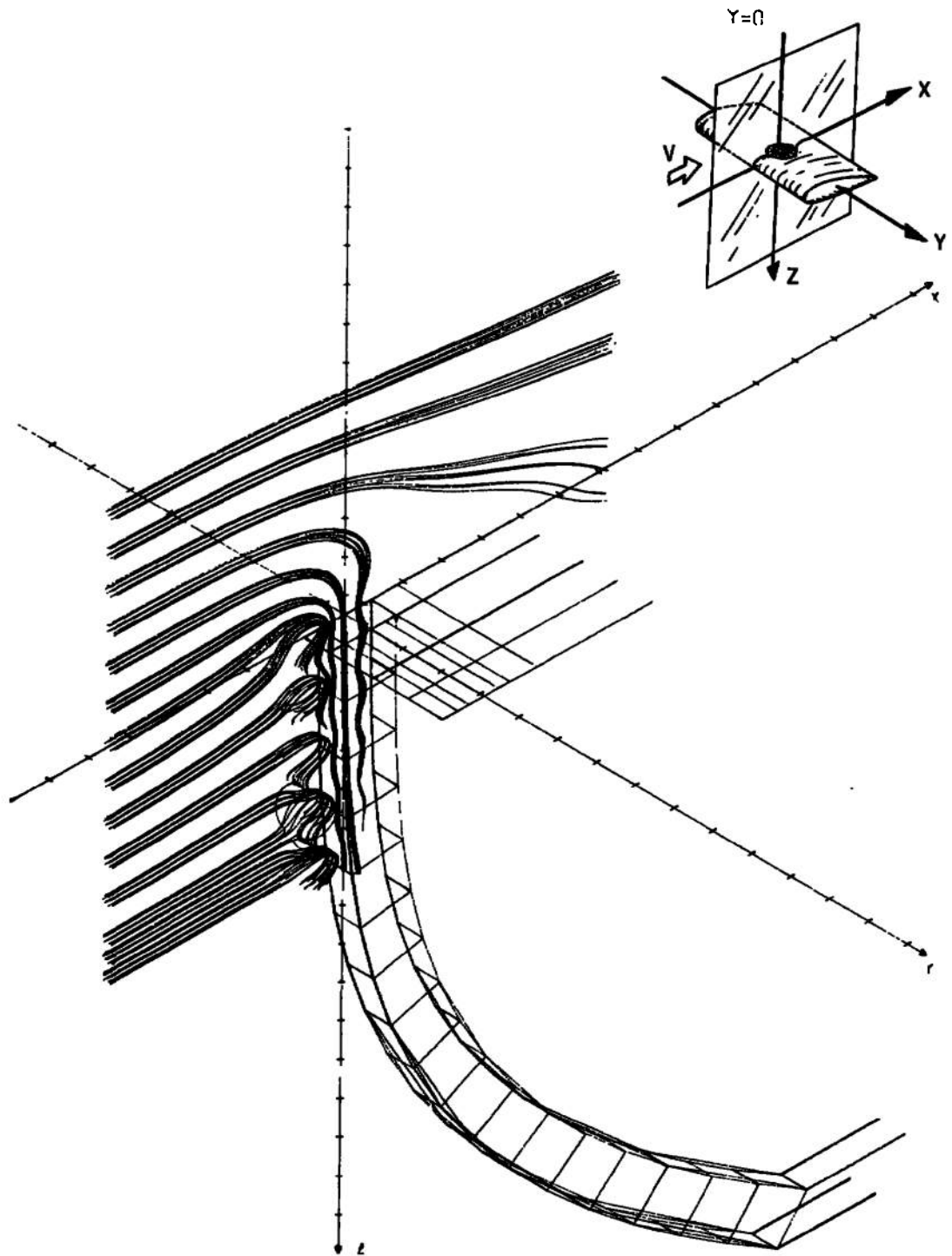
Fig. 13   Fan-in-Wing with Stream Tubes
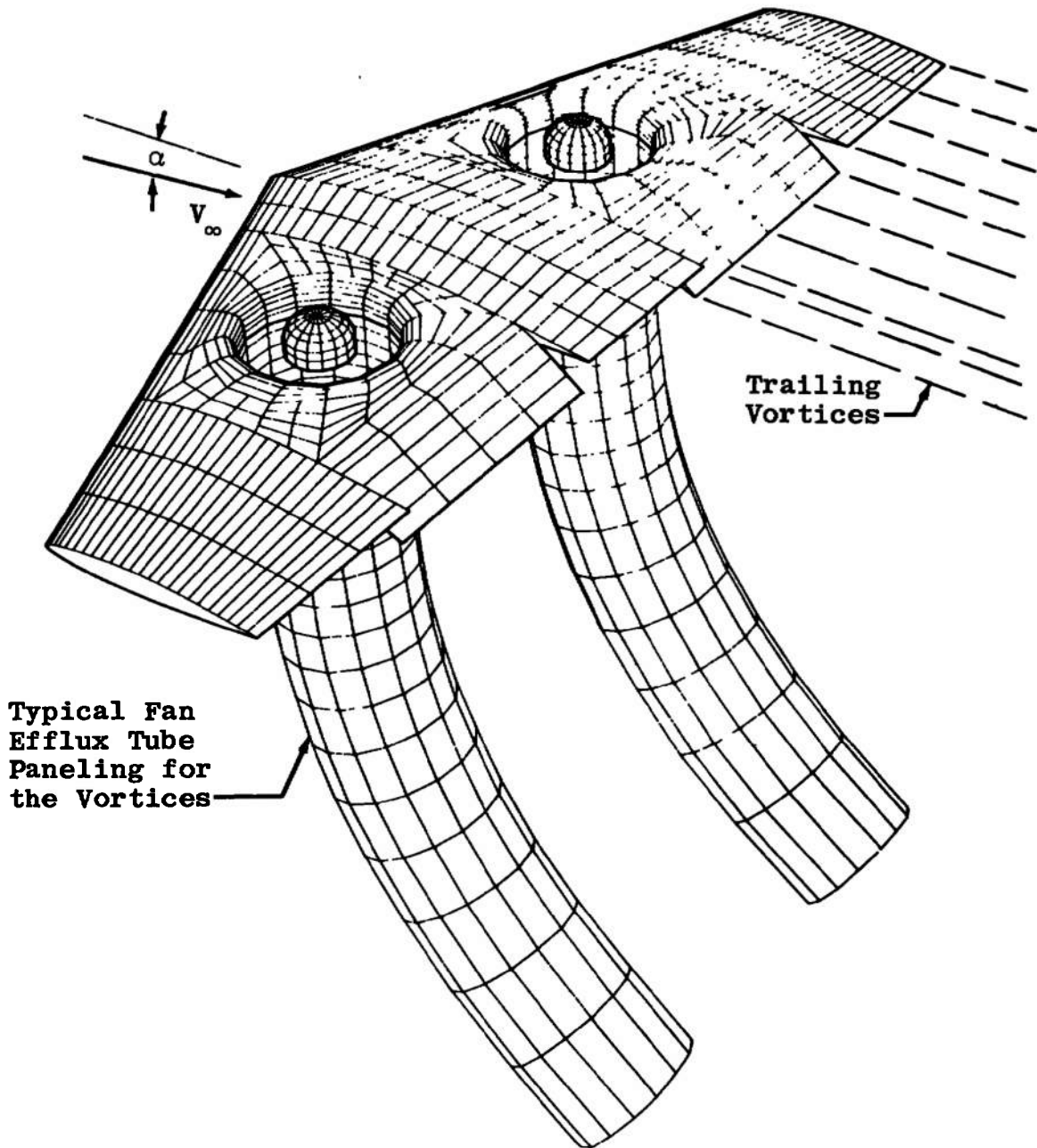
Arbitrary Planform, Thickness, Camber, Inlet Geometry, and
• Fan Inflow Distribution

• Source Panels on Wing and Centerbody Surfaces

• Vortices on Efflux Tube and Trailing Sheet

• Internal and Fan Face Vortices Omitted for Clarity

Fig. 14 Fan-in-Wing Configuration (Rubbert)
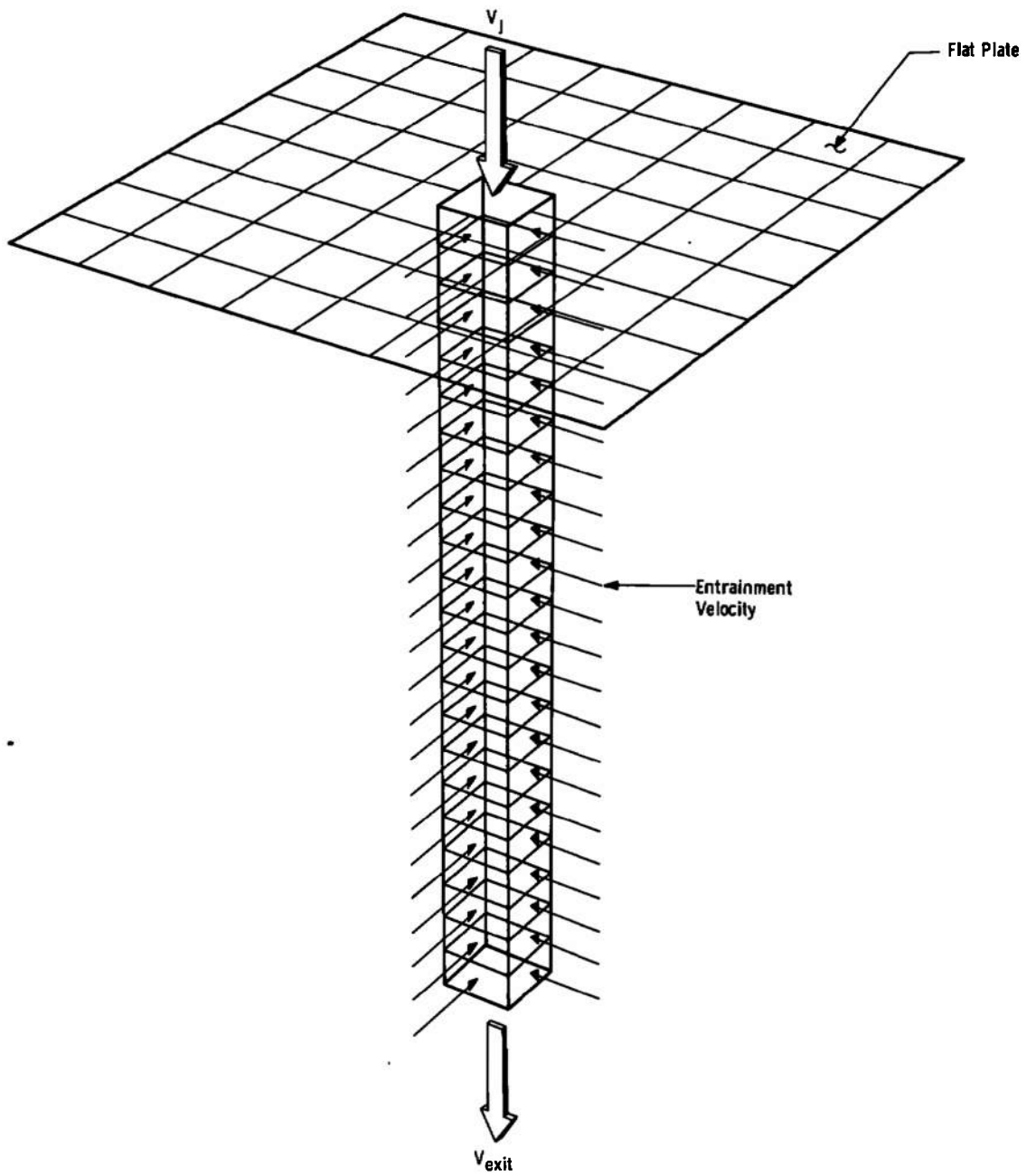
Fig. 15 Jet Exhausting into a Static Region
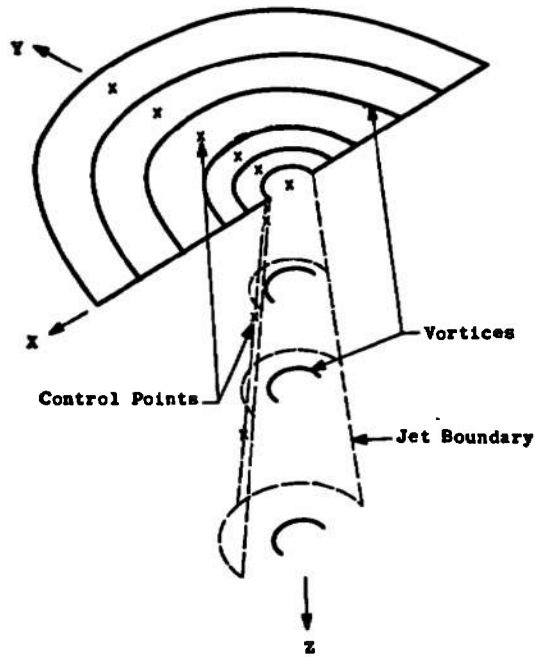
Circular model.
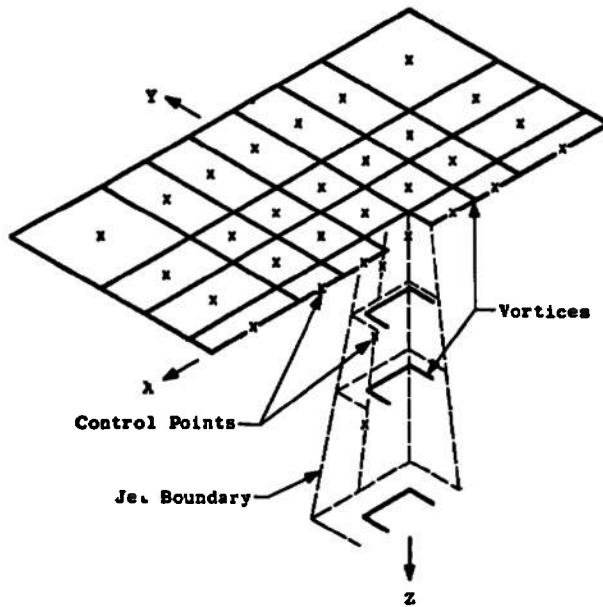
Square model.

Fig. 16 Vortex Models Used by West
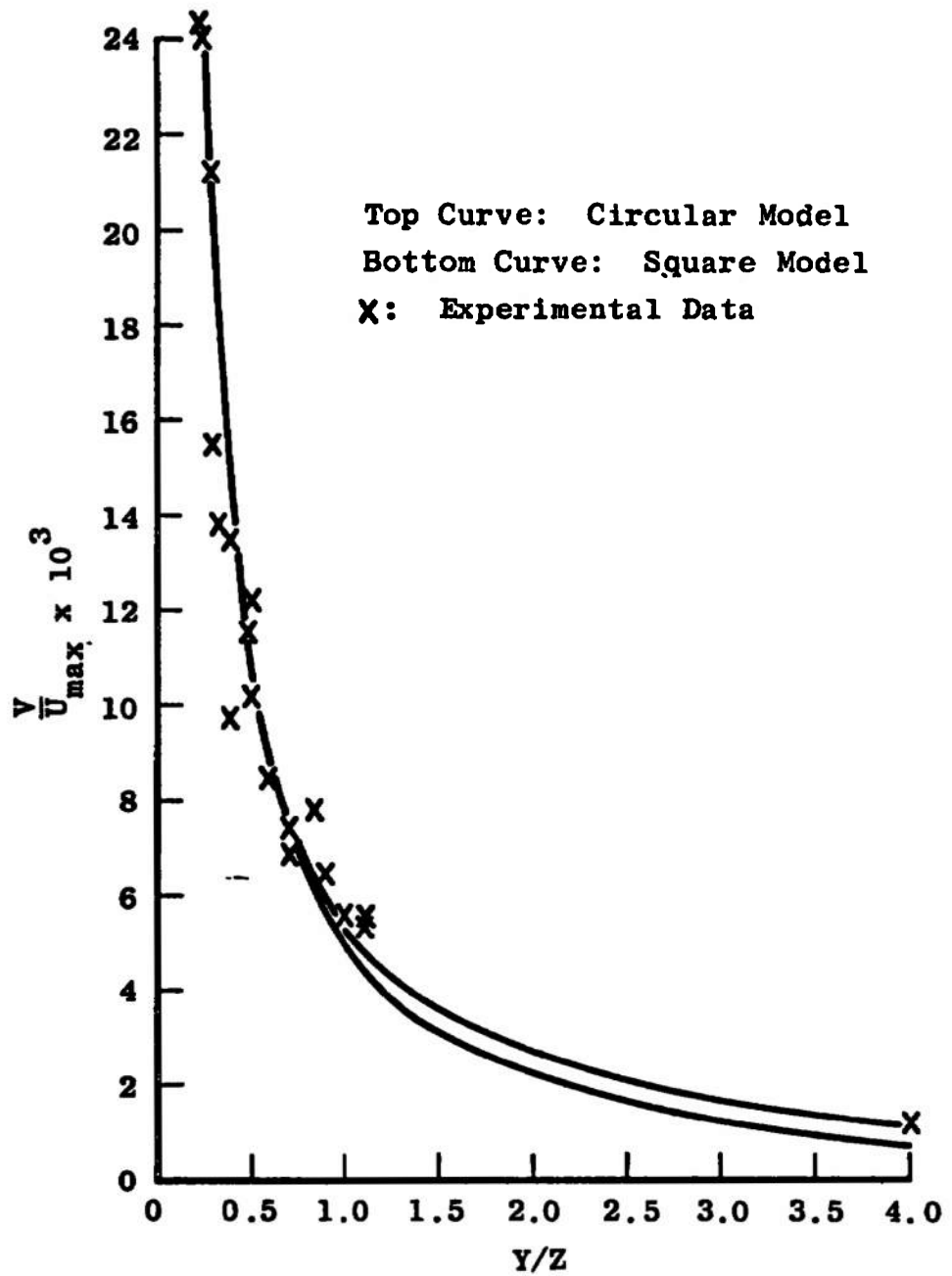
Fig. 17 Typical Comparison of Analytical and Experimental Data (West)
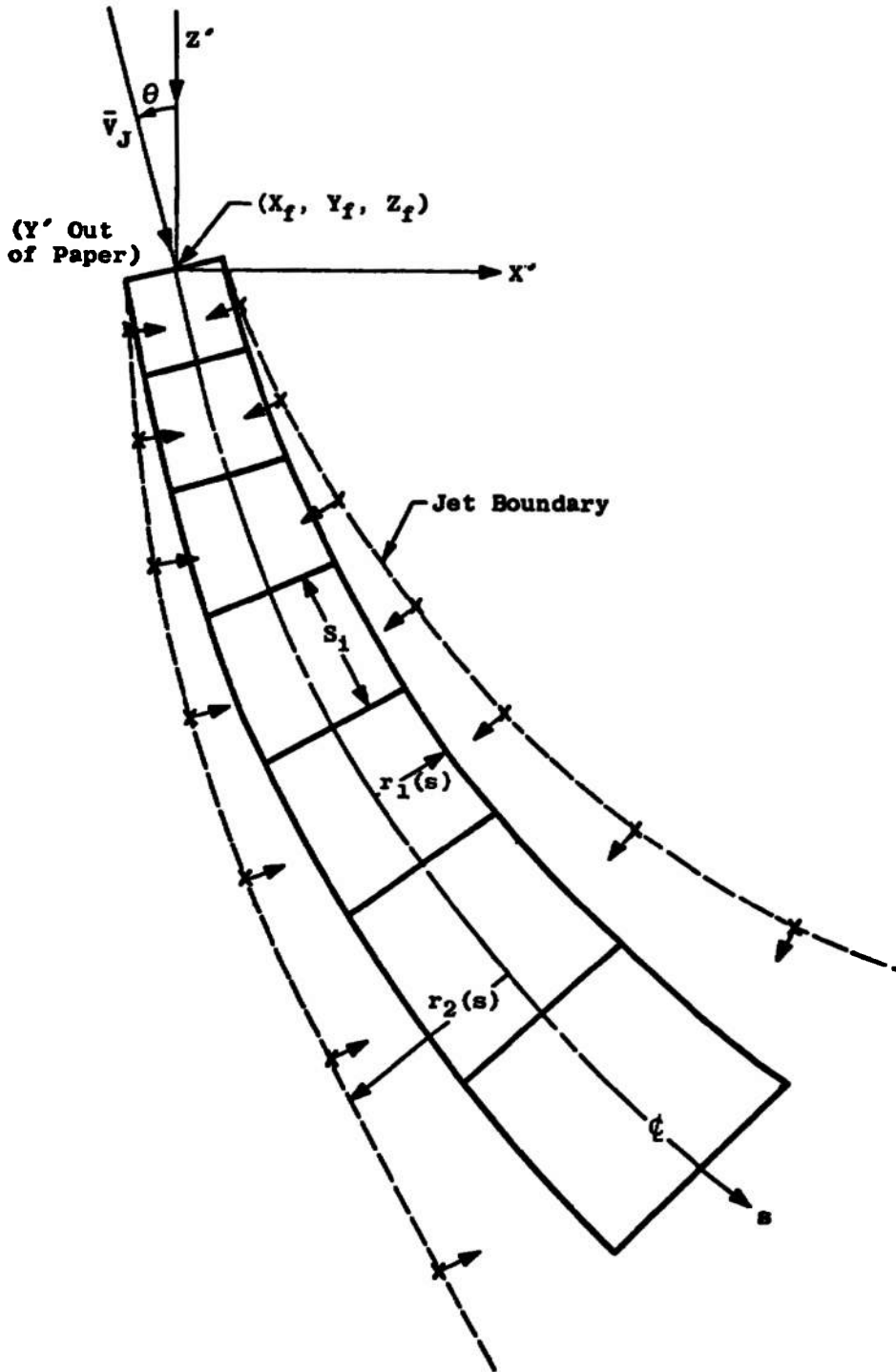
Fig. 18 Jet Tube Model Suggested by Fitch

Fig. 19 Model No. 1

Inlet Face - -Y
Wing Part 2

Inlet Face - +Y
Wing Part 1

Tube Half - -Y
Wing Part 4

Tube Half - +Y
Wing Part 3

Ring
Wing Part 5
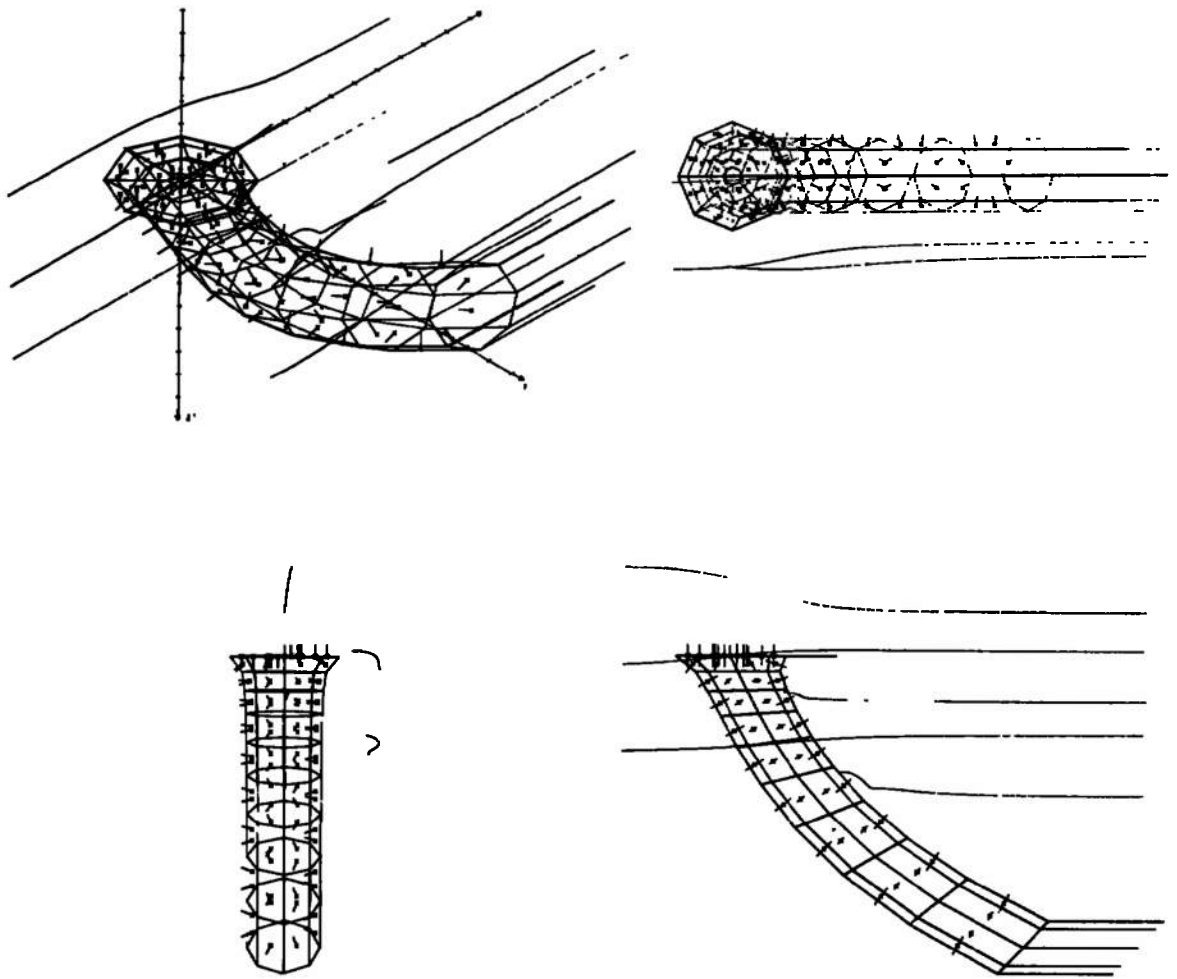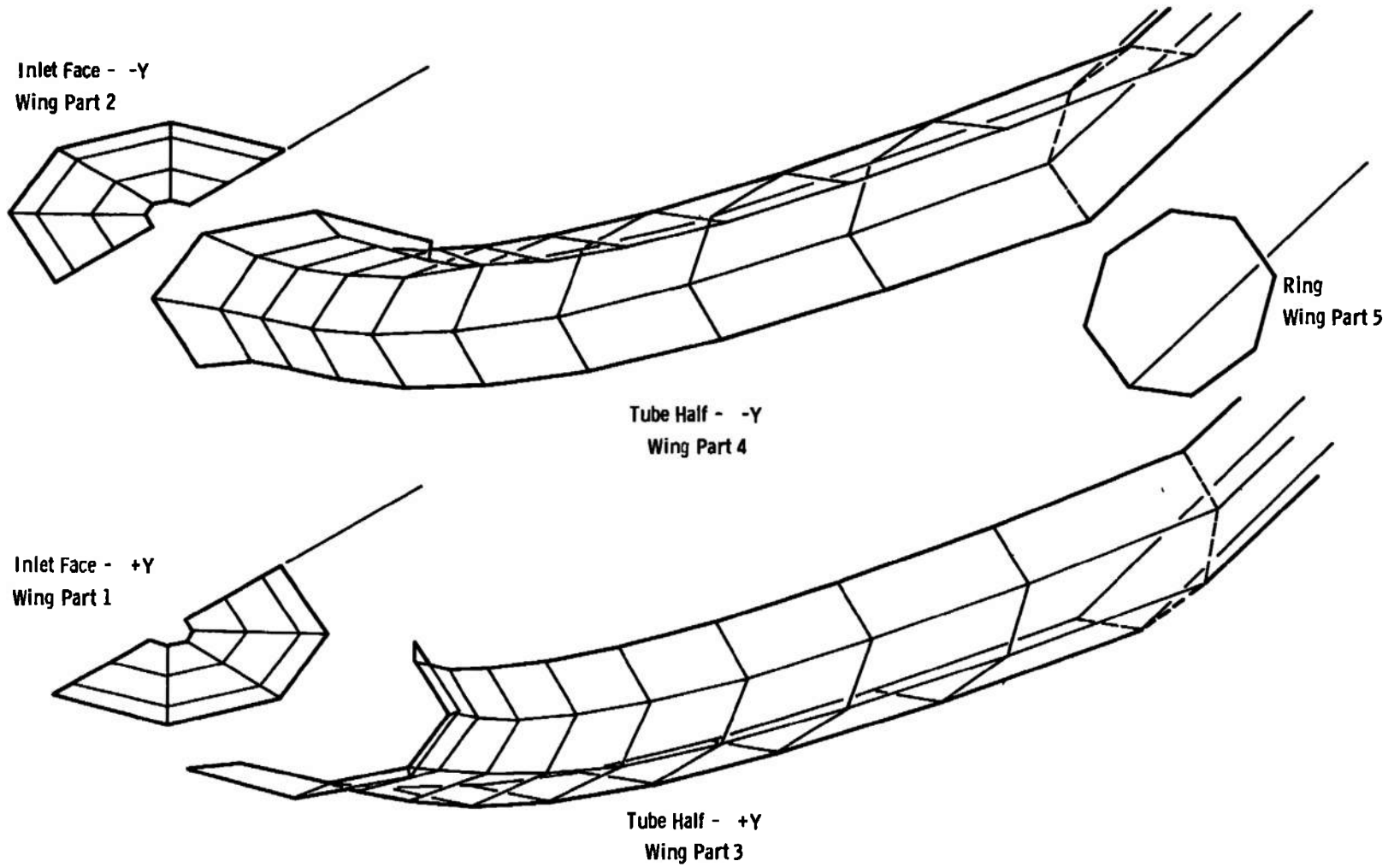
Fig. 20 Exploded View of Lattice Construction
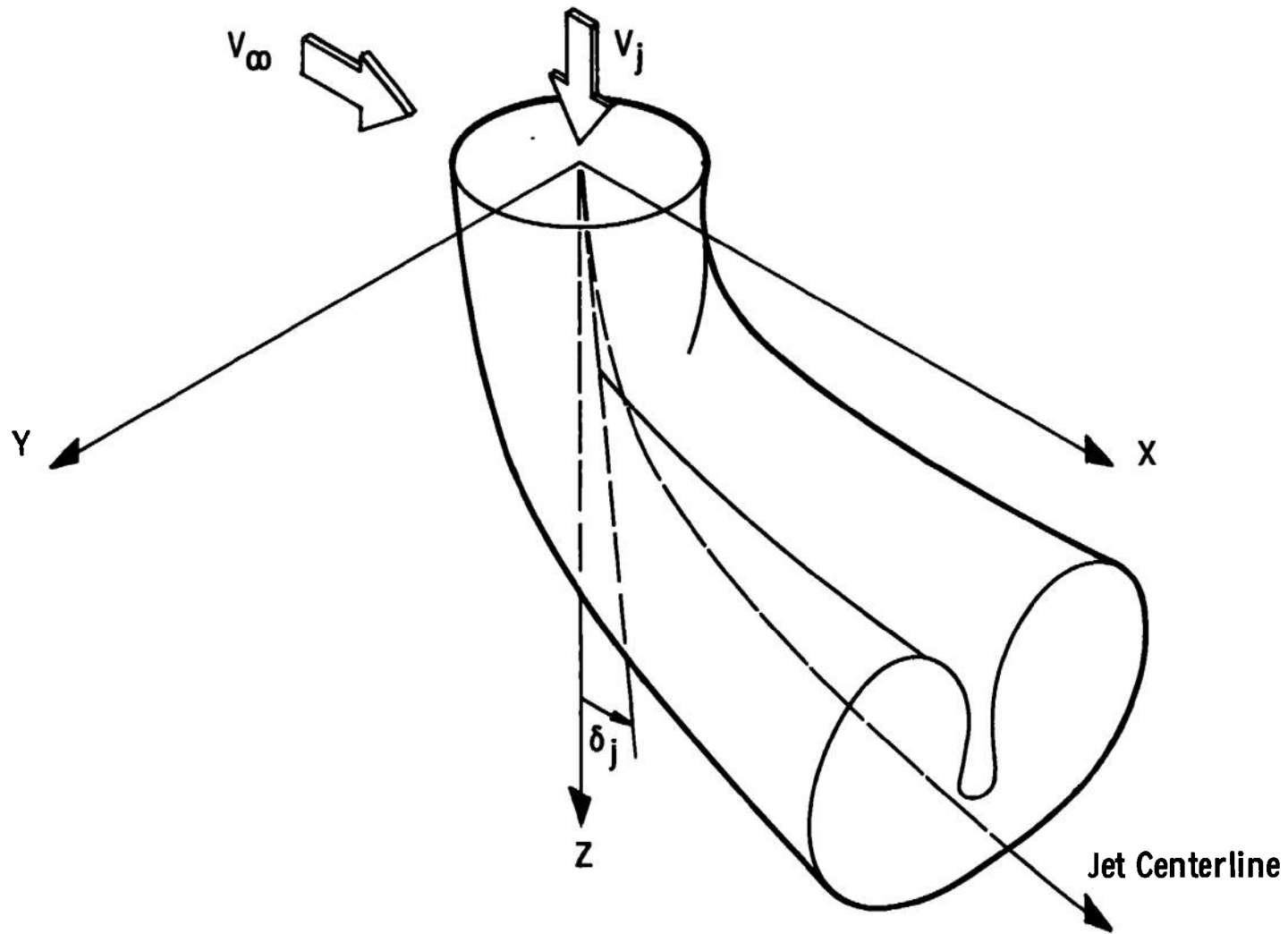
Fig. 21 Coordinate System
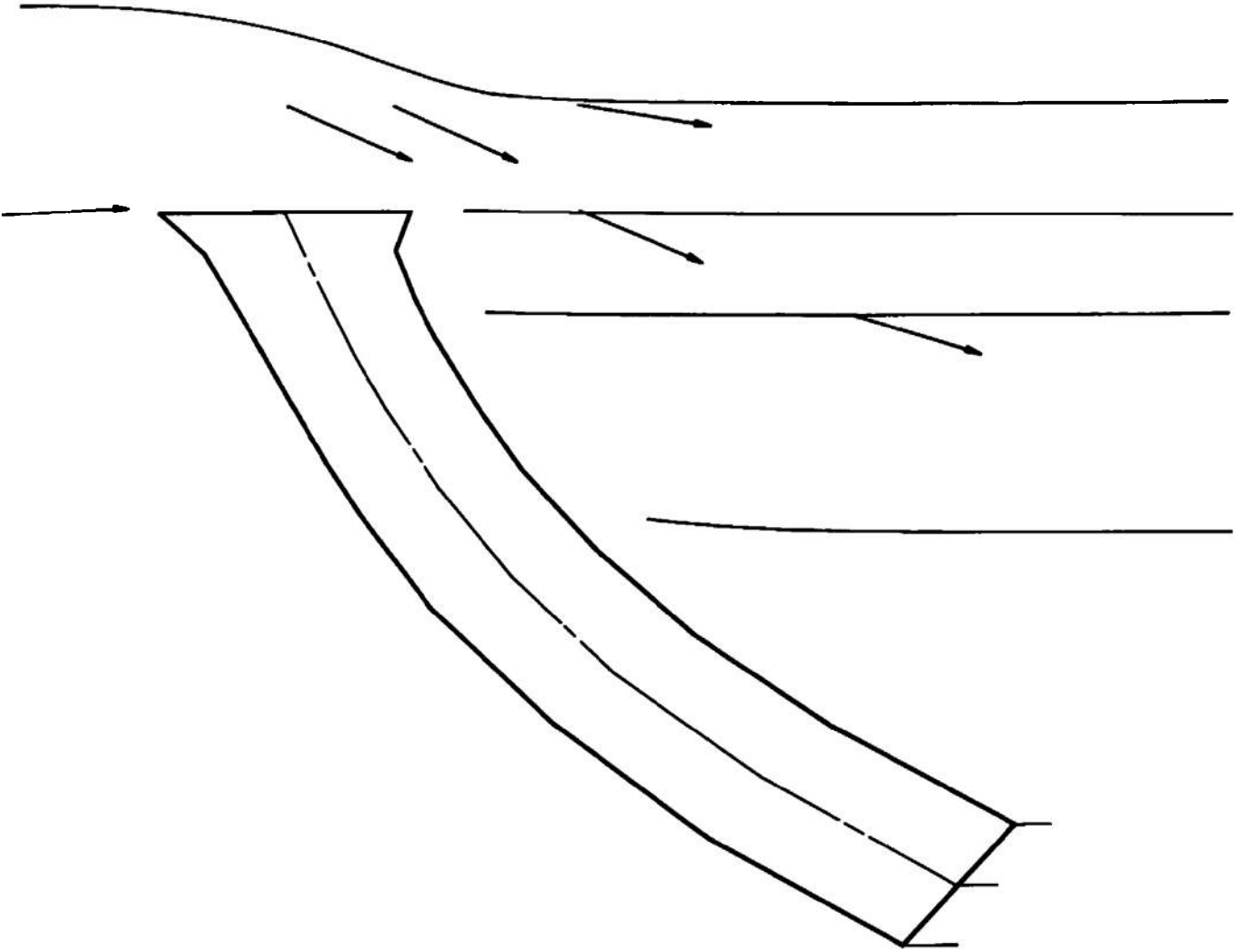
Fig. 22 Model No. 1—Analytical Streamlines, $K_{inlet} = 1.125$
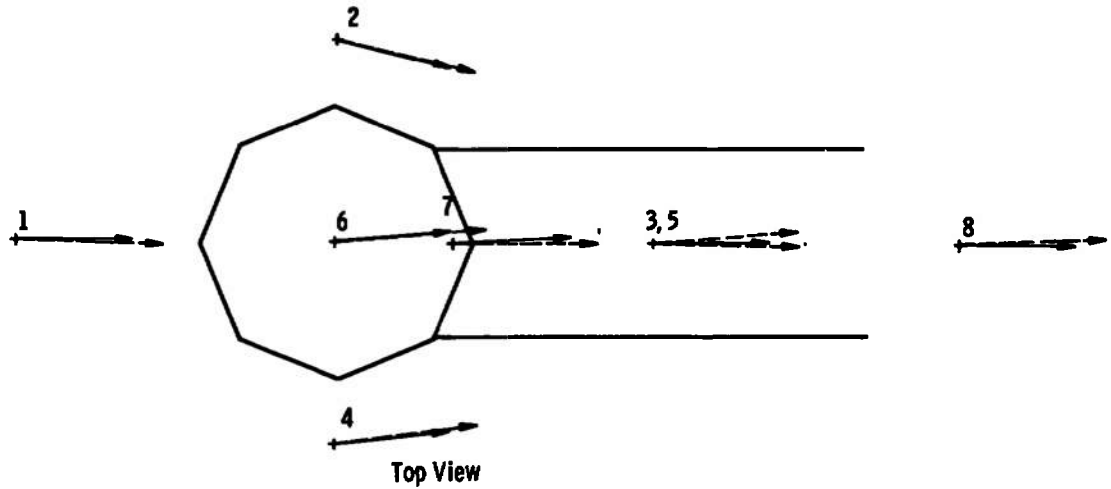
Point	Velocity	Pitch	Yaw
1	1.039	-3.20	-0.53
2	1.150	-11.94	14.04
3	0.853	1.42	-0.45
4	1.155	-9.45	-6.27
5	0.890	3.40	-0.39
6	1.310	30.11	-5.82
7	0.885	33.57	-3.73
8	0.965	0.22	-0.06
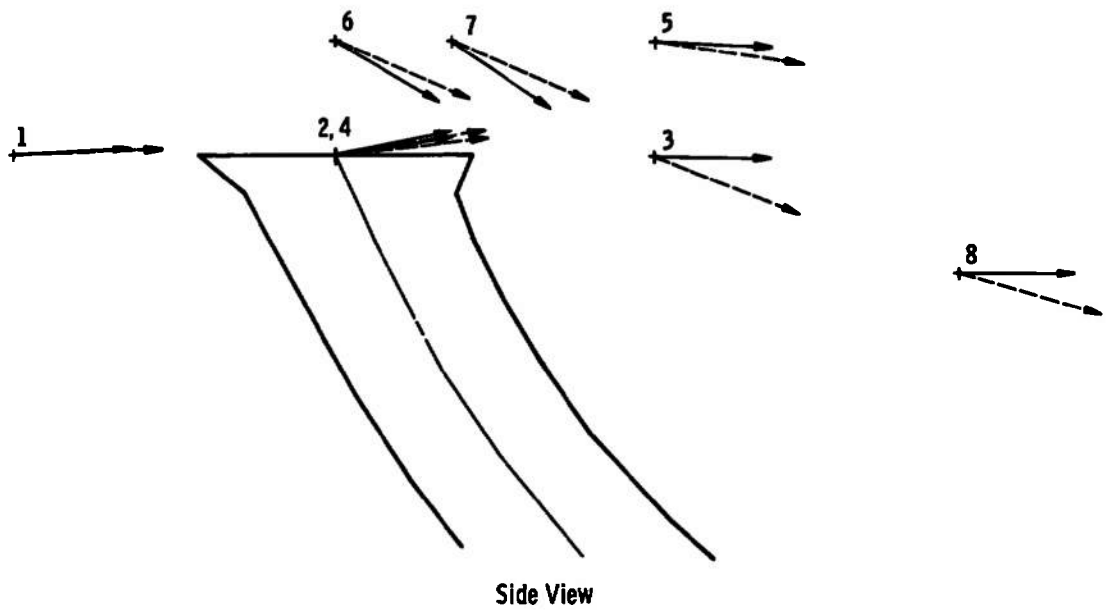
Fig. 23 Model No. 1—Comparison of Analytical and Experimental Flow Directions, K_{inlet} = 1.125

49

Lifting Body

Warped Delta Wing

Cascade of High Lift Wings
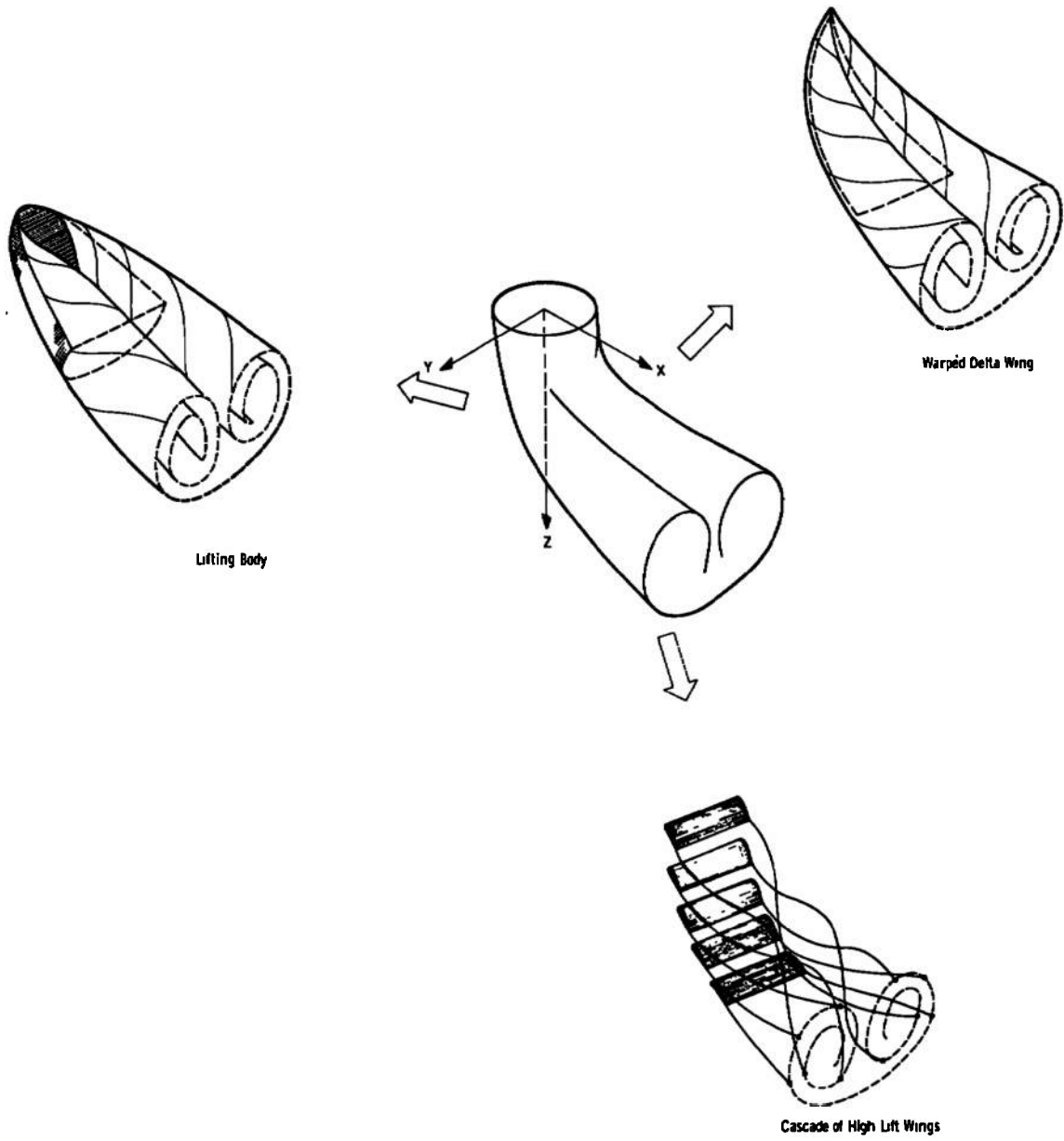
Fig. 24 Aerodynamic Configurations Which Generate Flow Fields
Similar to a Jet in a Crossflow

Fig. 25 Model No. 2

Wing Parts 3 and 4 -
Inlet (Not Shown)

Wing Parts 7 and 8

Wing Parts 1 and 2

Wing Part 9
Ring (Not Shown)

Wing Parts 5 and 6

Wing Parts 10 and 11
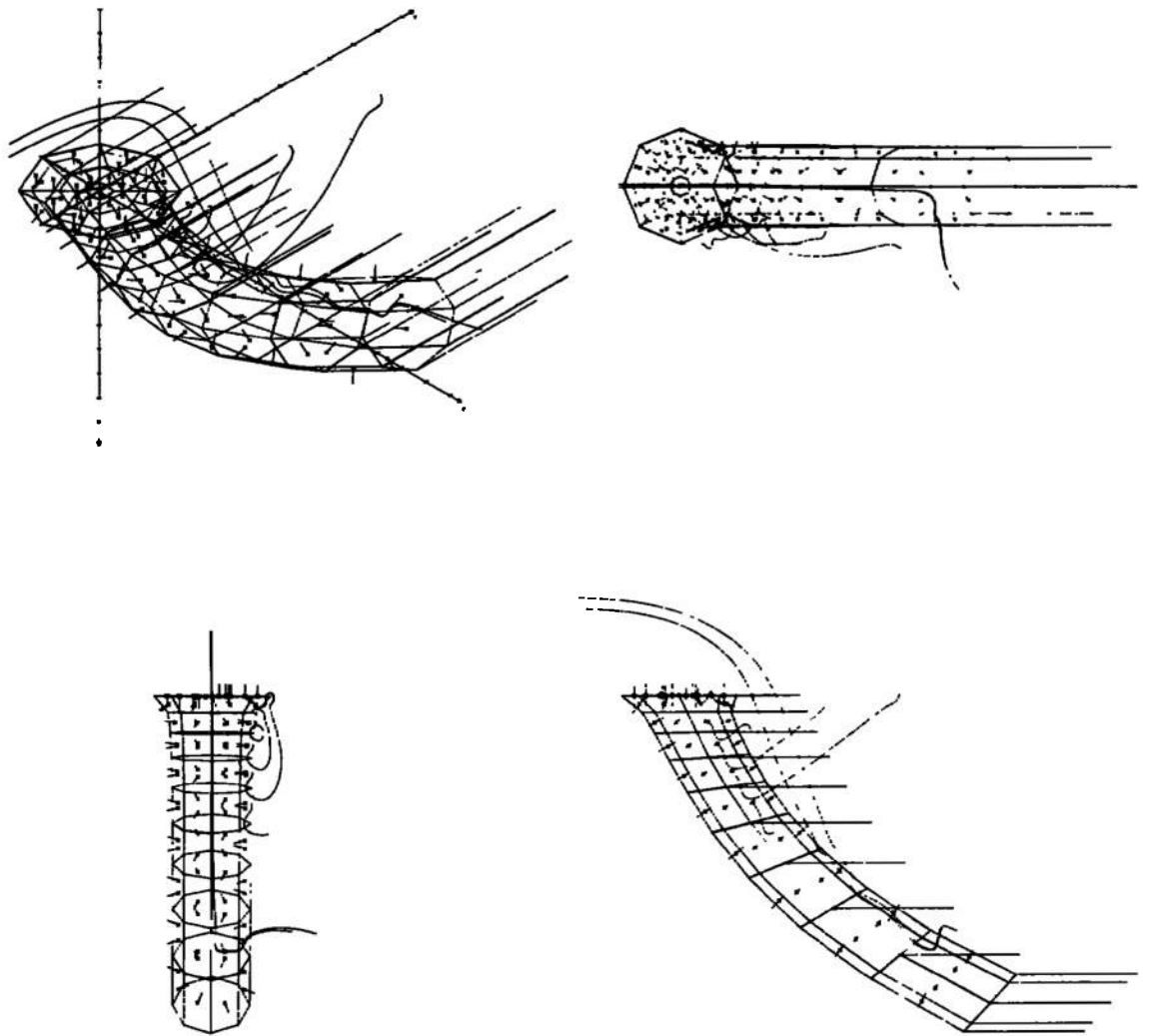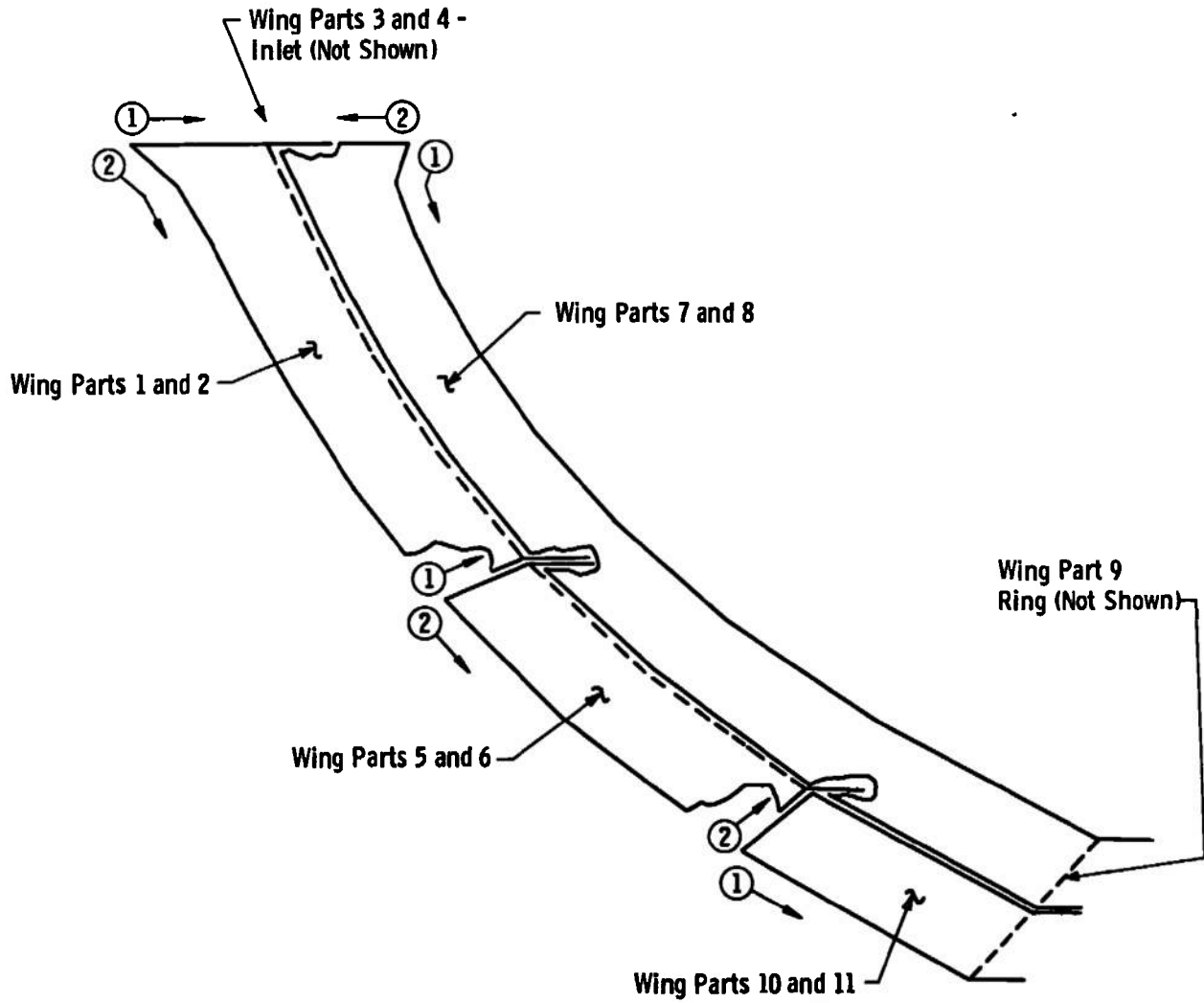
Fig. 26   Schematic of Model No. 2 Wing Part Layout
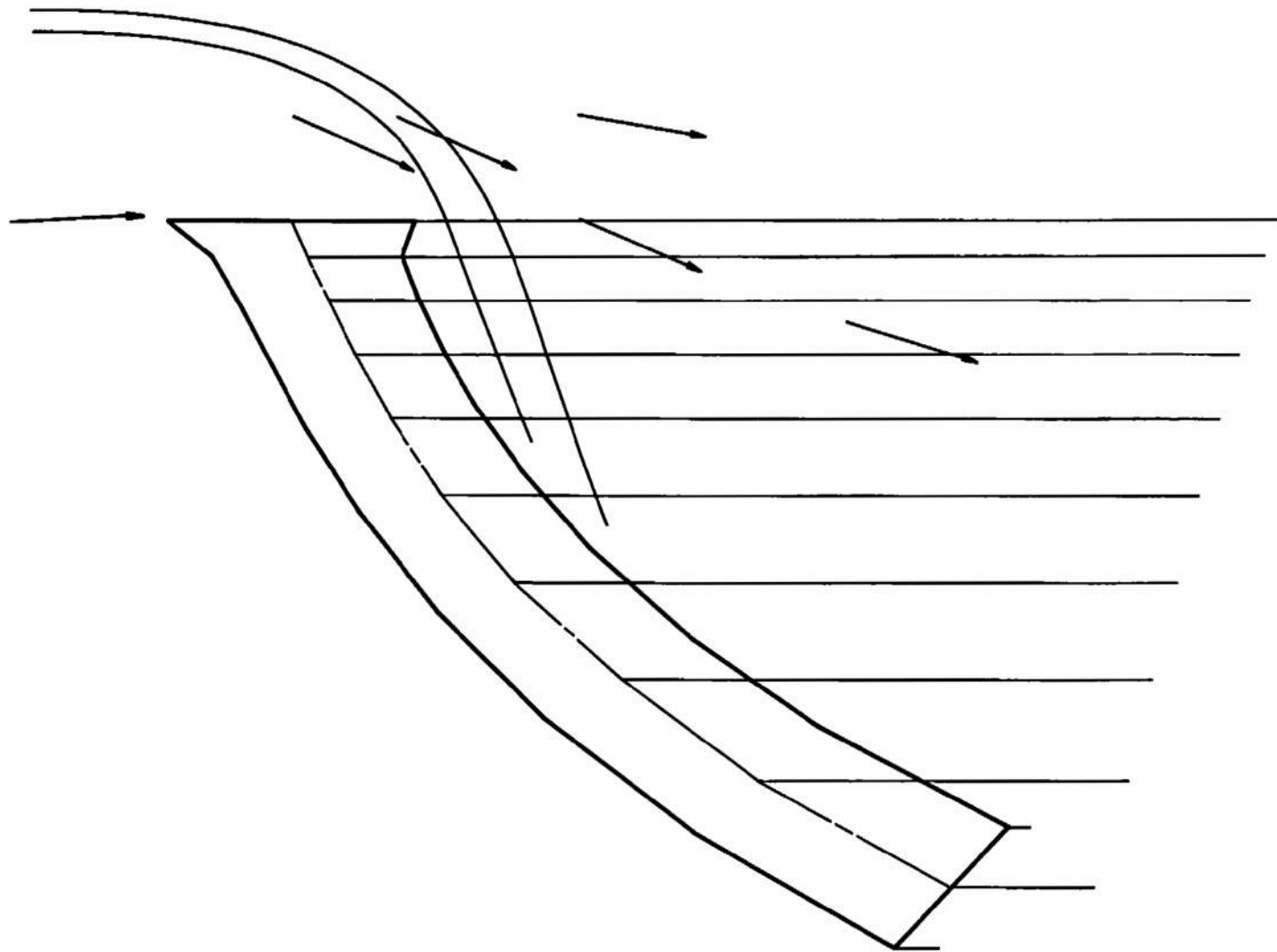
Fig. 27 Model No. 2—Analytical Streamlines, K_{inlet} = 1.125

Top View

Point	Velocity	Pitch	Yaw
1	1.091	-6.60	-0.43
2	1.426	-20.92	18.24
3	2.616	65.27	4.59
4	1.376	-22.91	-15.21
5	1.483	43.38	0.59
6	1.726	30.15	-2.23
7	1.608	41.06	-0.74
8	3.899	75.37	1.24

Key

- - - → Experimental Flow Direction

———→ Analytical Flow Direction

Side View
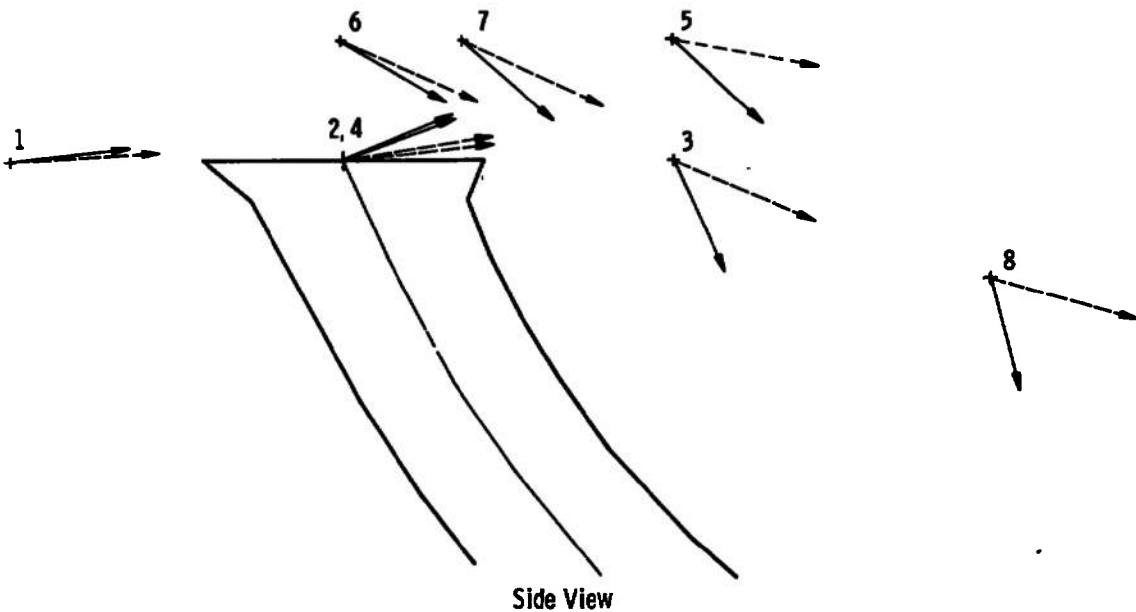
Fig. 28 Model No. 2—Comparison of Analytical and Experimental Flow Directions, K_{inlet} = 1.125
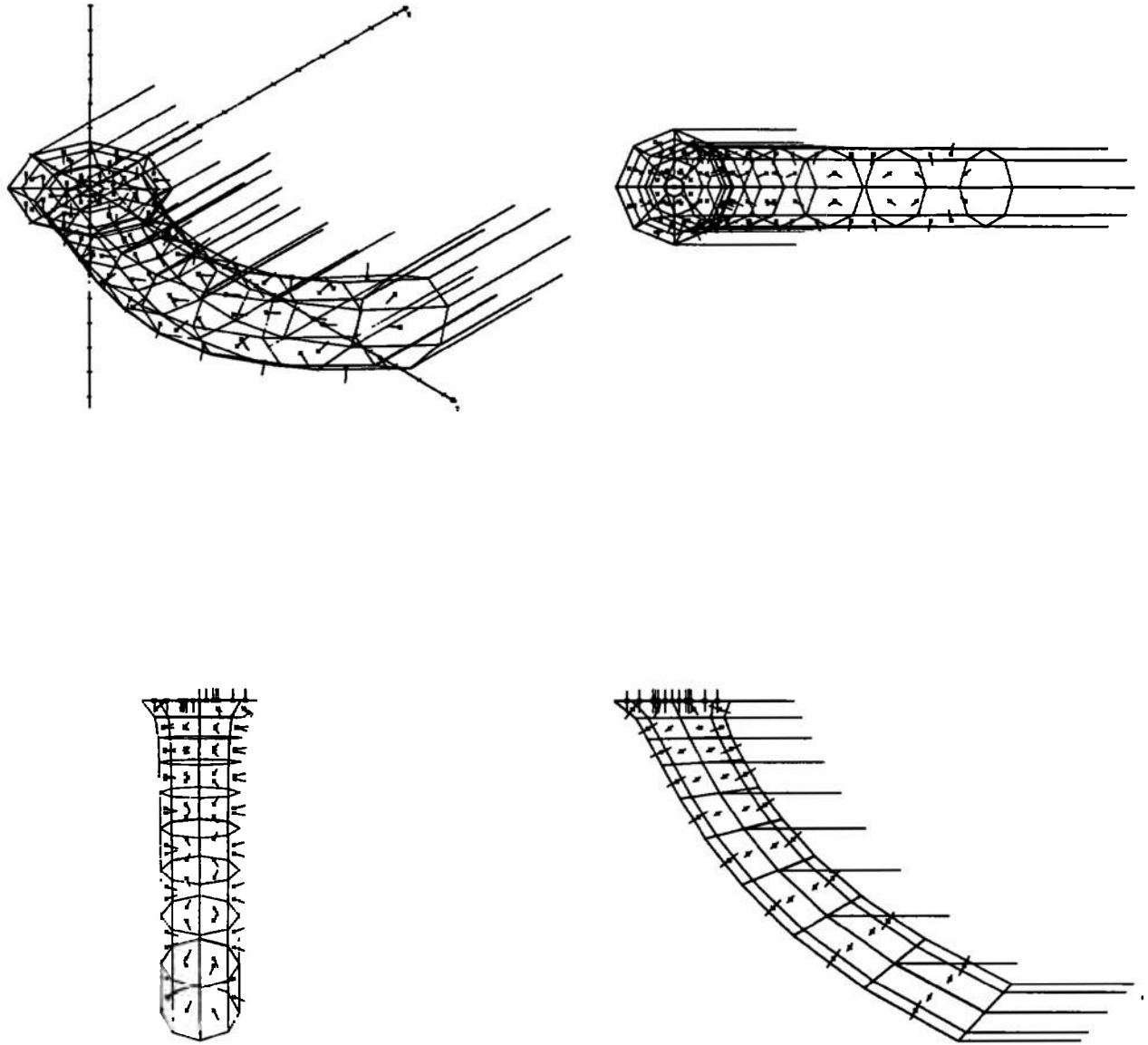
Fig. 29 Model No. 2a
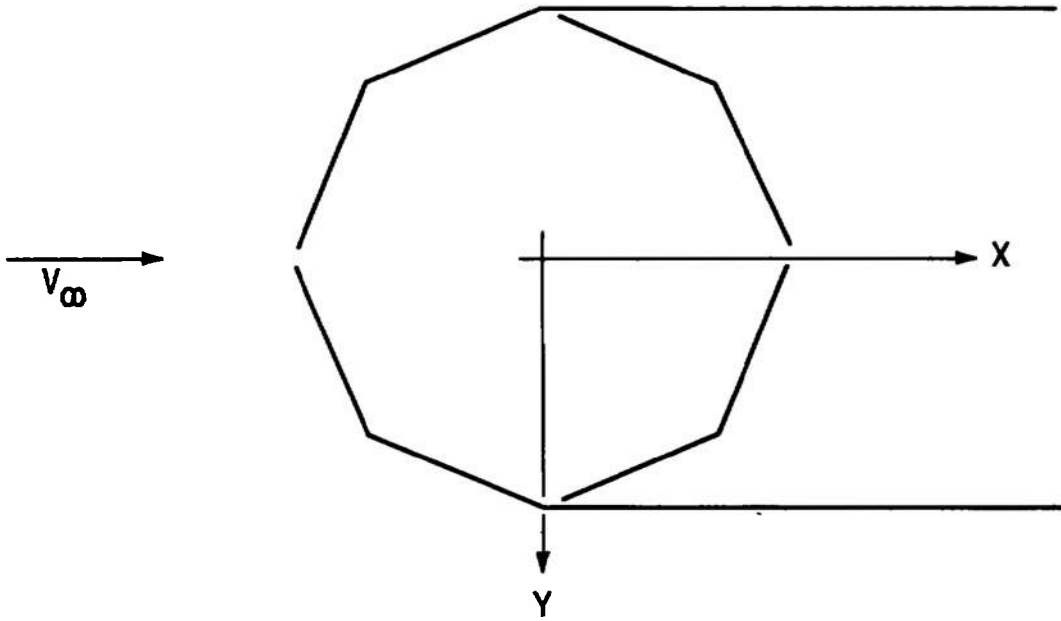
Model No. 2 – Trailing Vorticity from Upstream Half of Tube
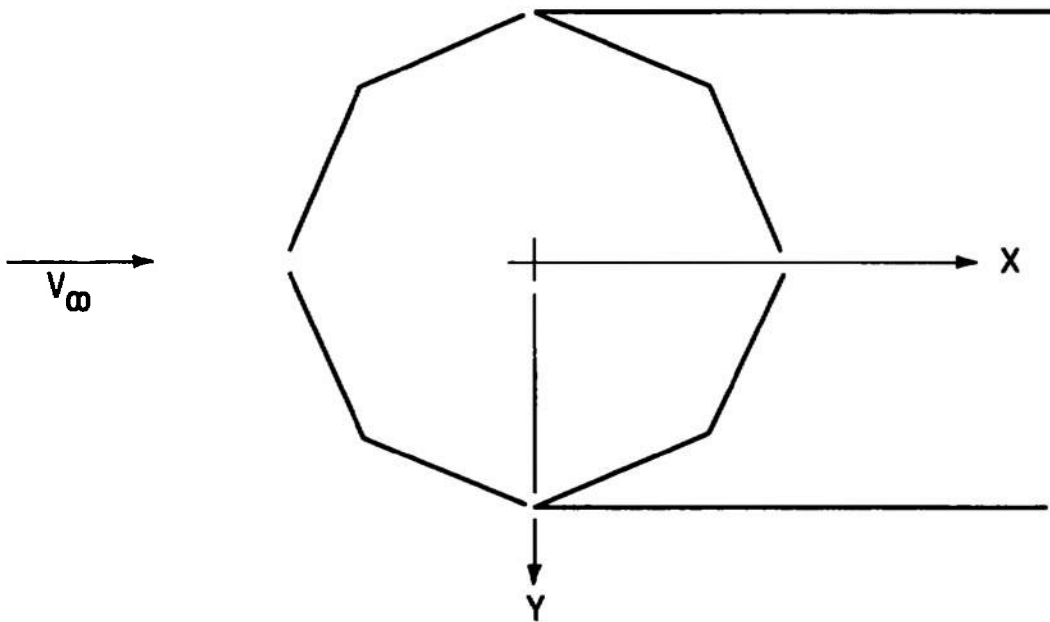
Model No. 2a – Trailing Vorticity from Downstream Half of Tube

Fig. 30 Schematic Showing Origin of Trailing Vortices
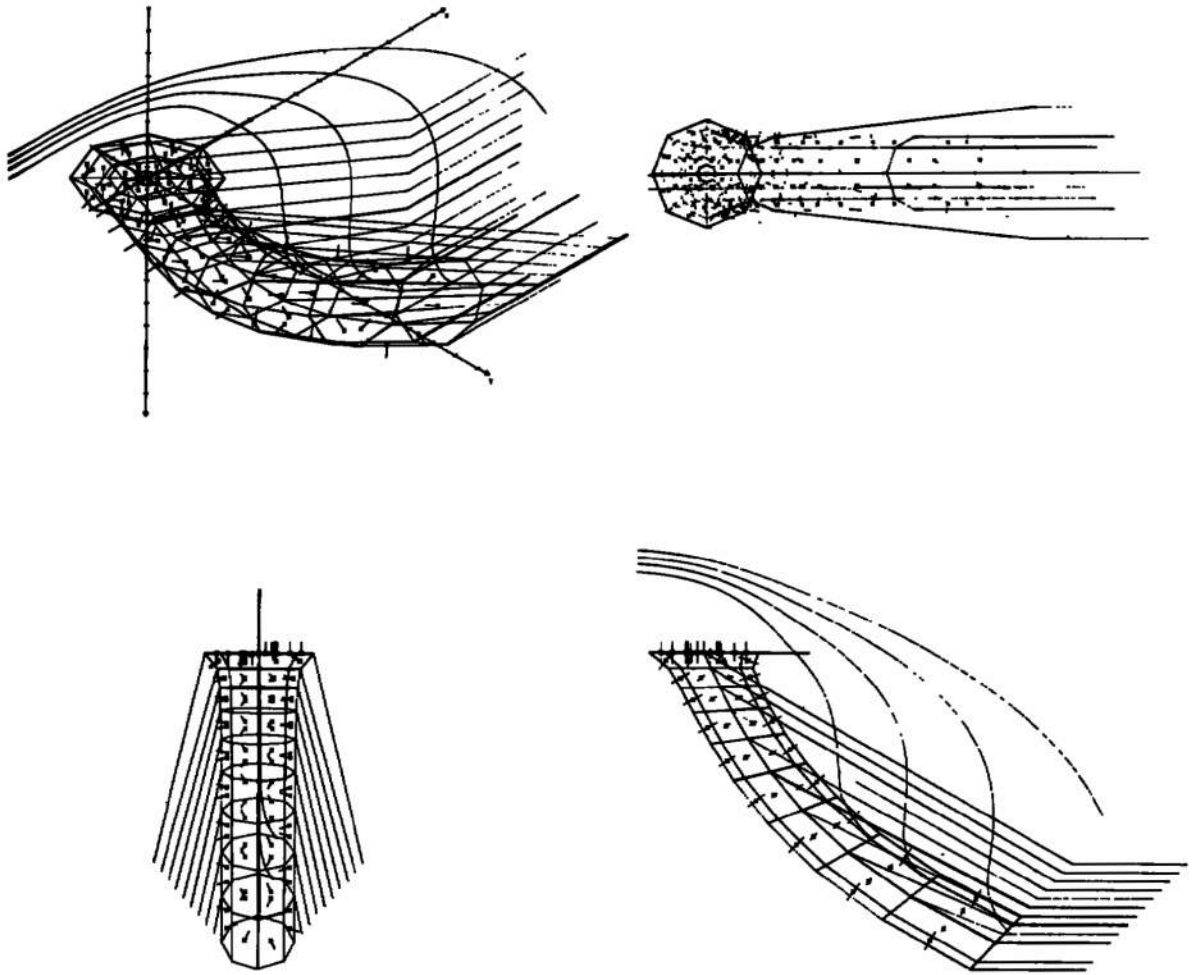
Fig. 31 Model No. 3
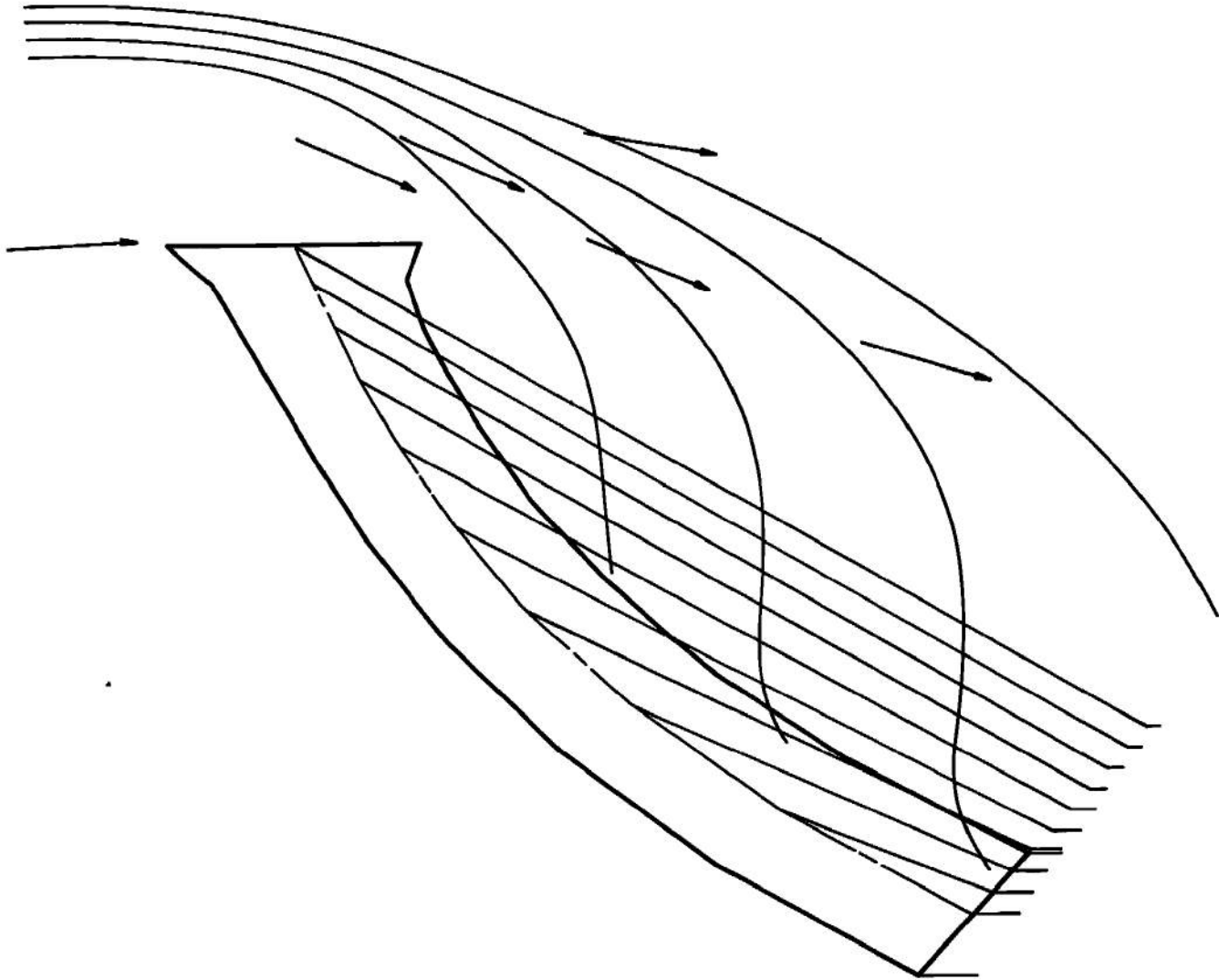
Fig. 32 Model No. 3—Analytical Streamlines, K_{inlet} = 1.125
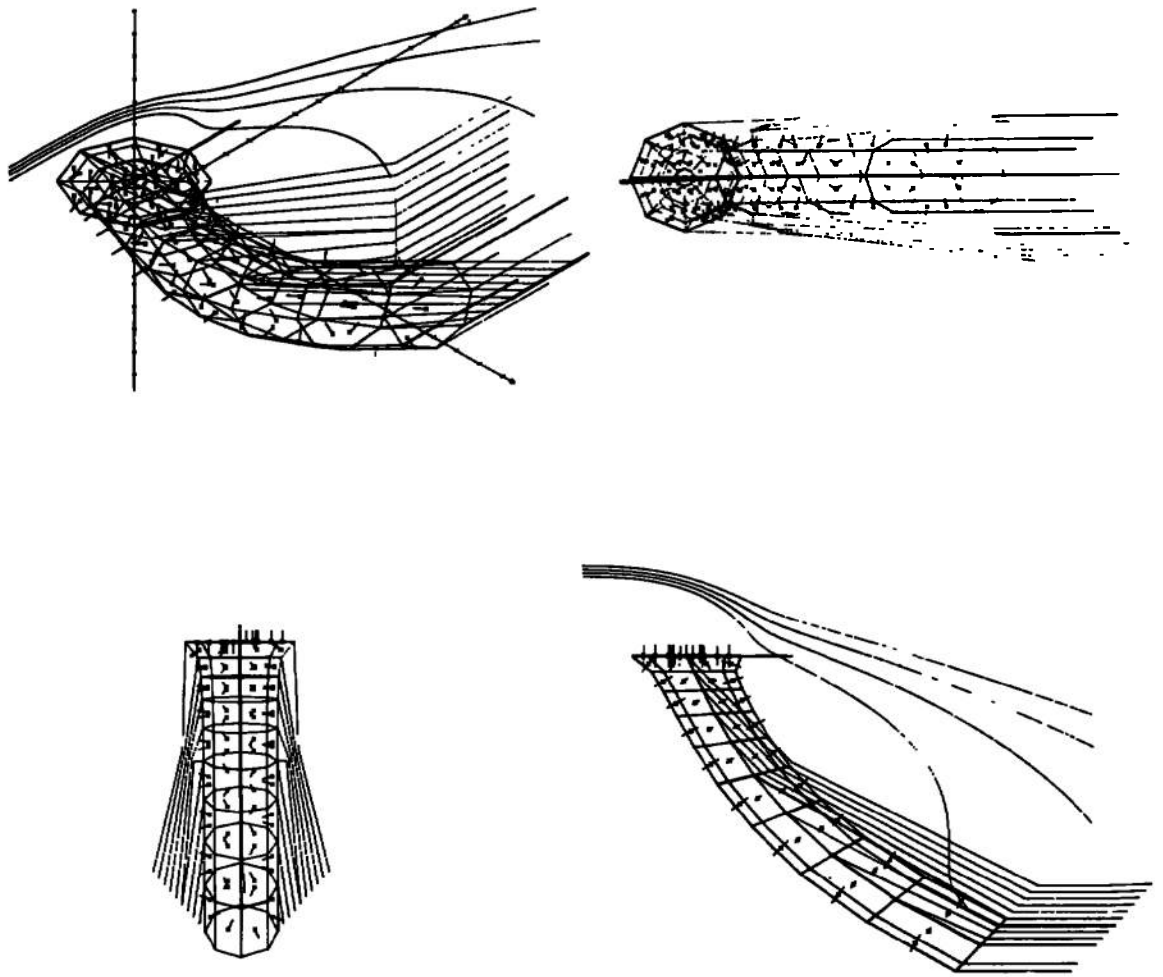
Fig. 33 Model No. 4
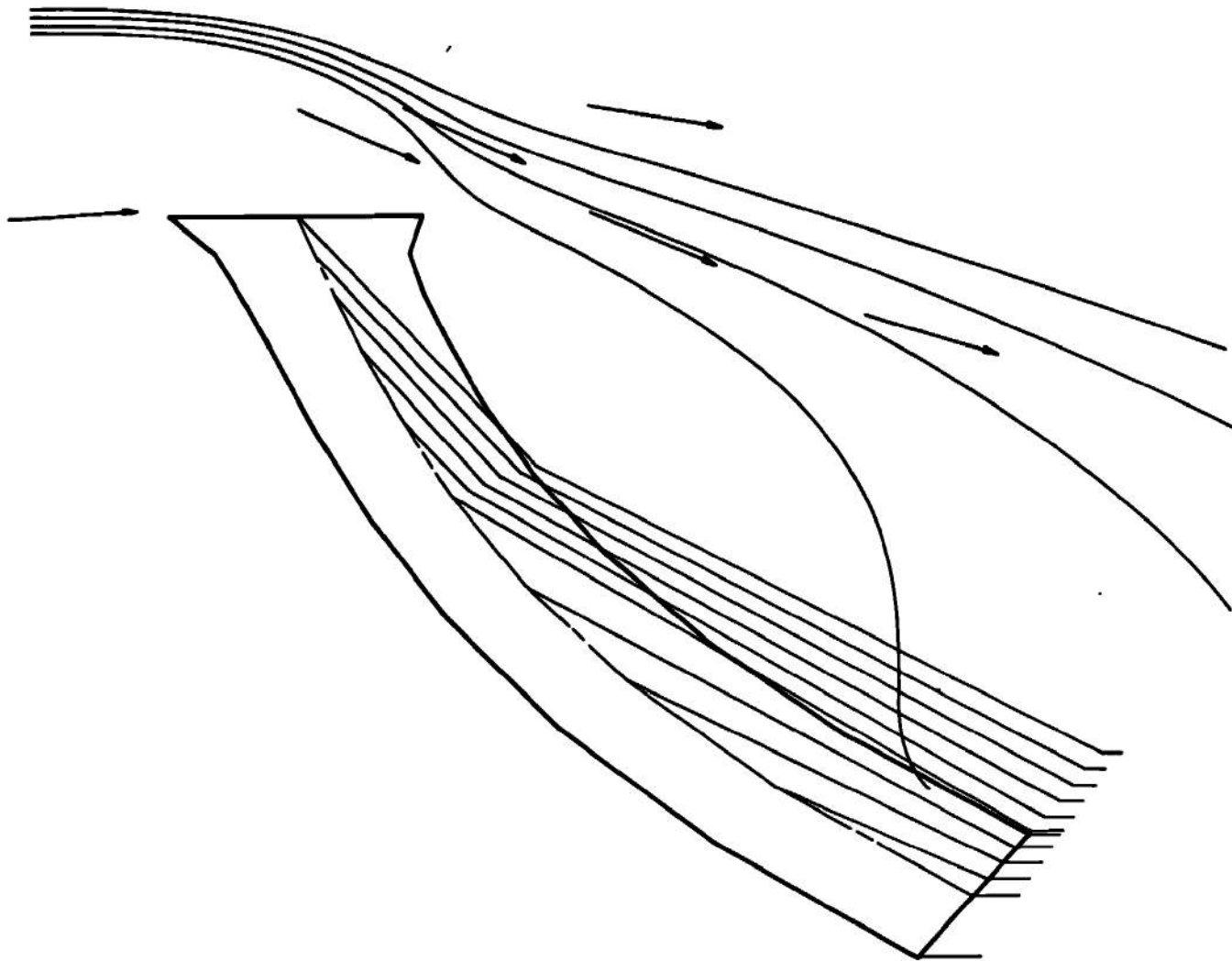
Fig. 34 Model No. 4—Analytical Streamlines, K_{inlet} = 1.125

Top View

Point	Velocity	Pitch	Yaw
1	1.055	-6.47	-0.38
2	1.354	-17.87	13.11
3	0.993	22.71	0.07
4	1.379	-18.02	-9.69
5	0.997	14.49	-0.12
6	1.459	30.64	-2.72
7	1.072	35.65	-1.65
8	1.053	27.28	-0.04

Key

— — ➤ Experimental Flow Direction

——➤ Analytical Flow Direction

Side View
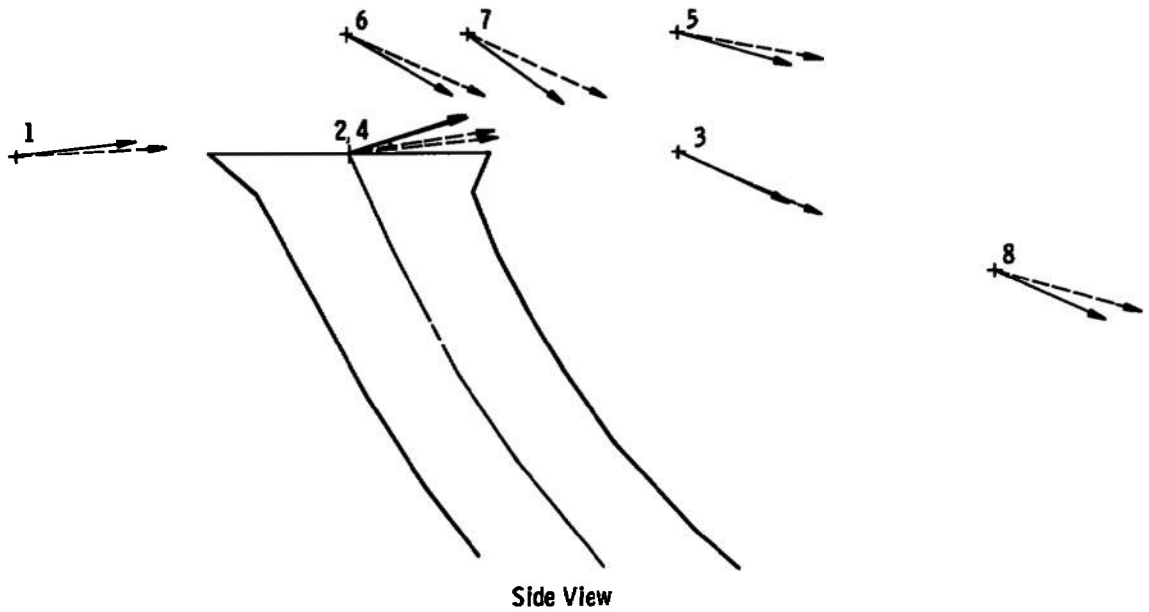
Fig. 35 Model No. 4—Comparison of Analytical and Experimental Flow Directions, K_{inlet} = 1.125
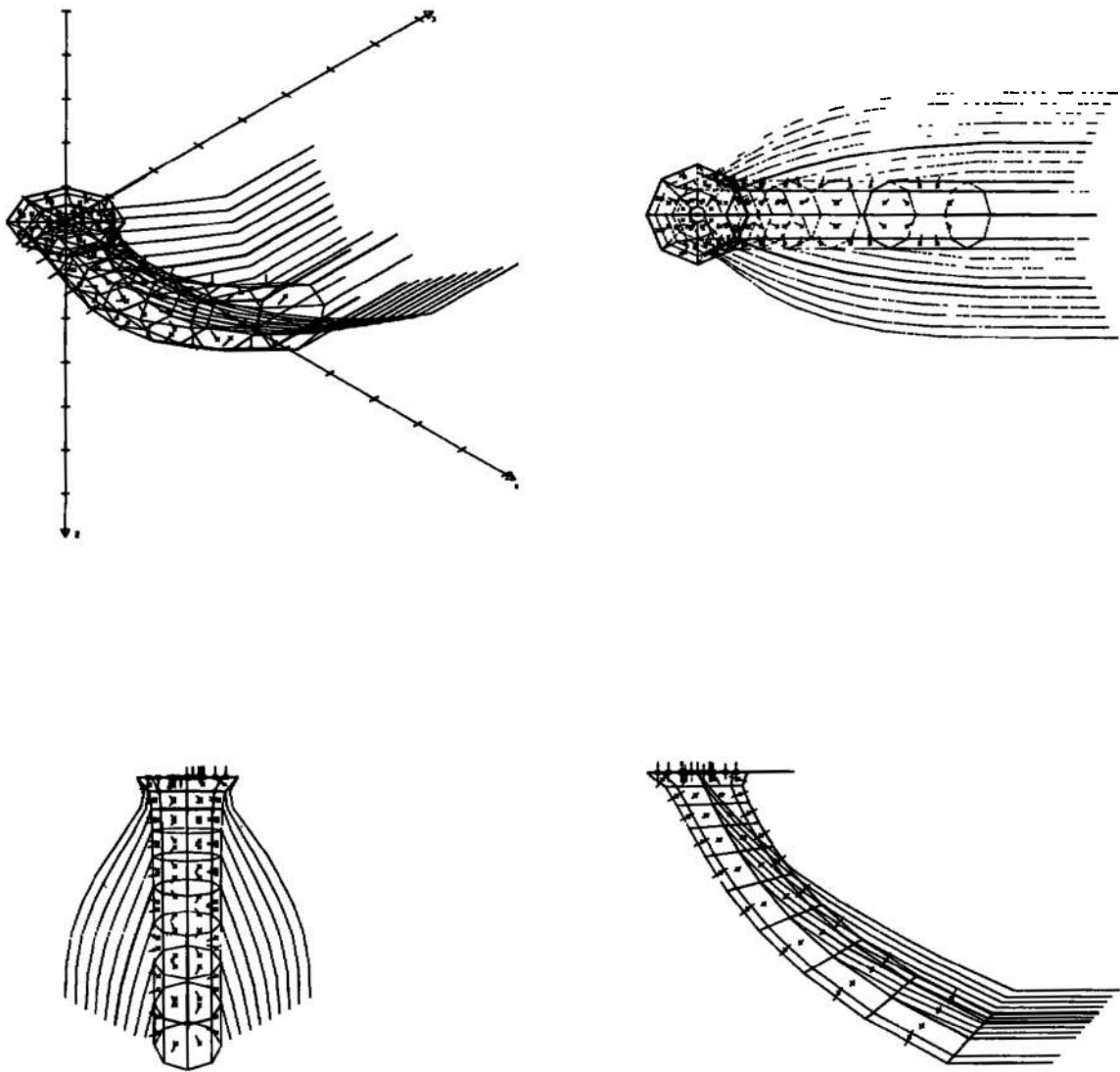
Fig. 36 Model No. 5
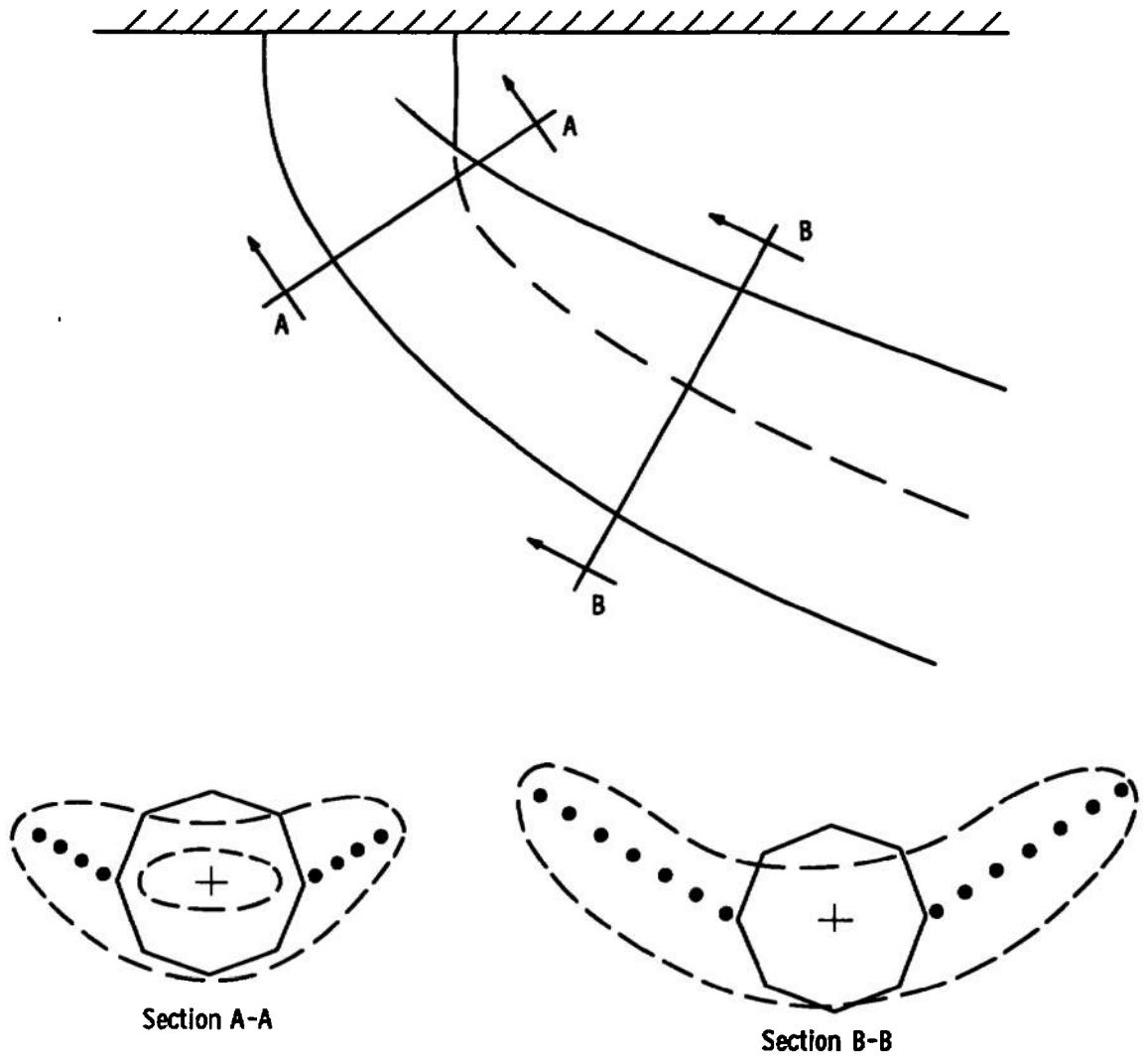
Fig. 37 Trailing Sheet Vortex Positions for Model No. 5
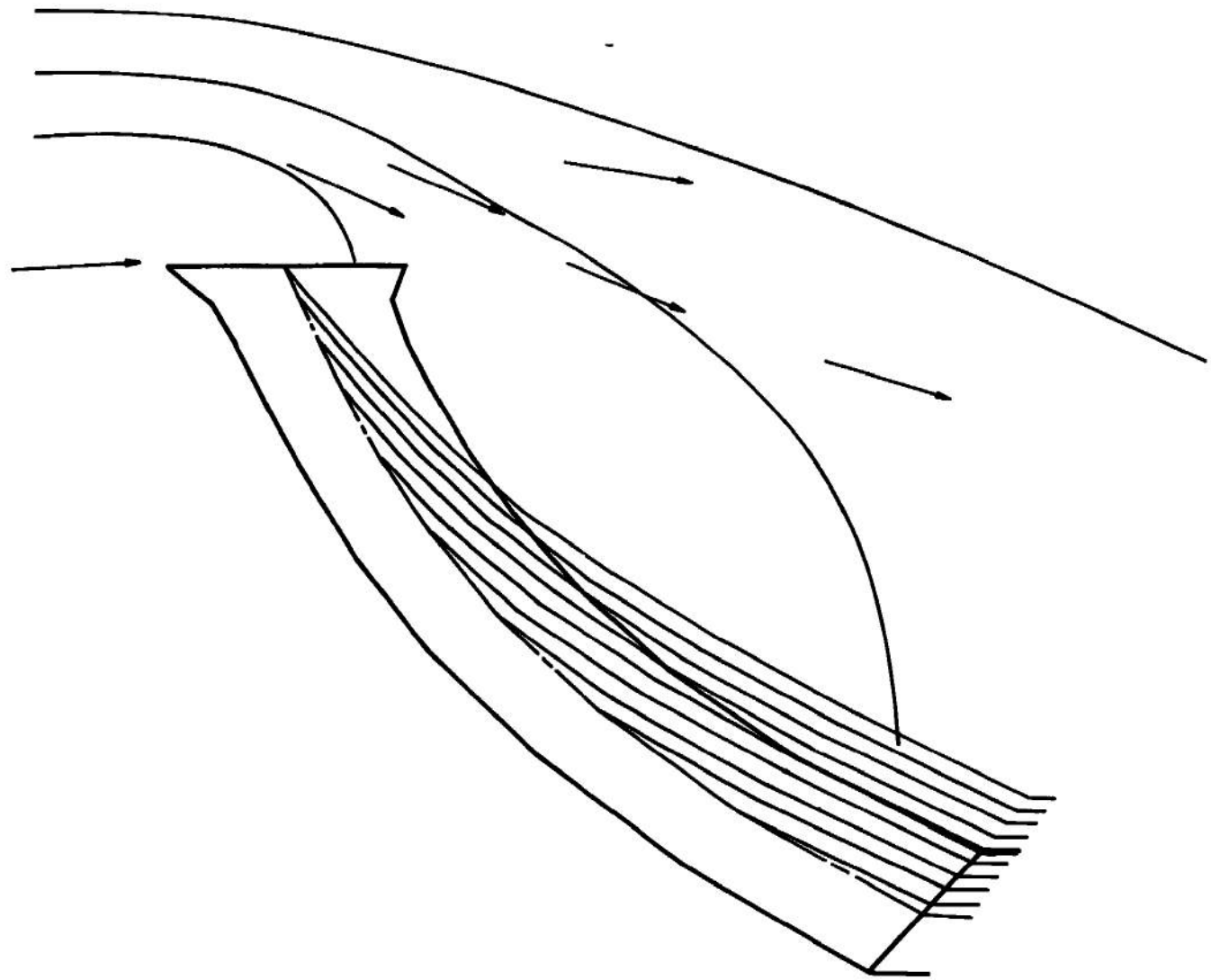
Fig. 38   Model No. 5—Analytical Streamlines, K_{inlet} = 1.125

Point	Velocity	Pitch	Yaw
1	1.081	-9.00	-0.37
2	1.534	-17.33	12.84
3	1.187	33.40	0.24
4	1.533	-17.10	-9.81
5	1.120	21.89	-0.04
6	1.574	28.94	-2.58
7	1.240	35.11	-1.60
8	1.147	39.32	0.34
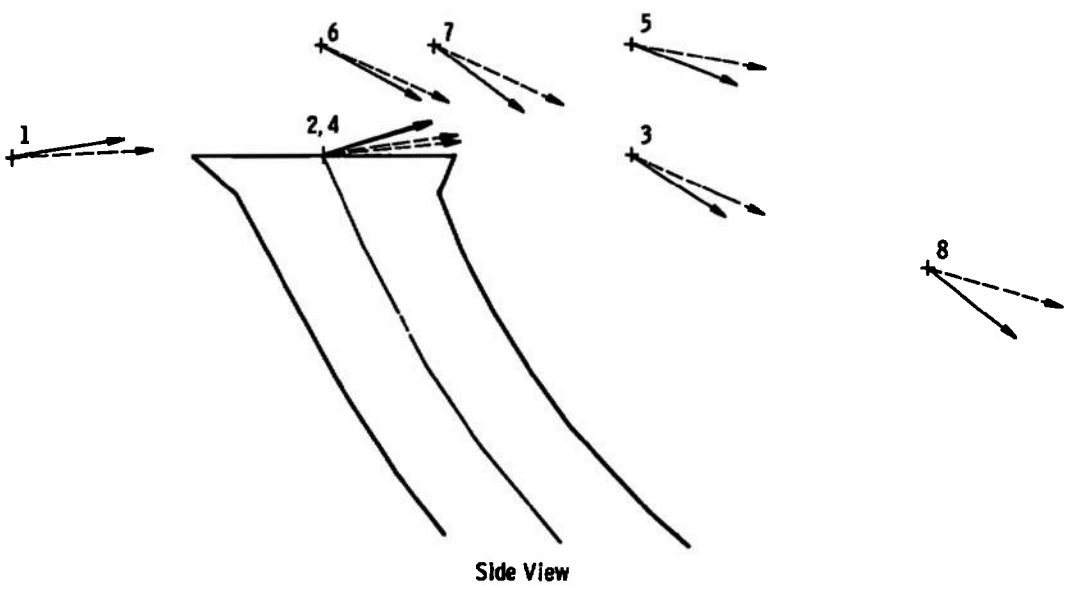
Fig. 39 Model No. 5—Comparison of Analytical and Experimental Flow Directions, K_{Inlet} = 1.125

Top View
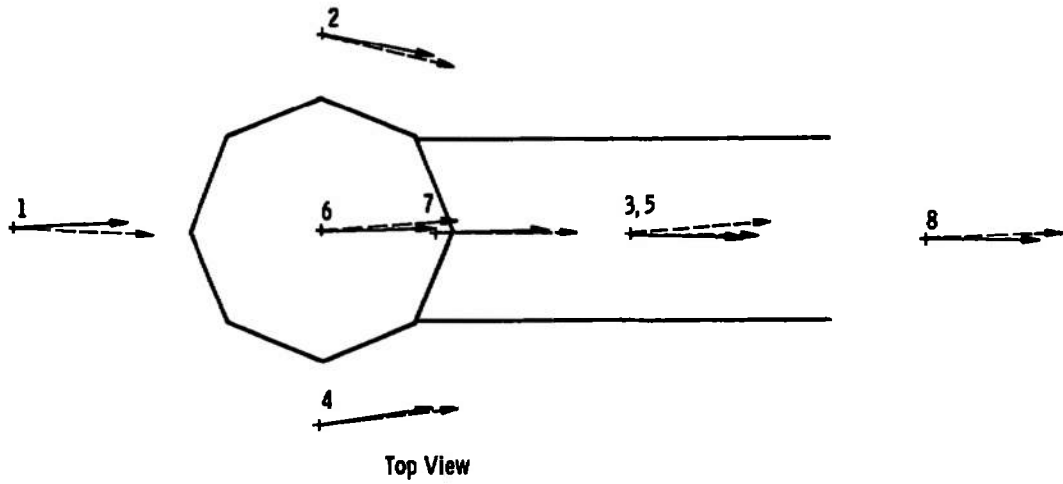
Key
--- → Experimental Flow Direction
—— → Analytical Flow Direction

Point	Velocity	Pitch	Yaw
1	1.067	-8.24	-0.33
2	1.479	-16.14	11.67
3	1.146	30.85	0.22
4	1.478	-15.94	-8.91
5	1.099	20.01	-0.04
6	1.503	26.82	-2.35
7	1.203	32.19	-1.42
8	1.105	35.72	0.30

Side View
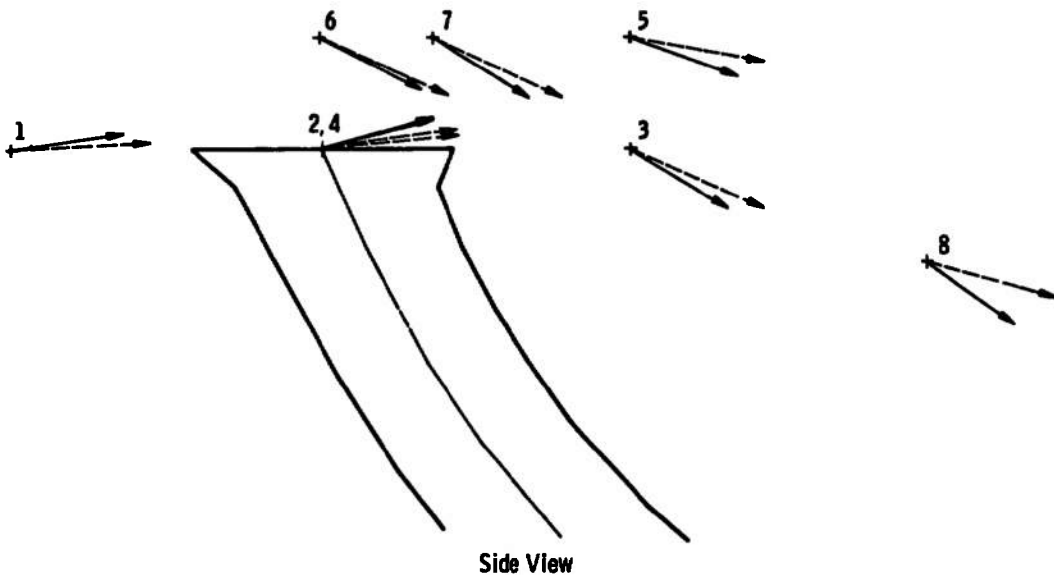
Fig. 40 Model No. 5—Comparison of Analytical and Experimental Flow Directions, $K_{Inlet} = 1.0$

Top View

Point	Velocity	Pitch	Yaw
1	1.112	-8.67	-0.33
2	1.495	-17.11	13.26
3	1.204	33.89	-0.05
4	1.481	-16.14	-10.64
5	1.229	21.91	-0.15
6	1.552	29.58	-2.70
7	1.219	35.89	-1.76
8	0.980	42.27	-0.12

Key

‒ ‒ ‒→ Experimental Flow Direction

——→ Analytical Flow Direction

Side View

Fig. 41 Model No. 6—Comparison of Analytical and Experimental Flow Directions, K_{inlet} = 1.125

Point	Velocity	Pitch	Yaw
1	1.013	-4.88	-0.14
2	1.257	-10.06	6.42
3	1.001	18.36	-0.02
4	1.255	-9.54	-5.07
5	1.017	11.45	-0.05
6	1.238	16.13	-1.26
7	1.080	19.07	-0.56
8	0.969	18.51	0.04
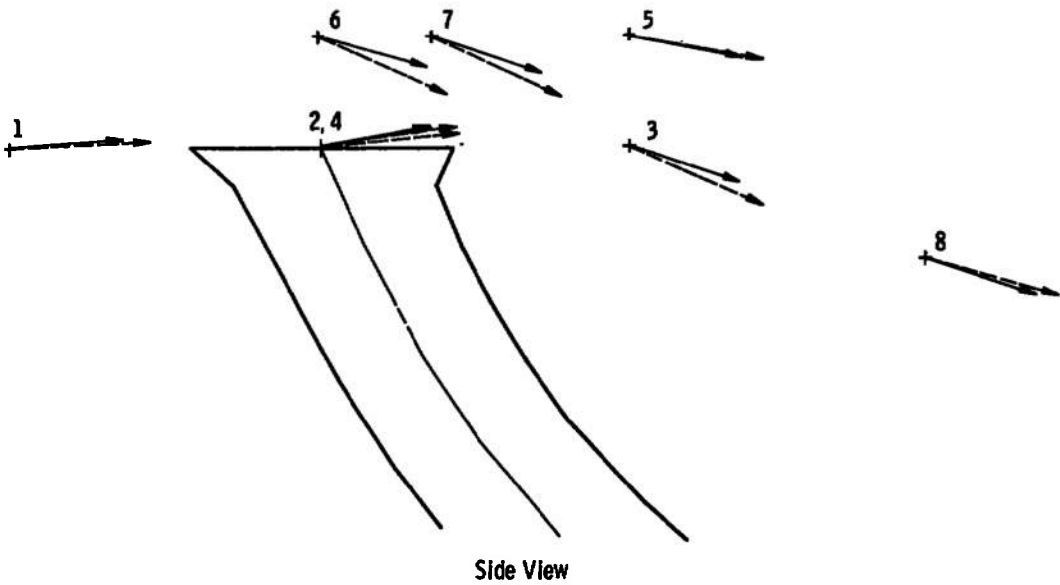
Fig. 42 Model No. 6—Comparison of Analytical and Experimental Flow
Directions, K_{inlet} = 0.5

Point	Velocity	Pitch	Yaw
1	1.111	-8.82	-0.37
2	1.508	-17.49	13.04
3	1.210	34.59	-0.03
4	1.508	-17.38	-10.01
5	1.242	22.40	-0.13
6	1.562	29.50	-2.68
7	1.234	36.04	-1.64
8	0.981	43.12	0.10
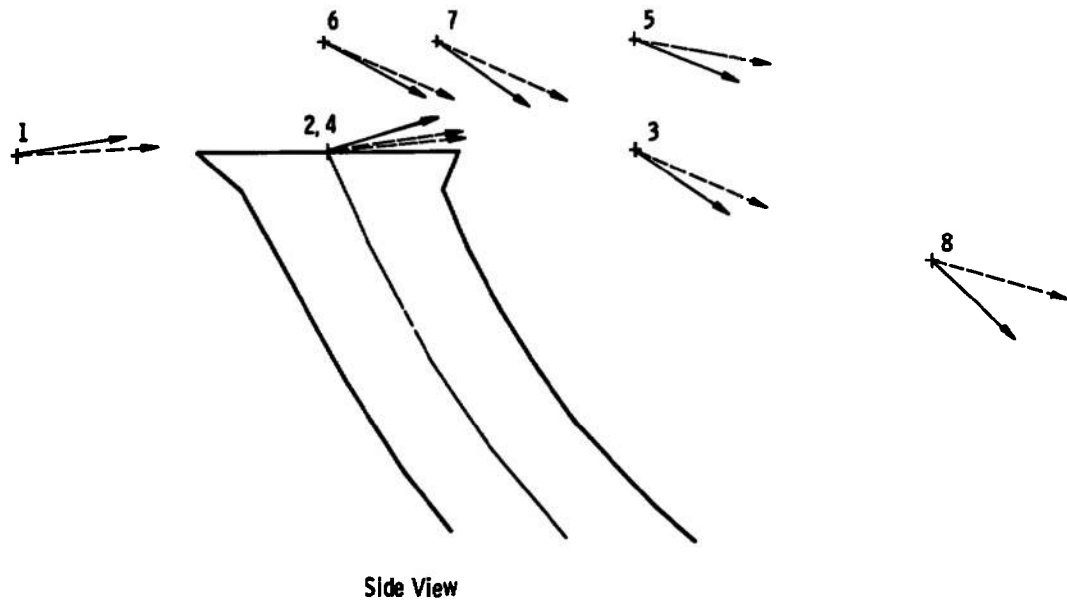
Fig. 43 Model No. 7—Comparison of Analytical and Experimental Flow Directions, K_{inlet} = 1.125

Top View

Point	Velocity	Pitch	Yaw
1	1.029	-6.09	-0.23
2	1.331	-12.67	8.27
3	1.039	23.39	0.15
4	1.334	-12.54	-6.23
5	1.037	14.70	-0.03
6	1.321	20.35	-1.72
7	1.114	23.88	-0.96
8	0.989	25.01	0.20

Key

- - - → Experimental Flow Direction

——→ Analytical Flow Direction

Side View
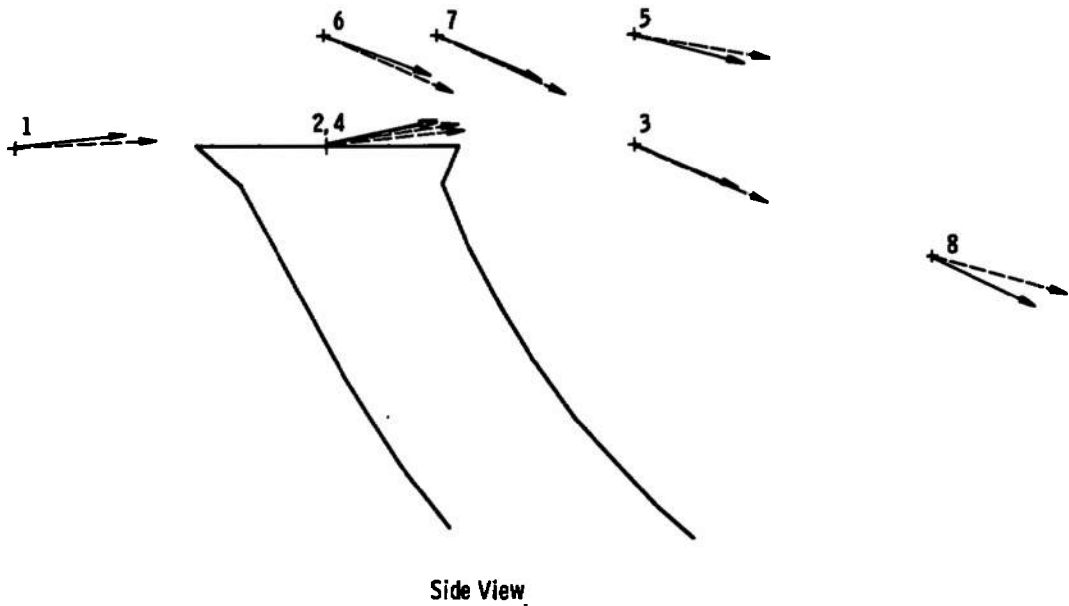
Fig. 44 Model No. 7—Comparison of Analytical and Experimental Flow Directions, K_{inlet} = 0.675
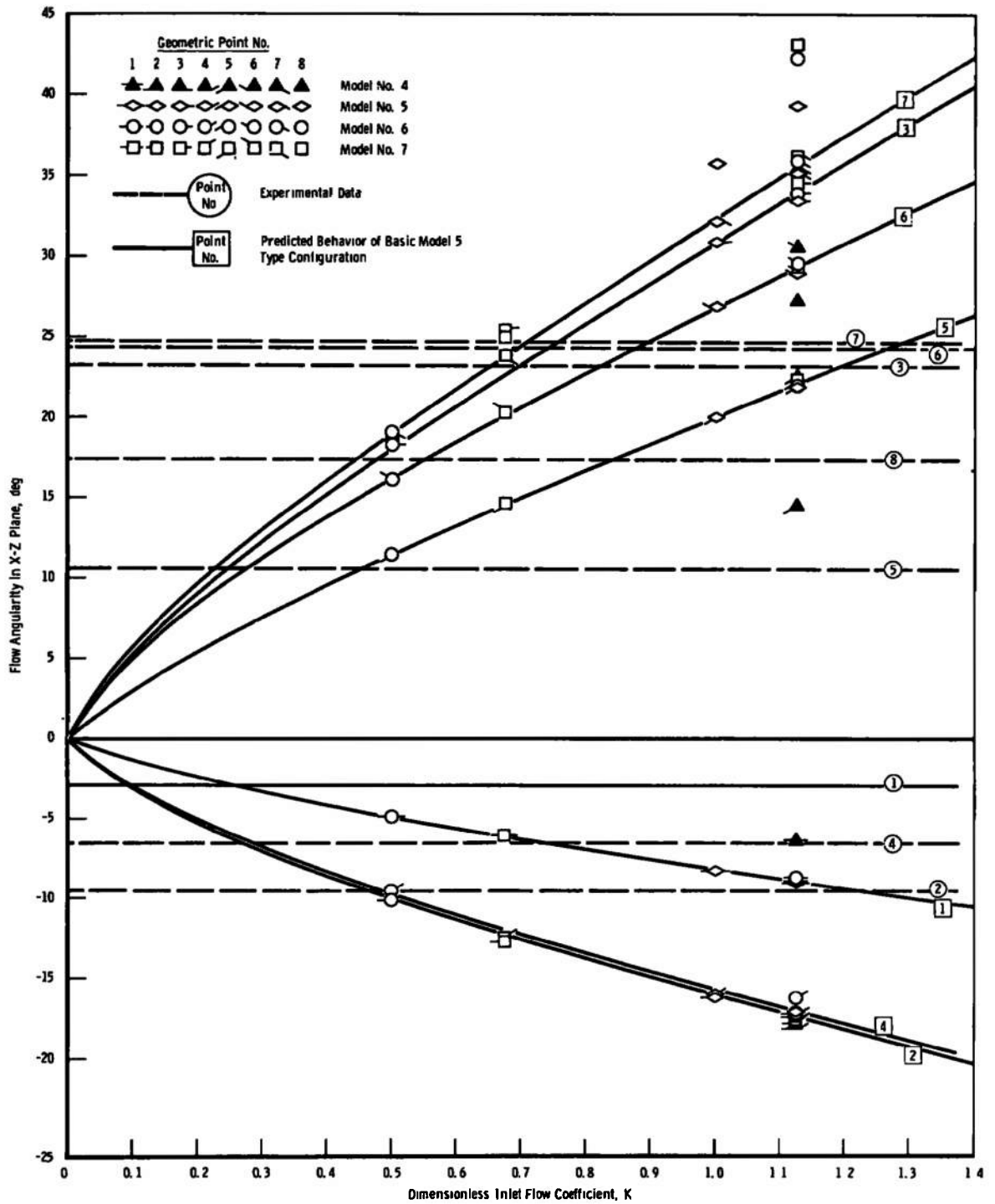
Fig. 45 Effect of Inlet Flow Coefficient on Flow Angularities
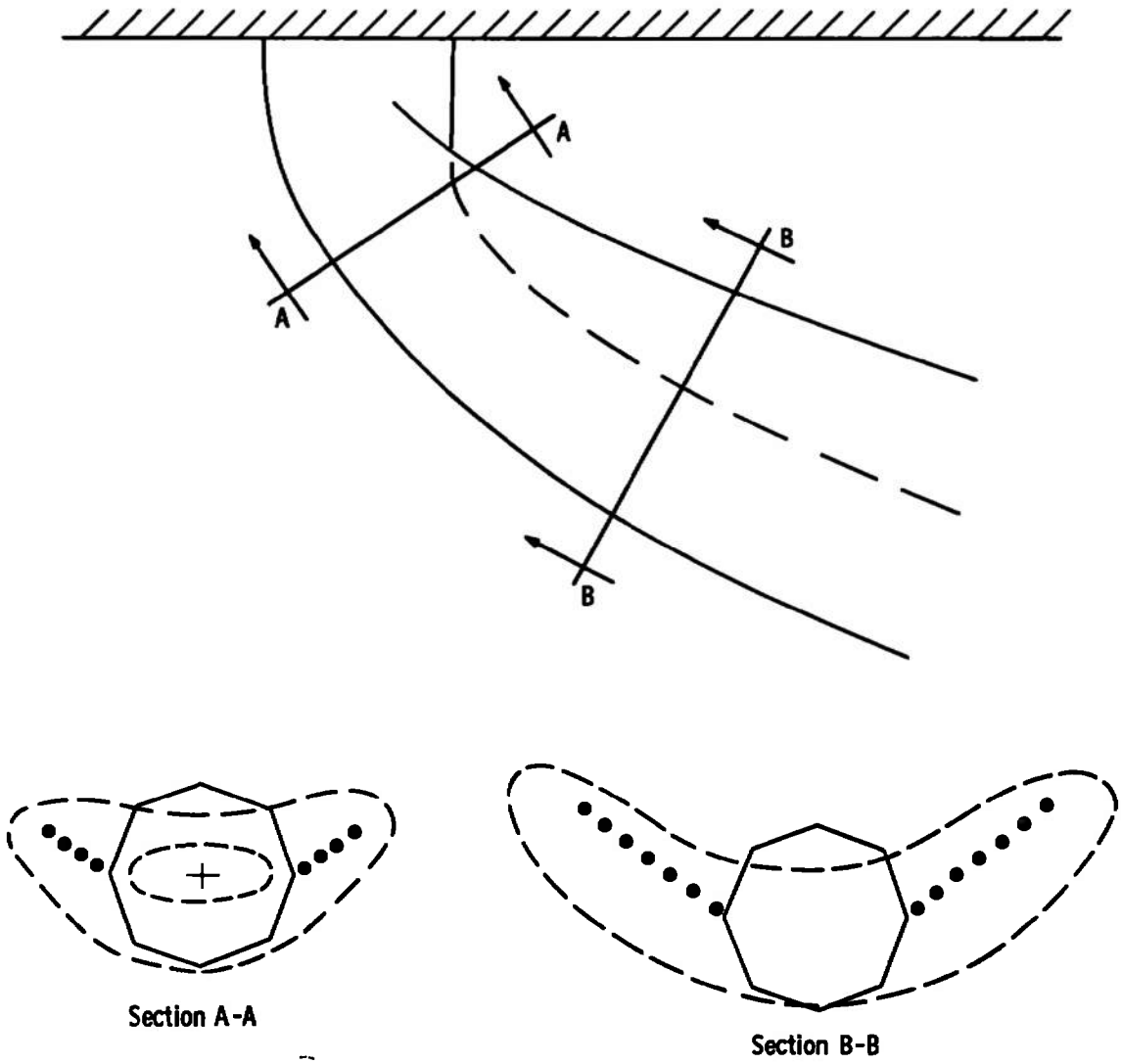
Fig. 46 Trailing Sheet Vortex Positions for Model No. 8
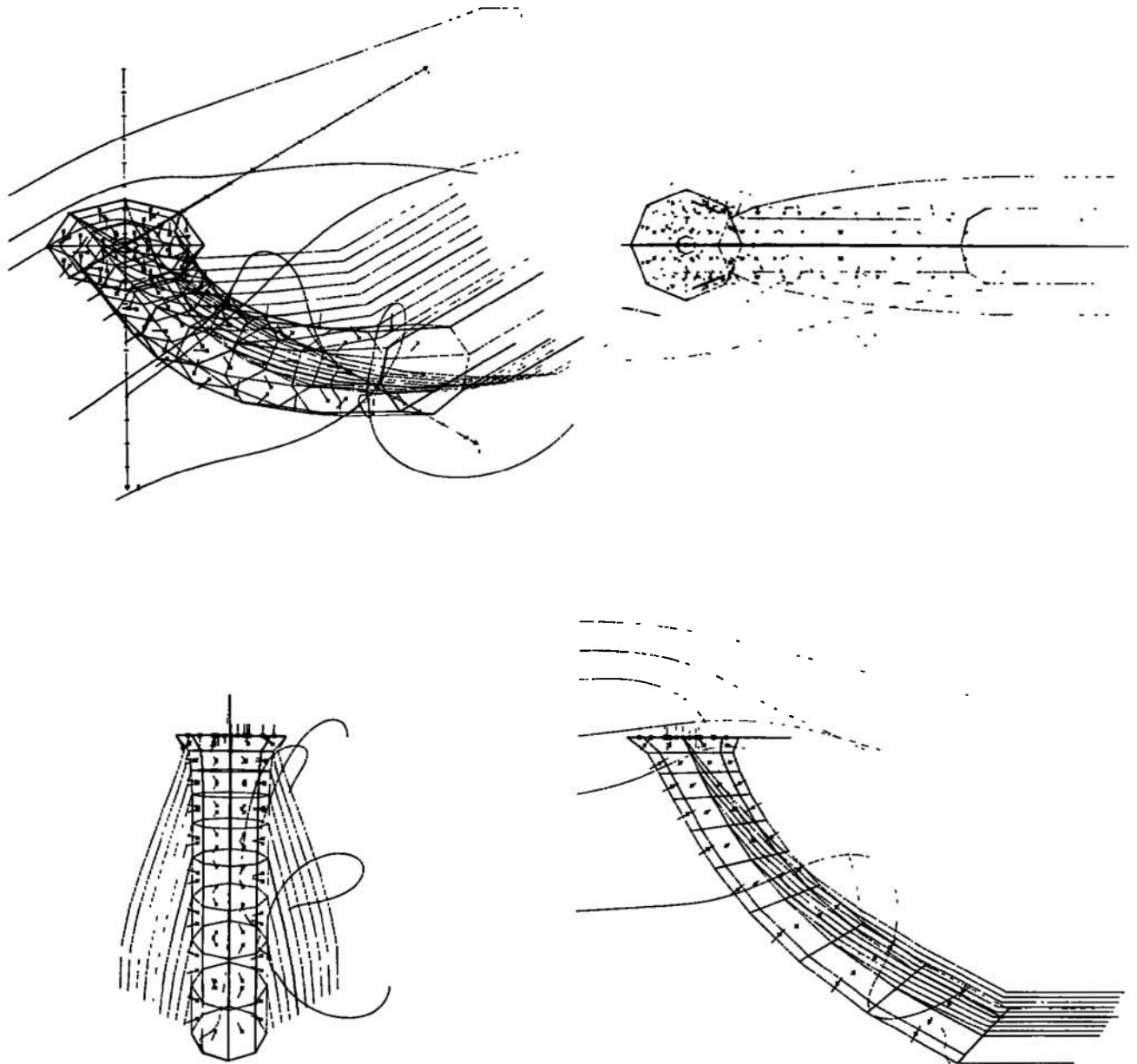
Fig. 47 Model No. 8

Fig. 48 Model No. 8--Analytical Streamlines, K_{inlet} = 1.125

Point	Velocity	Pitch	Yaw
1	1.057	-7.26	-0.30
2	1.365	-15.75	11.91
3	1.029	24.91	0.14
4	1.381	-15.70	-8.84
5	1.021	15.75	-0.09
6	1.364	29.21	-2.78
7	1.075	29.10	-1.99
8	0.988	27.39	0.19
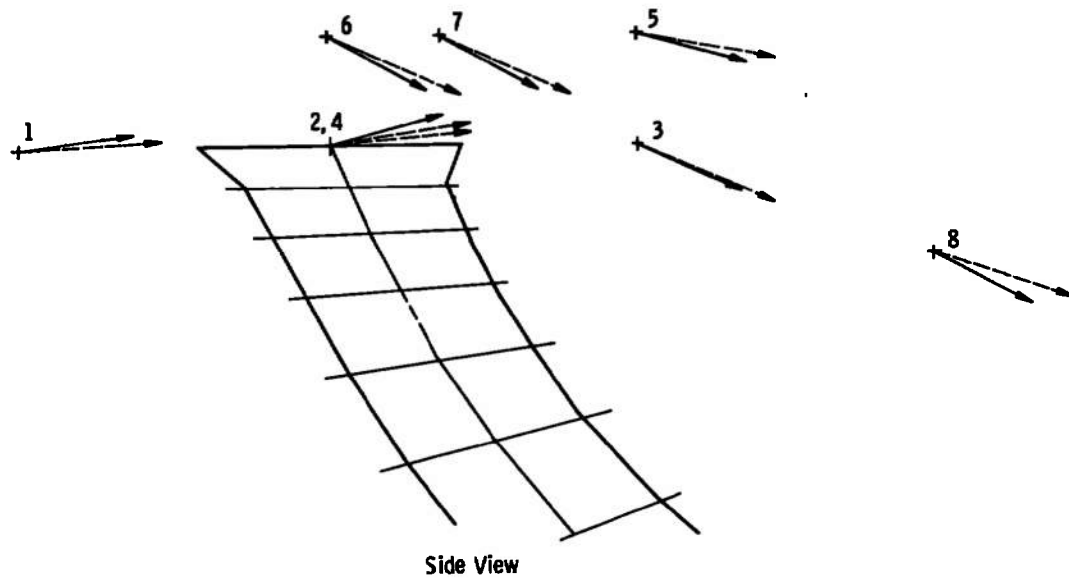
Fig. 49 Model No. 8—Comparison of Analytical and Experimental Flow Directions, K_{inlet} = 1.125
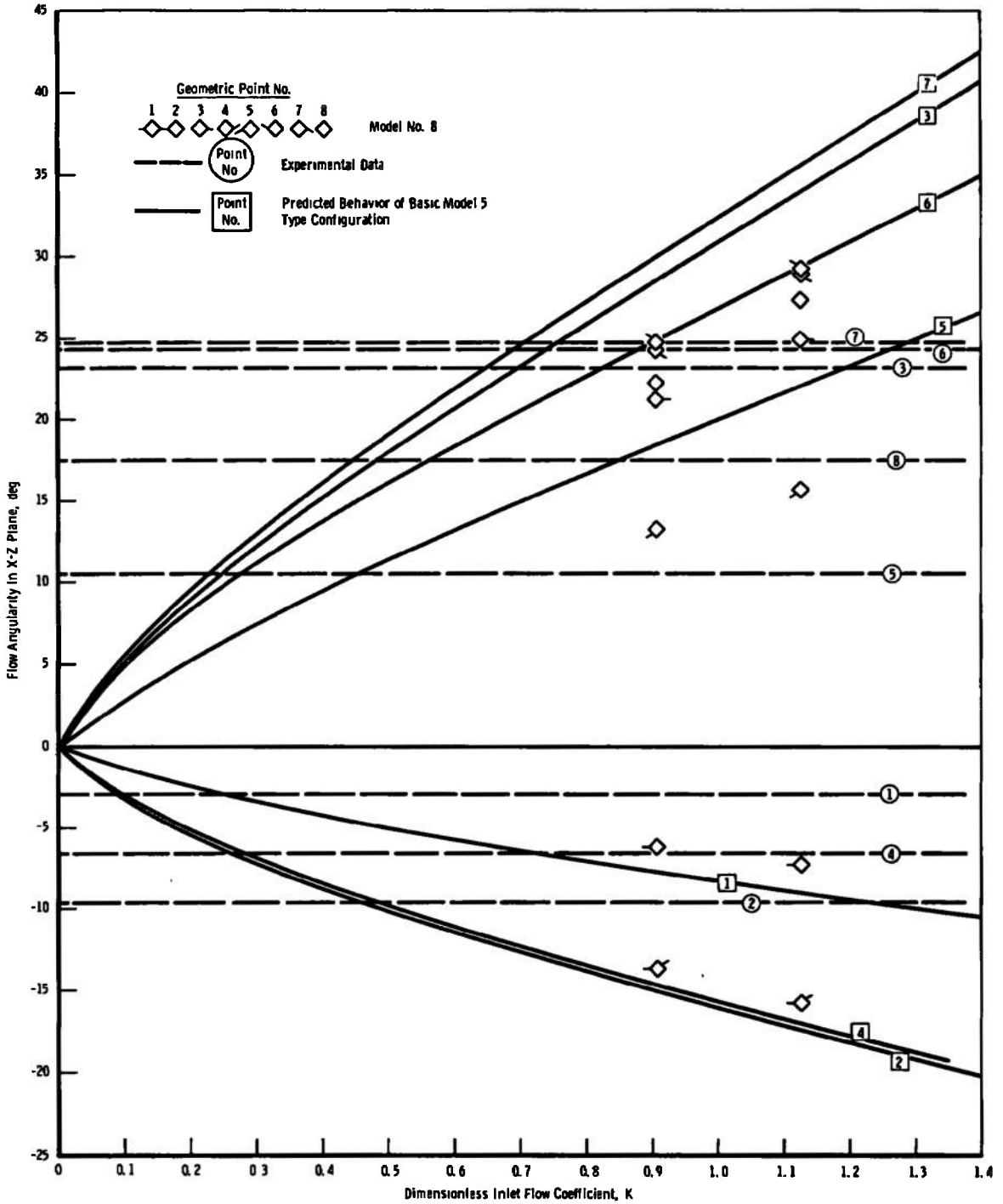
Fig. 50 Comparison of Model 5 Curves and Model 8 Data
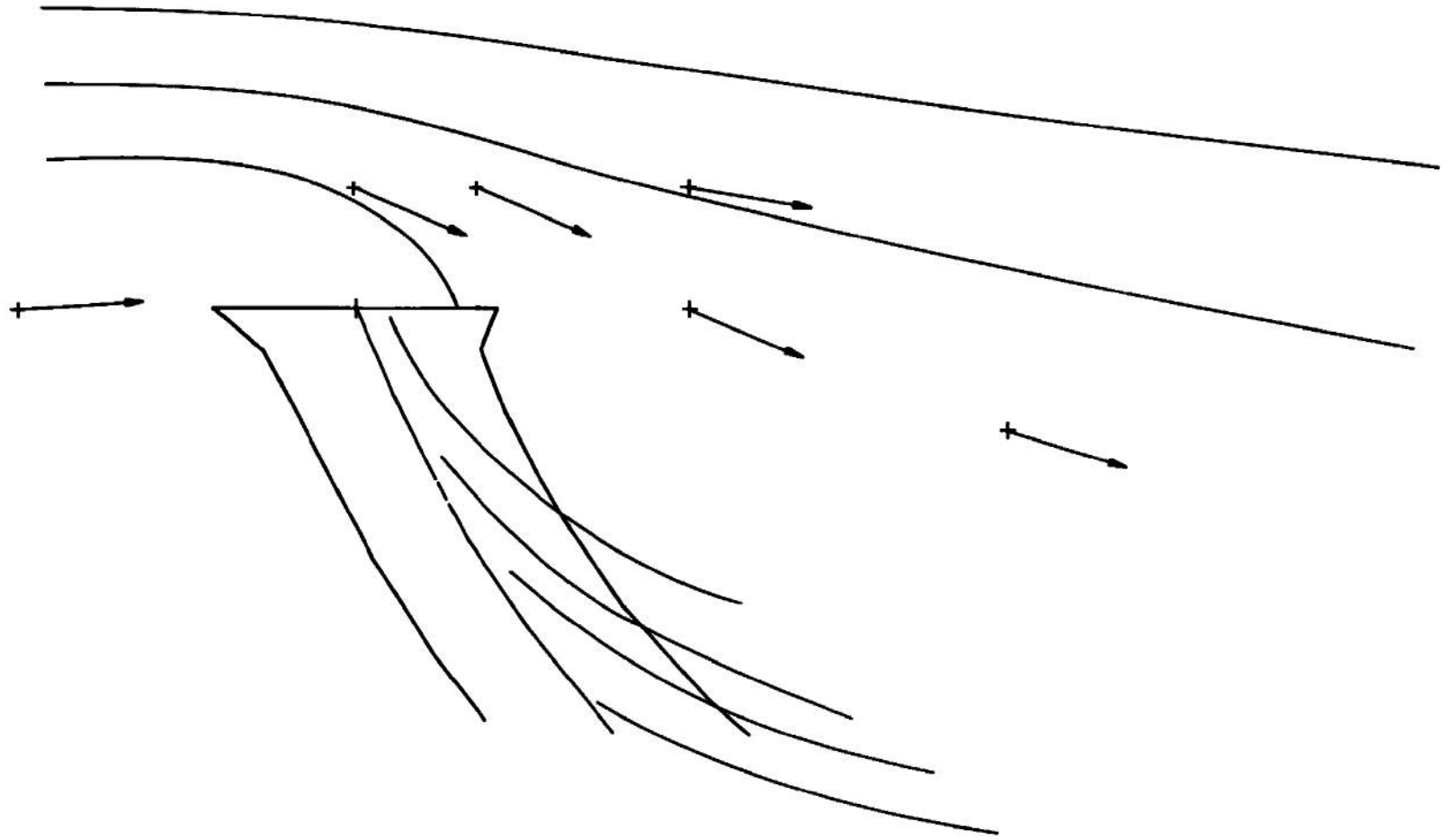
Fig. 51 Model No. 8—Analytical Streamlines, K_{inlet} = 0.906
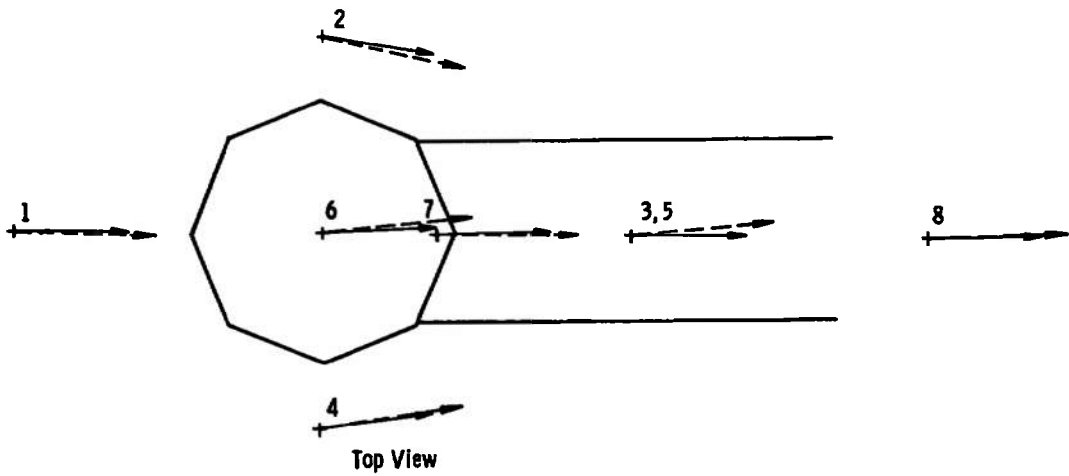
Point	Velocity	Pitch	Yaw
1	1.039	-6.21	-0.25
2	1.305	-13.64	9.79
3	1.002	21.25	0.11
4	1.319	-13.63	-7.24
5	1.009	13.31	-0.07
6	1.203	24.79	-2.29
7	1.054	24.30	-1.57
8	0.969	22.26	0.15
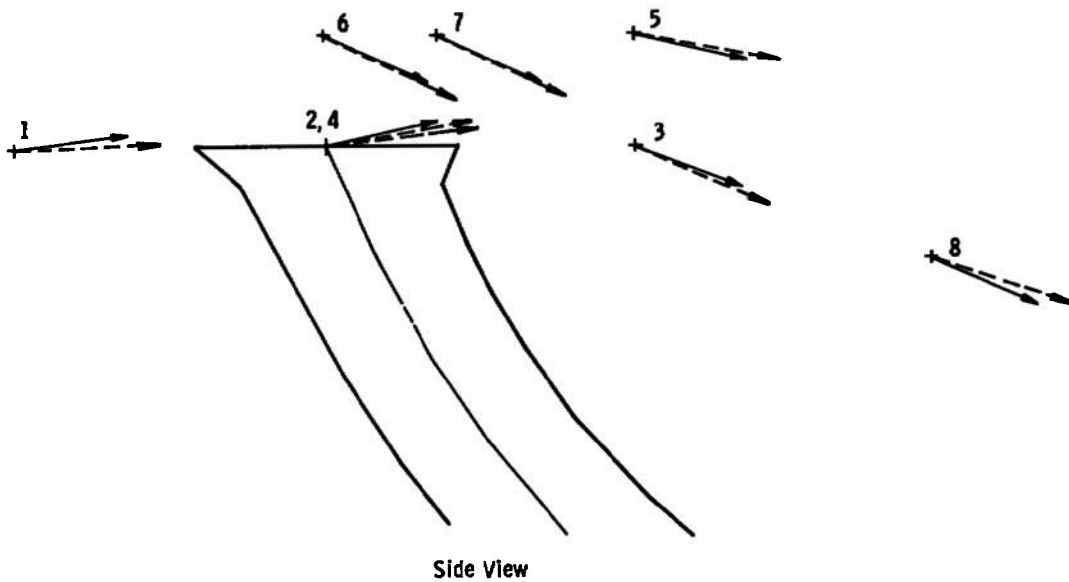
Fig. 52 Model No. 8—Comparison of Analytical and Experimental Flow
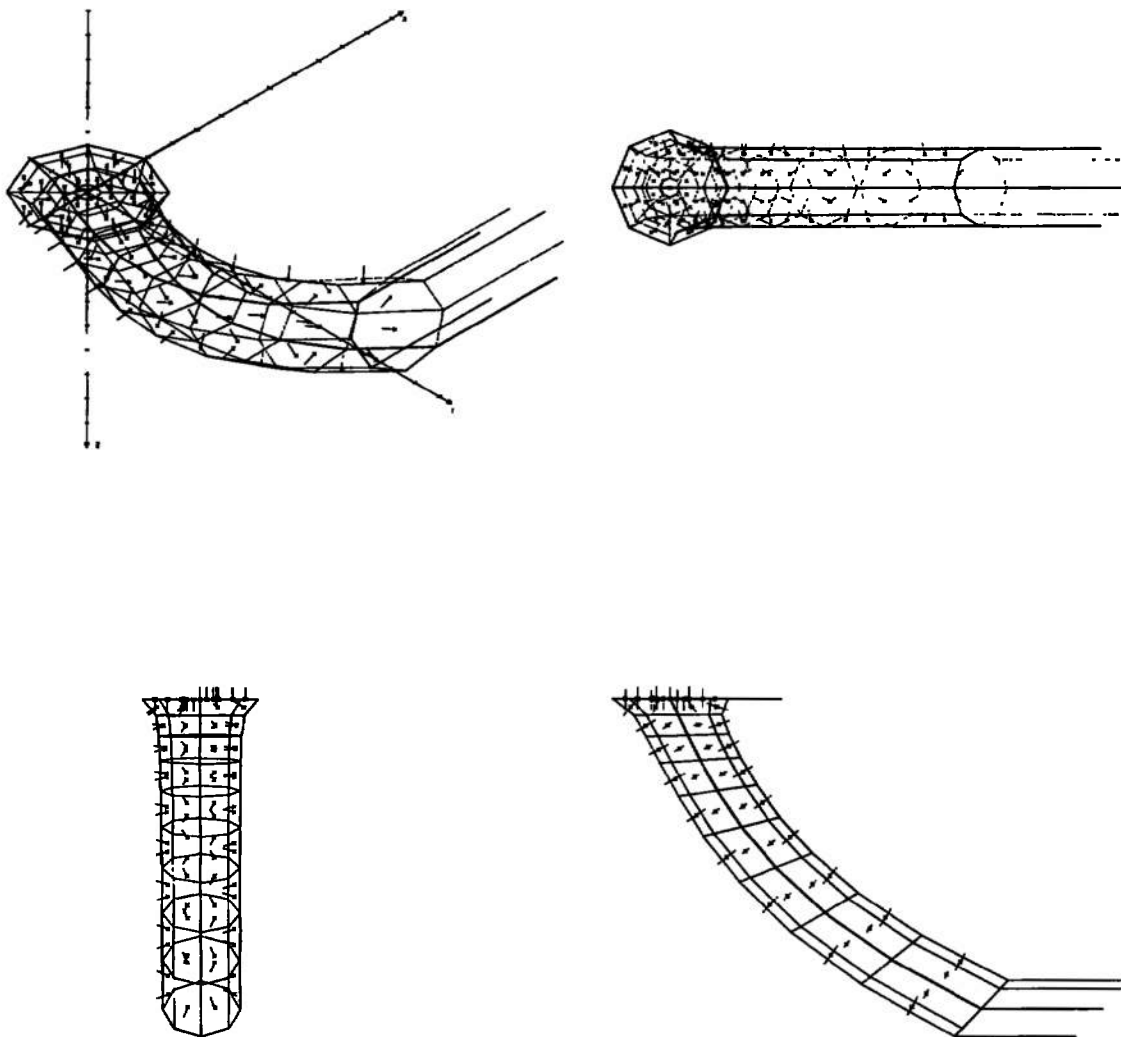Direction, K_{inlet} = 0.906
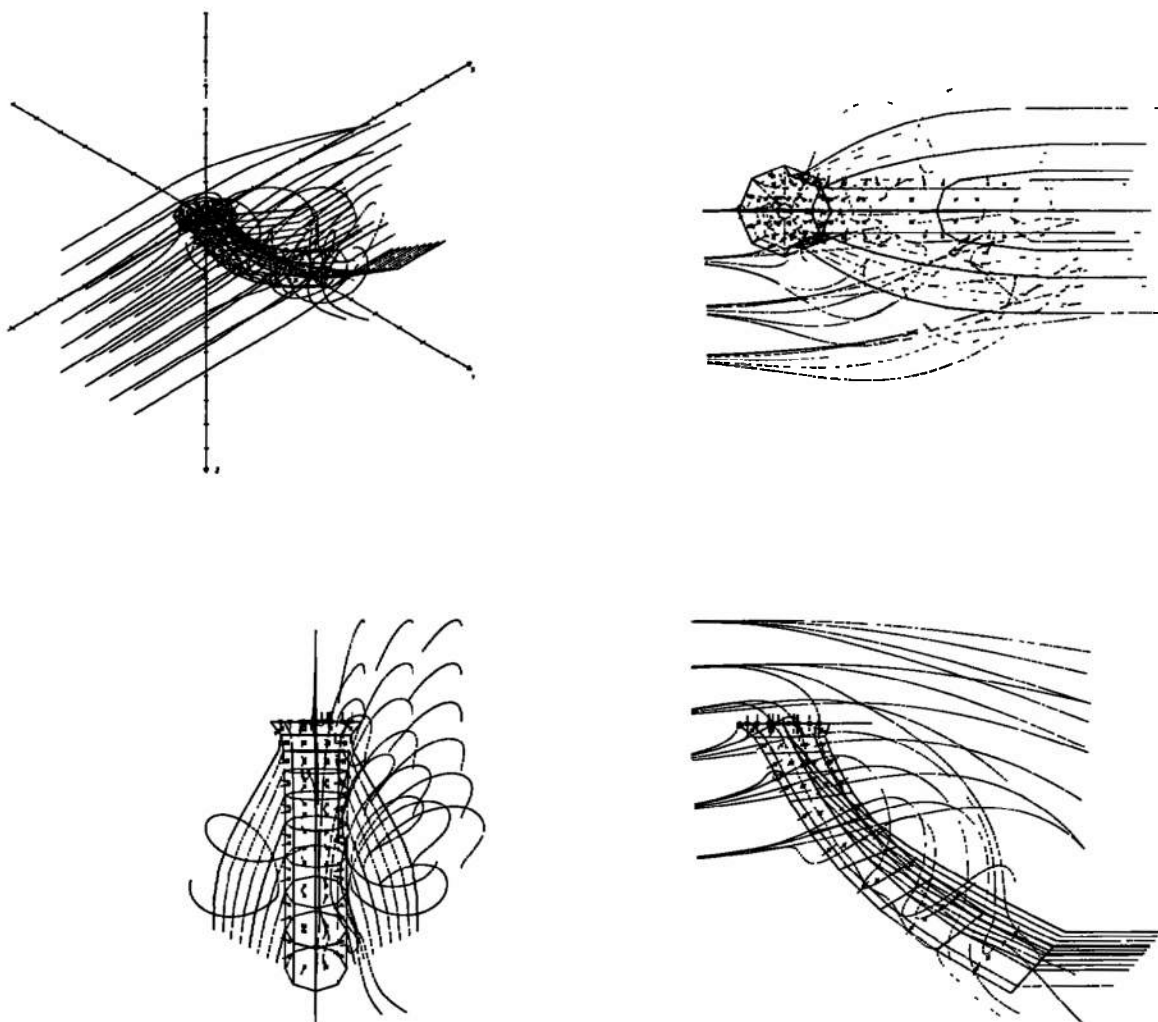
Fig. 53 Three-Dimensional Flow Simulation
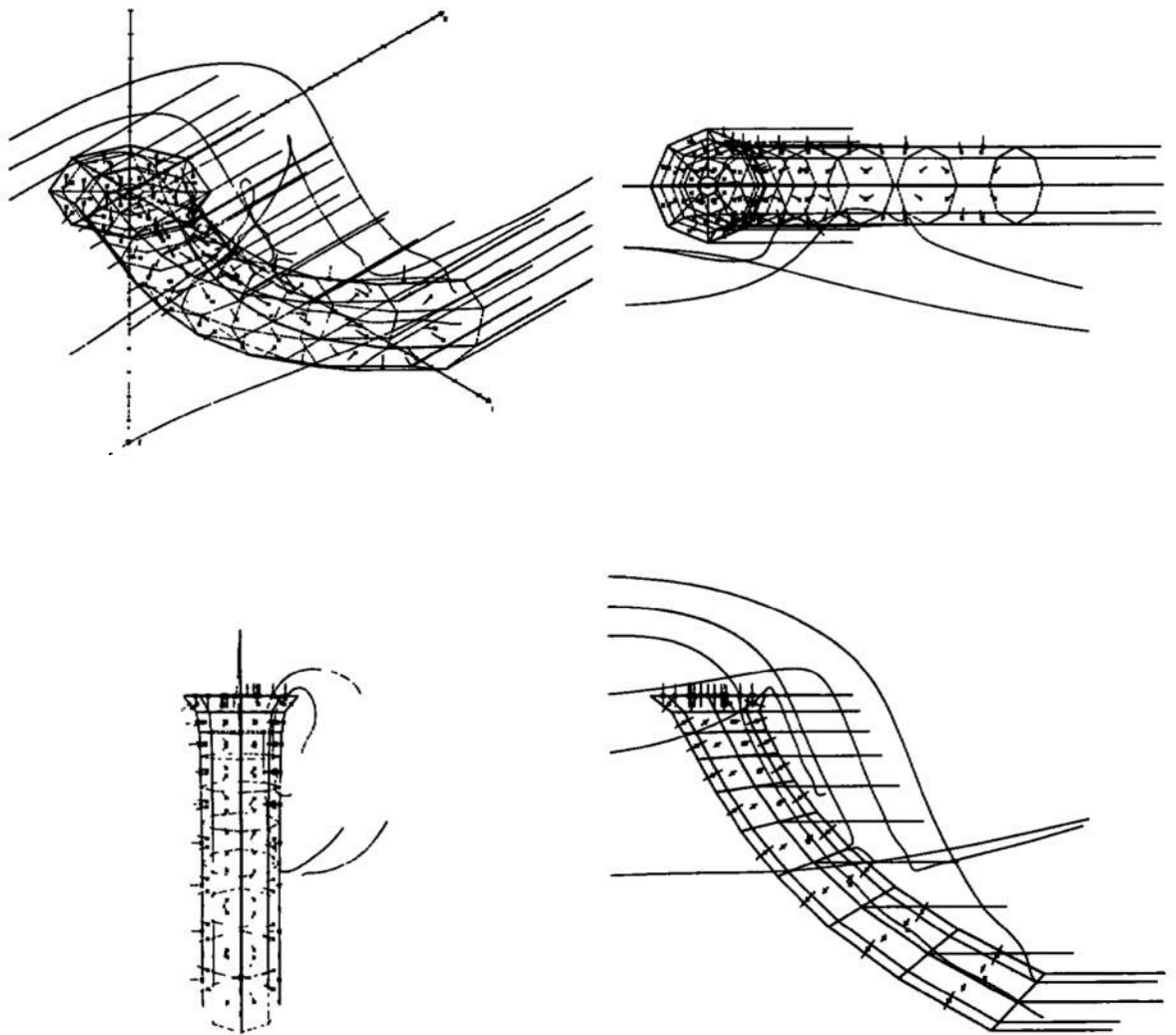
Fig. 54 Model No. 9

Fig. 55   Model No. 10
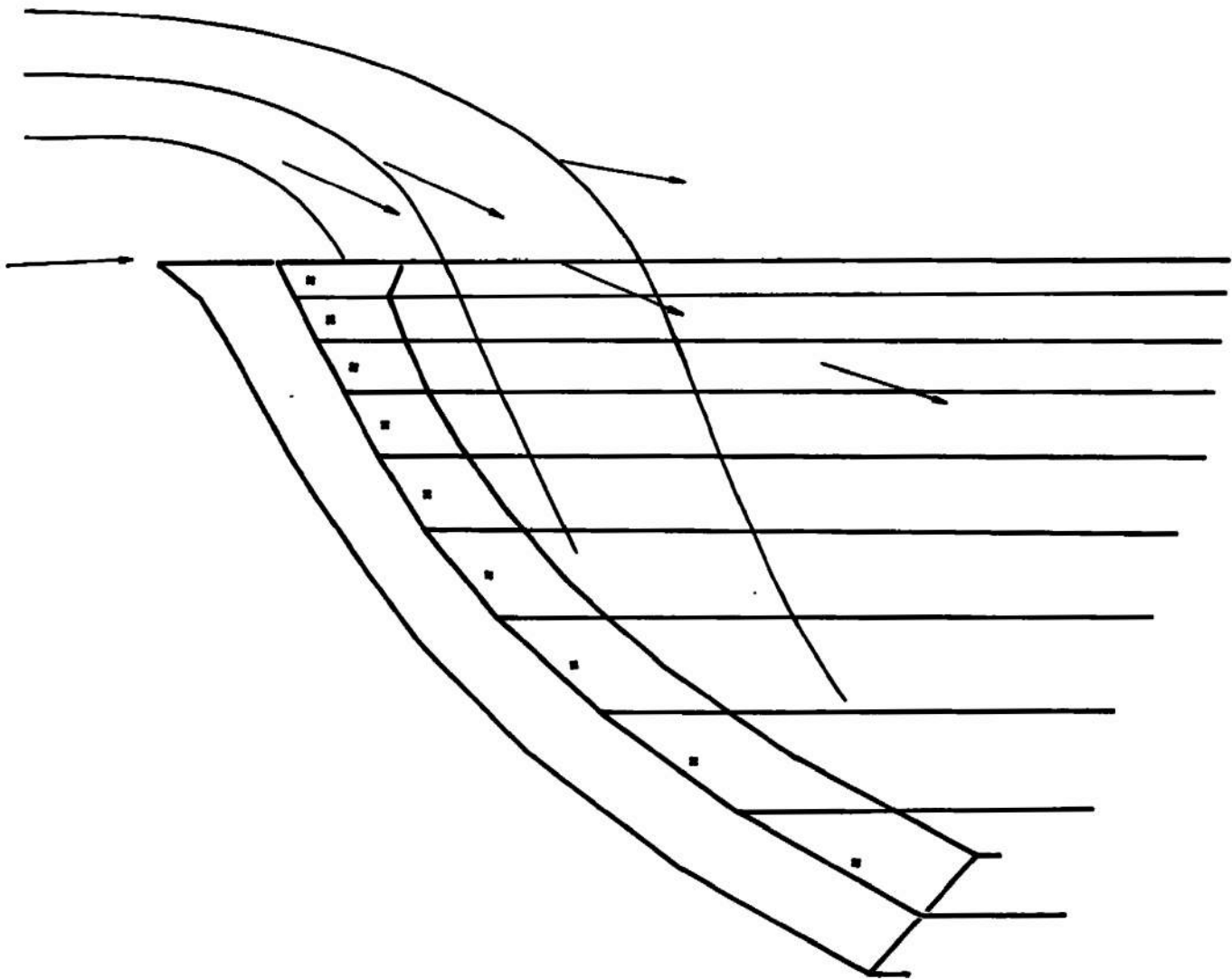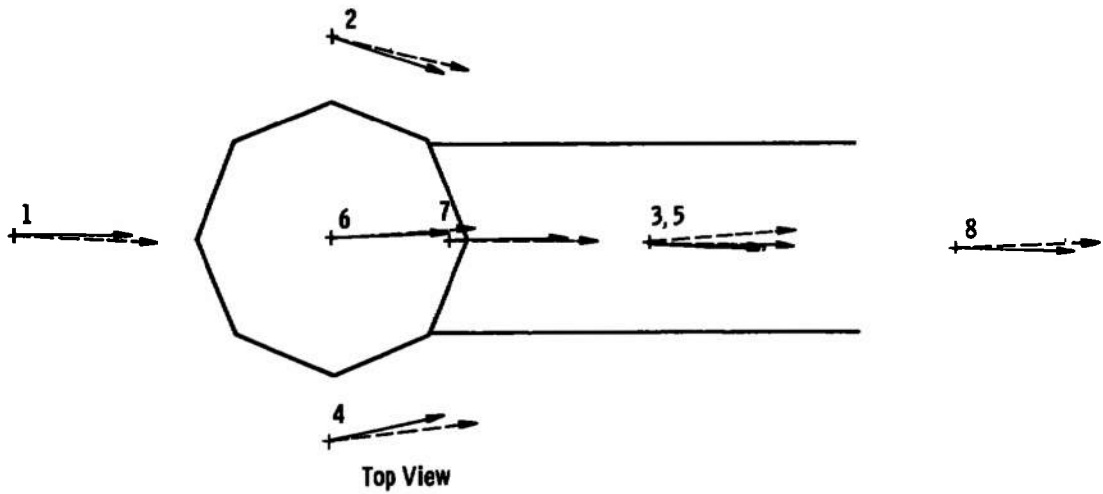
Fig. 56 Model No. 10—Analytical Streamlines, K_{inlet} = 1.125

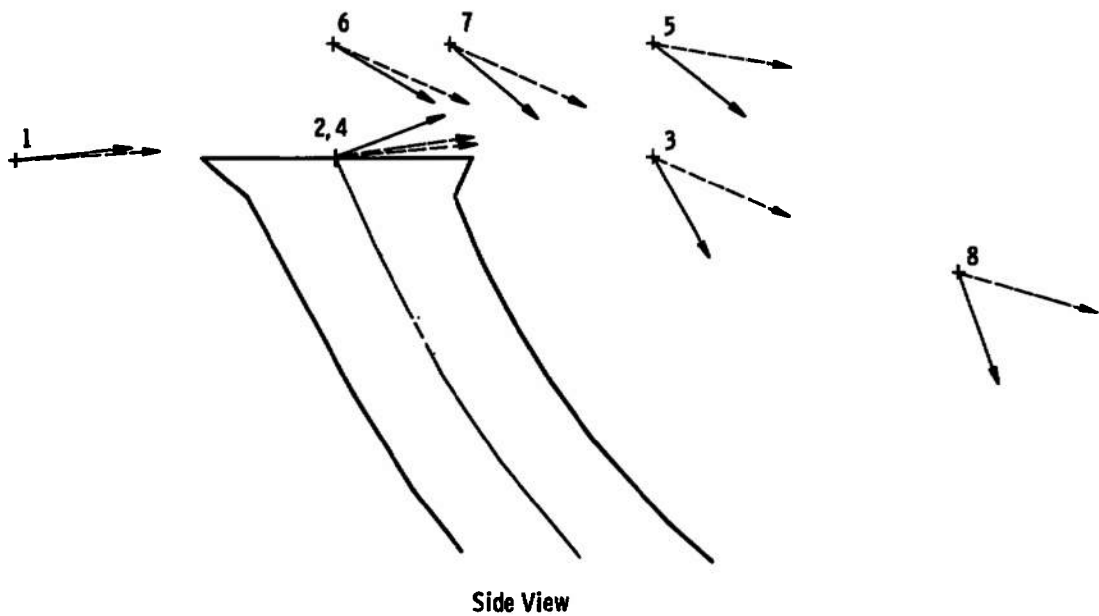| Point	Velocity	Pitch	Yaw
1	1.084	-5.94	-0.34
2	1.350	-21.92	17.38
3	2.135	61.32	1.86
4	1.314	-21.95	-14.31
5	1.334	39.22	0.04
6	1.662	30.73	-2.46
7	1.482	41.02	-1.34
8	2.869	69.39	1.12

Fig. 57 Model No. 10—Comparison of Analytical and Experimental Flow Directions, $K_{inlet} = 1.125$

Fig. 58 Model No. 11

$V_J/V_\infty = 2.145$
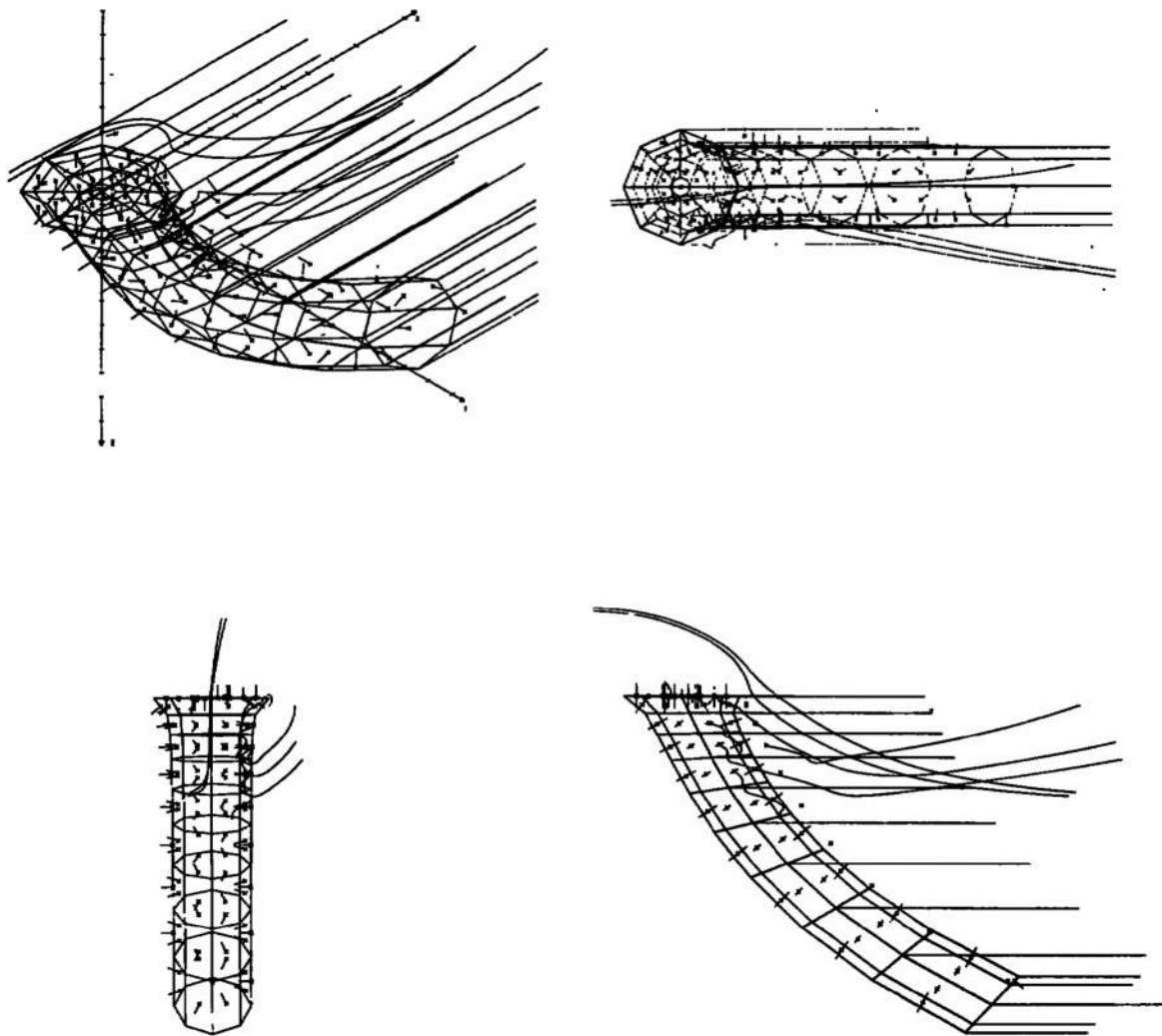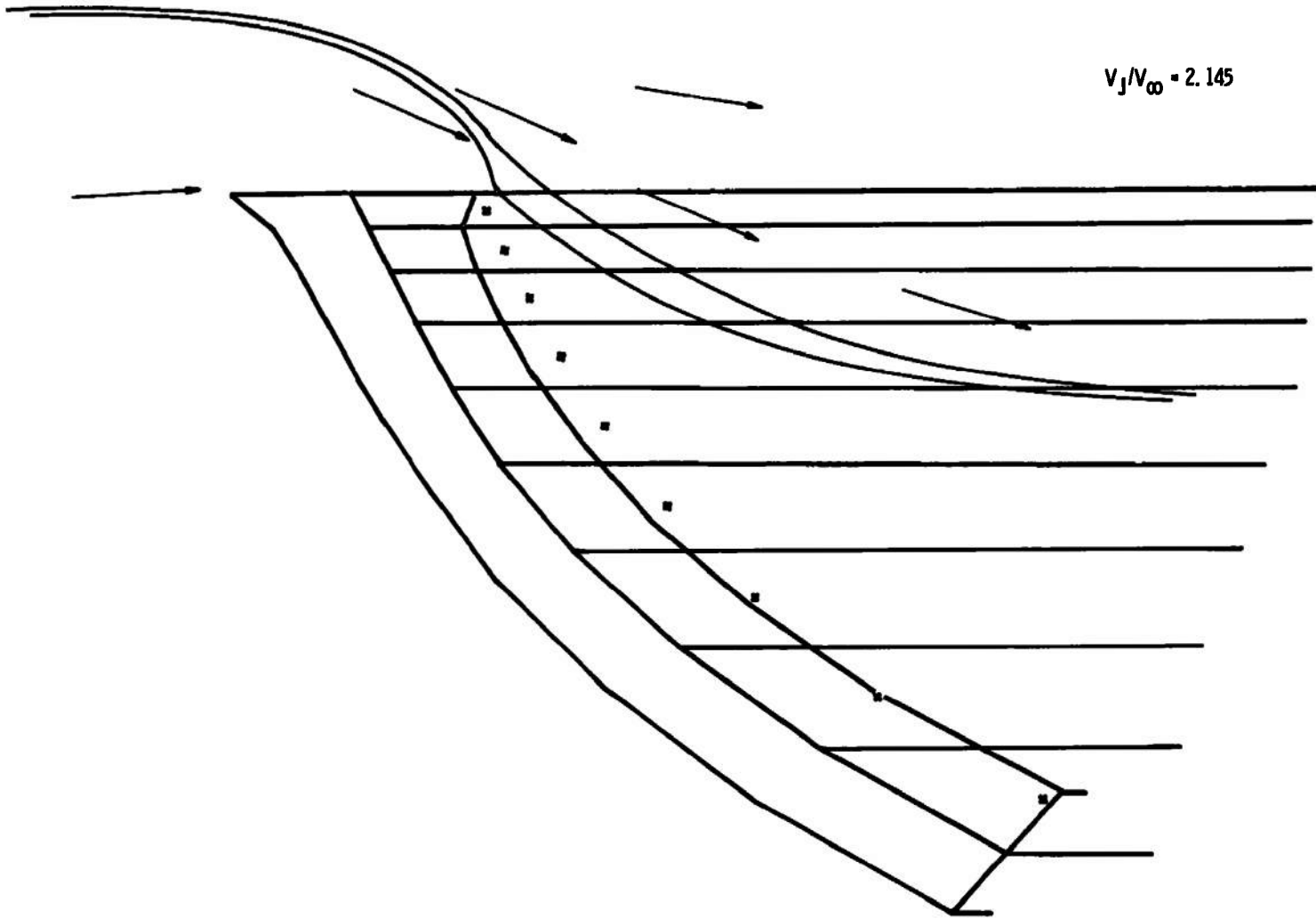
Fig. 59 Model No. 11—Analytical Streamlines $K_{inlet} = 1.125$

Fig. 60 Model No. 12

$V_J/V_\infty = 2.145$
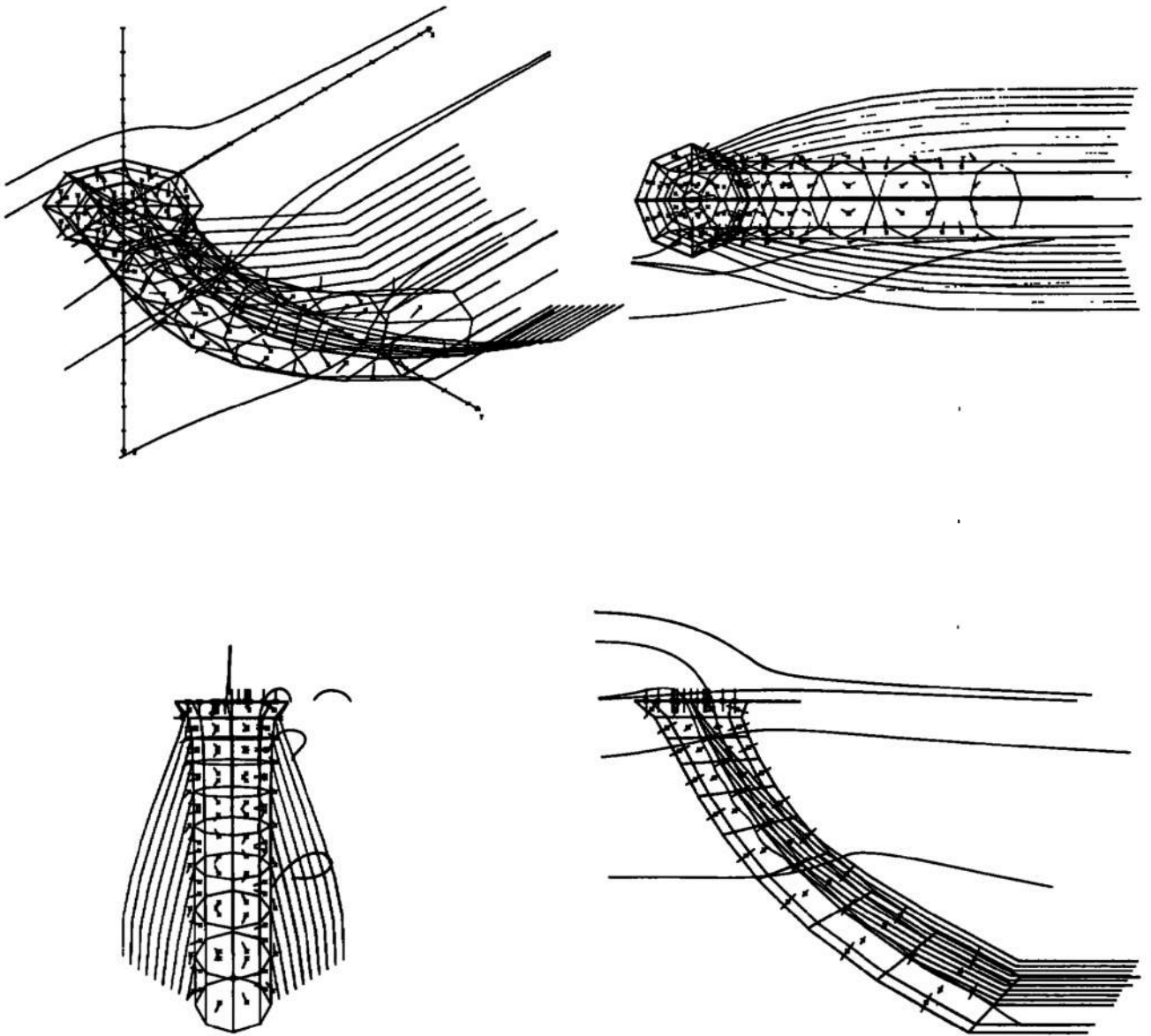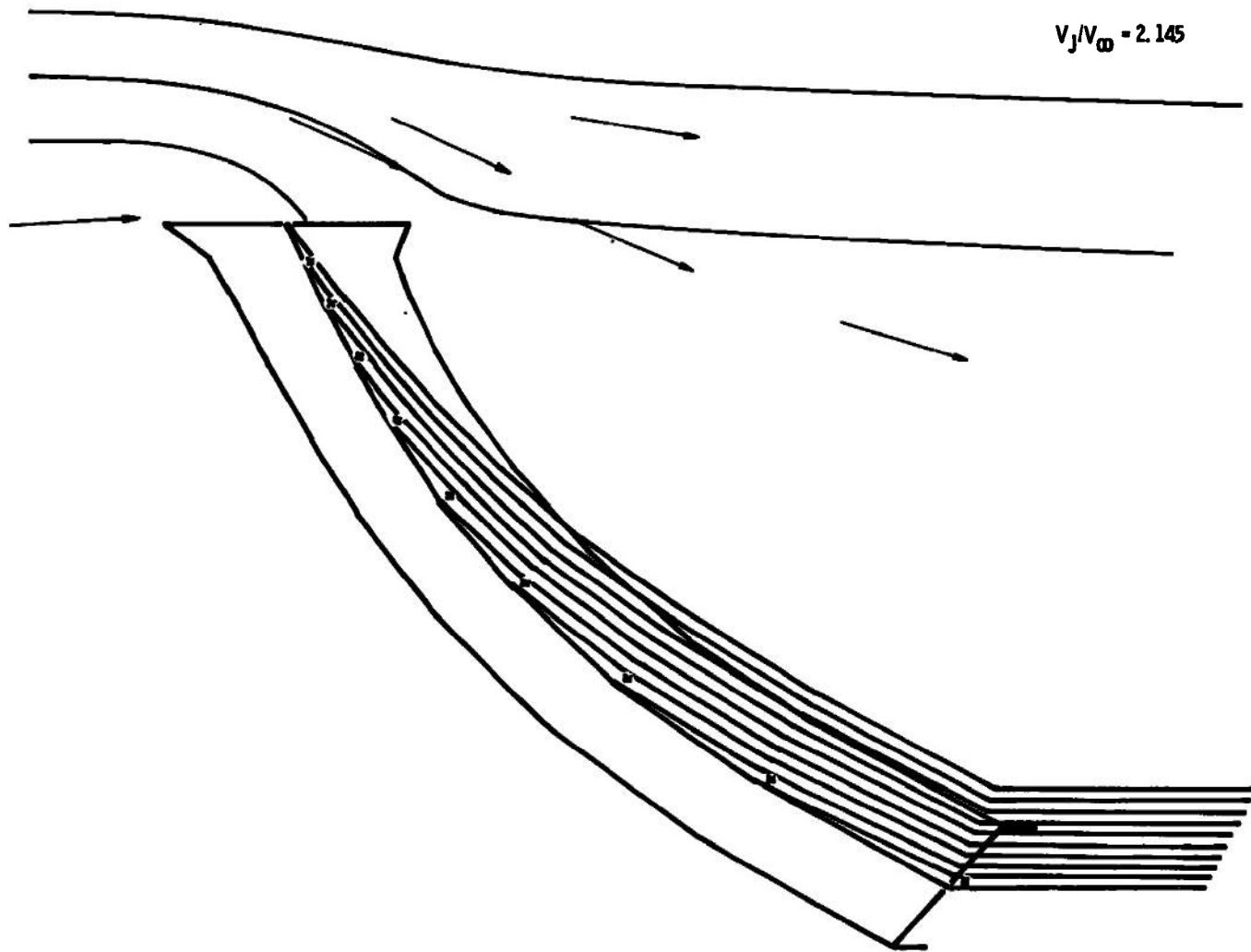
Fig. 61 Model No. 12—Analytical Streamlines, K_{inlet} = 1.125
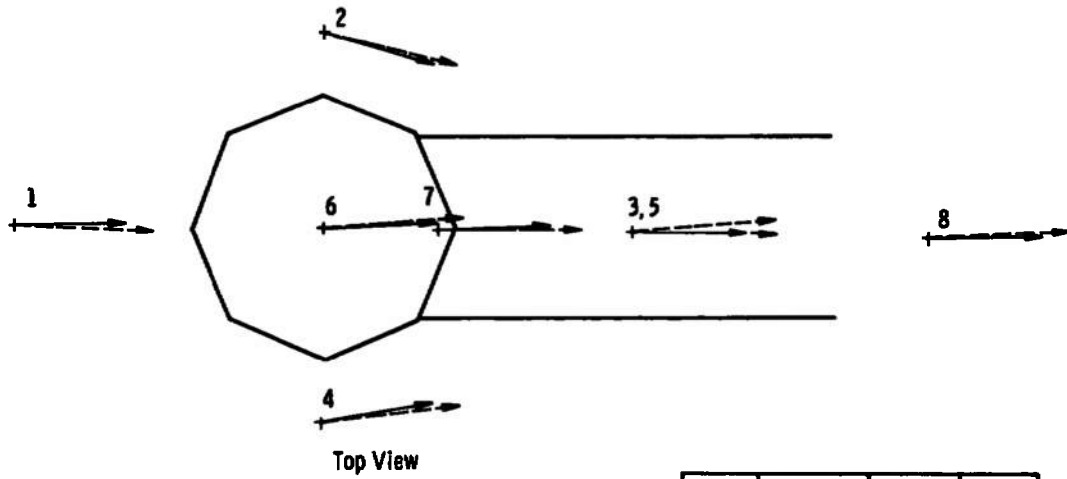
Top View

Point	Velocity	Pitch	Yaw
1	1.053	-4.08	-0.28
2	1.190	-13.10	14.44
3	0.868	5.39	-0.28
4	1.172	-11.42	-11.20
5	0.903	5.63	-0.23
6	1.350	32.70	-3.13
7	0.904	35.64	-2.45
8	0.965	4.81	-0.03

Key

----→ Experimental Flow Direction

——→ Analytical Flow Direction

Side View

Fig. 62 Model No. 12—Comparison of Analytical and Experimental Flow Directions, K_{inlet} = 1.125

APPENDIX II
VORTEX LATTICE PROGRAM

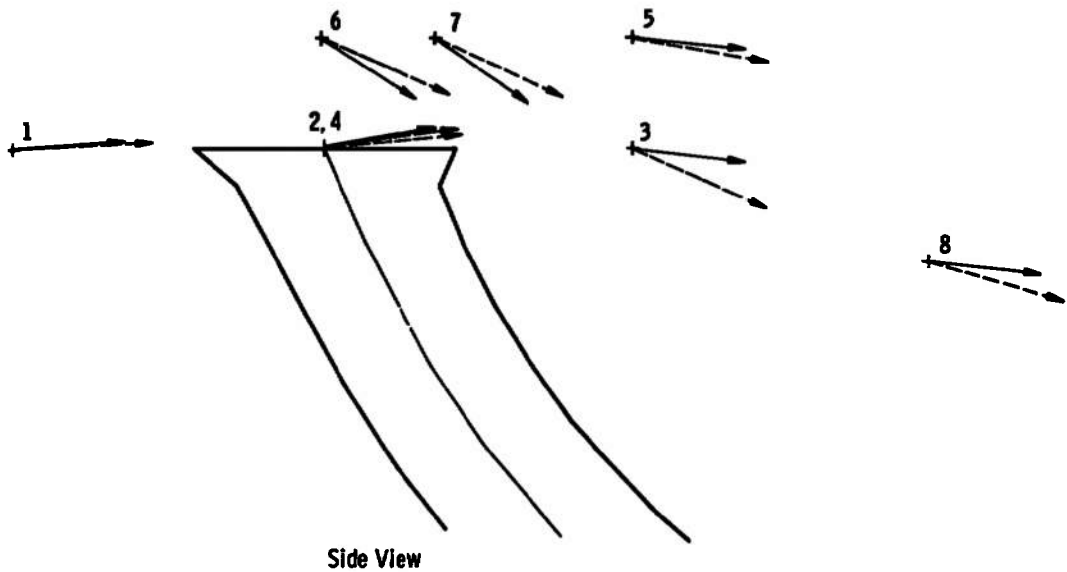The vortex lattice computer program used in this study is a modified version of that developed by Fitch (Ref. 1) and is similar to that used by Rubbert (Ref. 2). Models are constructed in a modular fashion through the use of rectangular arrays of horseshoe vortices called wing parts. Defining the model in this manner permits the user to change particular parts of the model without requiring modification of the entire input package. This is especially convenient in situations where one. part of the model is to be run at different attitudes to the others.

A typical wing part is illustrated in Fig. II-1 along with the nomenclature used throughout this report. The relative orientation of the leading edge, etc., is determined by the order of input information. This order is indicated in the figure by the number beside each geometric point. The first geometric coordinate specified defines the inboard end of the leading edge. The coordinates along the inboard tip to the trailing edge are specified next. If additional points (extra points) are needed to define the position of the trailing line vortex, these follow in order, until the last one is input. This order is repeated for the second column of coordinates beginning with the point located on the leading edge and proceeding in the chordwise direction to the last extra point. The process is continued column by column until the outboard tip is reached. Each successive wing part is defined in the same manner.

For simplification of the figures contained in this report, a shorthand notation was introduced to define the orientation of each wing part. The notation has been used in Fig. II-1b to represent the wing part shown in Fig. II-1a.

A wide variety of configurations are possible since the number of wing parts may be varied, a wing part may be made up of one or many horseshoe vortices and may be deformed into any three-dimensional shape desired.

Specification of a nonlifting wing part can be accomplished by using the extra points to route the trailing vortices to infinity along the same line. A simple example of lifting and nonlifting types is shown in Fig. II-2a and b, respectively. It is often convenient to build up a lifting system such as the one illustrated in Fig. II-2a using both nonlifting and lifting wing parts. It can be shown that the configuration presented in Fig. II-2c provides the same net result as that appearing in Fig. II-2a.
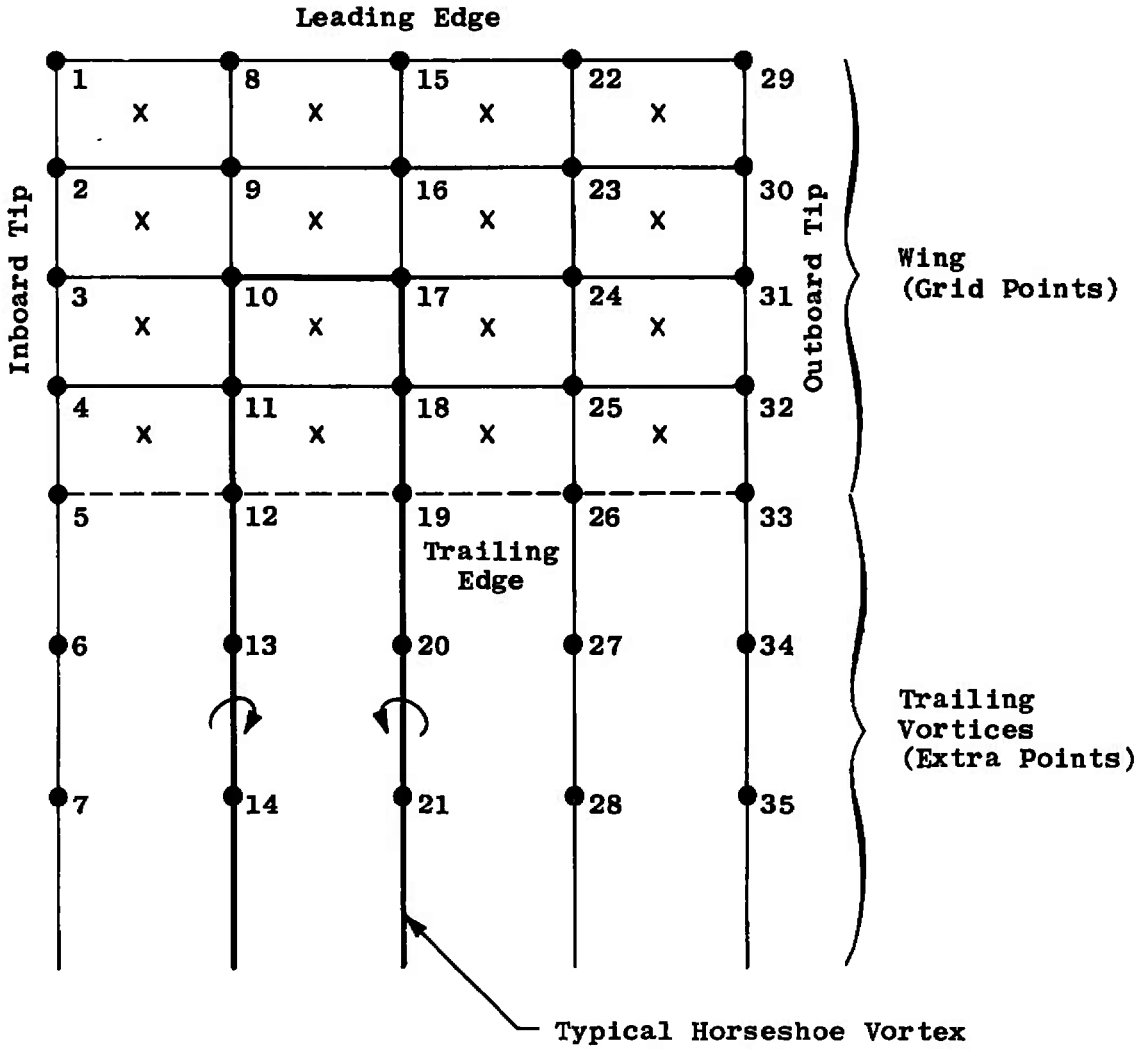
a. Typical Wing Part
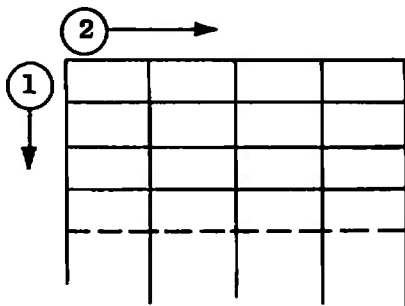
b. Short Hand Notation
Fig. II-1 Program Input Nomenclature
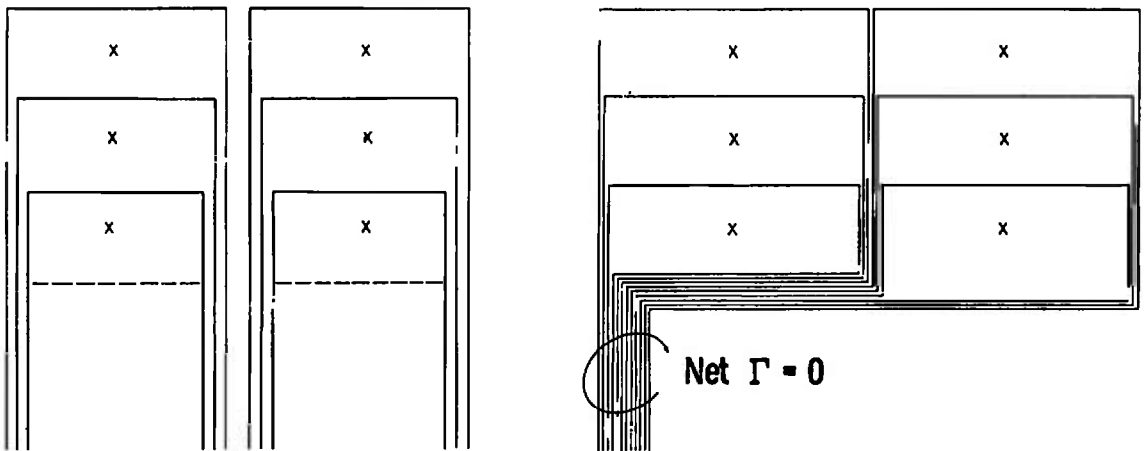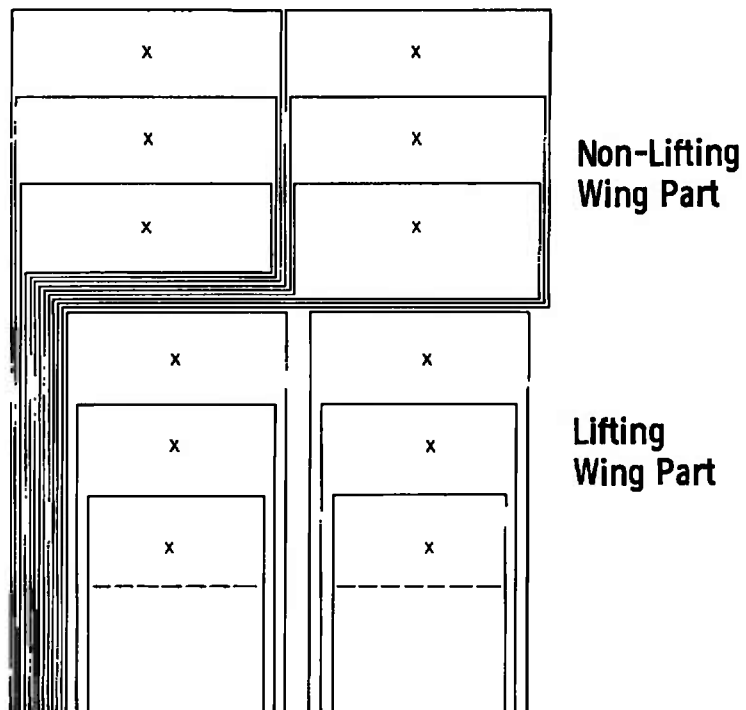
a. **Lifting Wing Part**

b. **Nonlifting Wing Part**

Net $\Gamma = 0$

Non-Lifting
Wing Part

Lifting
Wing Part

c. **Multi-Wing Part Lifting System**
Fig. II-2 Methods of Lattice Construction

DOCUMENT CONTROL DATA - R & D

(Security classification of title, body of abstract and indexing annotation must be entered when the overall report is classified)

1 ORIGINATING ACTIVITY (Corporate author)	2a. REPORT SECURITY CLASSIFICATION
Arnold Engineering Development Center, Arnold Air Force Station, Tennessee 37389	UNCLASSIFIED
	2b. GROUP N/A

3 REPORT TITLE

SIMULATION OF A HIGH DISC LOADING FREE PROPELLER
IN A CROSS FLOW BY THE VORTEX-LATTICE METHOD

4 DESCRIPTIVE NOTES *(Type of report and inclusive dates)*
November 10, 1969--June 1971--Final Report

5 AUTHOR(S) *(First name, middle initial, last name)*

R. L. Parker, Jr. and F. L. Heltsley, ARO, Inc.

6 REPORT DATE	7a. TOTAL NO. OF PAGES	7b. NO. OF REFS
November 1972	99	10

8a. CONTRACT OR GRANT NO	9a. ORIGINATOR'S REPORT NUMBER(S)
b. PROJECT NO. 69BT	AEDC-TR-72-139
c. Program Element 64207F	9b. OTHER REPORT NO(S) (Any other numbers that may be assigned this report)
d.	ARO-OMD-TR-72-98

10. DISTRIBUTION STATEMENT

Approved for public release; distribution unlimited.

11 SUPPLEMENTARY NOTES	12. SPONSORING MILITARY ACTIVITY
Available in DDC	Air Force Flight Dynamics Laboratory Wright-Patterson Air Force Base Ohio 45433

13 ABSTRACT

A study was conducted to develop an analytical model for the investigation of flow fields about intermediate disc loading lift devices for VTOL applications. Classical vortex-lattice theory was used in conjunction with experimental data for representing a free propeller in a crossflow. The jet phenomena to be simulated by the method are discussed. A number of previous attempts at vortex-lattice modeling are presented. Analytical stream lines and field vectors are compared with available experimental data. The results are evaluated and recommendations are made for further model development.

DD FORM 1473 1 NOV 65

14. KEY WORDS	LINK A		LINK B		LINK C	
	ROLE	WT	ROLE	WT	ROLE	WT
analytical model						
VTOL application						
potential flow						
propeller						
jet simulation						

AFSC
Arnold AFS Tenn